A numerical model for solving the linearized gravity-wave equations by a multilayer method

Alexandru Doicu[1], Dmitry S. Efremenko[2], and Thomas Trautmann[2]

[1]Independent researcher, 82110 Germering, Germany

[2]Deutsches Zentrum für Luft- und Raumfahrt (DLR), Institut für Methodik der Fernerkundung (IMF), 82234 Oberpfaffenhofen, Germany

Correspondence: Dmitry S. Efremenko (dmitry.efremenko@dlr.de)

Abstract. We developed a numerical model to solve for solving the linearized gravity-wave equations by using a multilayer approach . Specifically, the model handles the linearized equations including that explicitly accounts for viscosity, thermal conduction, and ion drag. The solution methods are based on the matrix exponential formalism and encompass two main approaches: (i) strategy is based on a matrix-exponential formalism and comprises two classes of methods: global matrix methods and (ii) scattering matrix methods. Both methods are focused on determining either (i) the amplitudes of the characteristic solutions or (ii) the discrete values of the solution vector. Ascending and descending wave modes are distinguished based on the criterion that the real parts of the eigenvalues of the characteristic equation for ascending modes are smaller than those for descending modes. In global matrix methods, ascending and descending modes can be defined (i) at the upper and lower boundaries or (ii) in each layer. In contrast, scattering matrix methods necessitate explicitly determining the mode type within each layer. The model accommodates two types of lower boundary conditions and can handle both The model supports both single-frequency waves and time wavepackets. Our simulations demonstrate that the solution methods are numerically stable and achieve comparable accuracies. Among them, waves and time-dependent wave packets. Particular emphasis is placed on the global matrix method, which exploits the structured form of the multilayer system to achieve high computational efficiency while maintaining numerical accuracy. Numerical experiments demonstrate that all methods yield identical accuracy, although the global matrix method for computing the amplitudes of the characteristic solutions is the most efficient. is significantly more efficient than the scattering matrix method, especially for time-dependent wave packets. The impact of ion drag on wave characteristics is quantified within this framework. The implementation is freely available as open-source code at https://github.com/AlexandruDoicu/Gravity-Waves.

1 Introduction

Time-step methods (Liu et al., 2013; Heale et al., 2014; Fritts et al., 2015) are commonly used to solve fully nonlinear sets of governing equations , allowing for upper-atmospheric gravity waves, thereby allowing the modeling of wave breaking, secondary wave generation, and weakly nonlinear effects. However, as compared to linear methods for gravity waves (Midgley and Liemohn, 1966; Volland, 1969a, b; Francis, 1973; Yeh and Liu, 1974; Klostermeyer, 1972, 1980) (Midgley and Liemohn, 1966; Volland, 1969a, b; Francis, 1973; Yeh and Liu, 1974; Klostermeyer, 1972, 1980; Knight et al., 2024) they are computationally expensive. In (Pütz et al., 2019) Pütz et al. (2019) it was found that a time-step model took several hours to run, while a linear method only took several seconds. In this regard, linear methods are more suitable for analyzing measured data.

The linearized equations can be transformed into a linear system of ordinary differential equations with variable coefficients that depend on the background atmospheric parameters and their height derivatives (the atmospheric parameters are assumed to be horizontally uniform but vertically varying). A common technique for integrating the linearized equations is the multilayer method first applied by Pfeffer and Zarichny (1962). In this method, the atmosphere is divided into a sequence of thin layers, and in each layer, a linear system of ordinary differential equations with constant coefficients is solved. The analytic wave solutions in neighboring layers are matched by the continuity condition of the variables across the interface. There are two methods for deriving a linear system of ordinary differential equations with constant coefficients.

1. In the standard physical multilayer method, the atmospheric parameters, and in particular, the temperature and wind velocity, are assumed to be constant within each layer (Midgley and Liemohn, 1966; Volland, 1969a, b; Francis, 1973; Yeh and Liu, 1974). As a result of the piecewise constant approximation, the height derivatives of the atmospheric parameters are zero within each layer.

2. In the nonstandard numerical multilayer method, the coefficients as a whole are approximated by their values in the middle of the layer (Klostermeyer, 1972). As a result, the height derivatives of the atmospheric parameters (approximated by their values in the middle of the layers) are also included in the resulting system of equations.

The criticism of standard physical multilayer methods by Hines (1973) concerns whether the equations describing the state variables in a layer are physically realistic. He concluded that it is impossible to find the appropriate variables when either (i) the viscosity and the wind velocity are nonzero or (ii) the thermal conductivity and the temperature height derivative are nonzero. However, as mentioned by Knight et al. (2022), Hines' concern about the physical meaning of the state variables is not relevant for a nonstandard numerical multilayer method. The reason is that in a purely mathematical context, it is sufficient to prove that the method, converges to a correct solution in the infinitesimally thin layer limit. A justification of this result, based on a matrix–exponential representation for the solution, can be found in (Klostermeyer, 1980)Klostermeyer (1980).

According to Volland (1969a), a layer is said to be isothermal if the background temperature is constant, and homogeneous if the kinematic viscosity , and so, the thermal diffusivity, is constant. In the case of an isothermal, homogeneous, and windless atmosphere, as in (Midgley and Liemohn, 1966; Volland, 1969a, b; Francis, 1973; Yeh and Liu, 1974)Midgley and Liemohn (1966); Volland (1969a, b); Francis (1973); Yeh and Liu (1974), the dispersion relation, associated to the system of ordinary differential equations, separates into three pairs of ascending and descending gravity-wave, viscosity-wave, and thermal conduction-wave modes. The viscosity-wave and thermal conduction-wave modes are also referred to as dissipative modes. The main distinction between the two pairs of dissipative modes and the pair of gravity-wave modes is that the latter have smaller vertical wavenumber imaginary parts. This means that ascending gravity-wave modes do not decrease in amplitude as rapidly with increasing altitude as dissipative modes. On the other hand, if it is assumed that in each layer, the assumption of locally constant kinematic viscosity is unrealistic as discussed in Knight et al. (2019). If one assumes instead that the dynamic viscosity is constant within each layer, it is generally not possible to differentiate distinguish between ascending and descending modes for some certain wavenumbers, frequencies, and background parameters (Knight et al., 2022, 2019, 2021). In this context, Knight et al. (2022) explained that the problem of distinguishing ascending from descending modes is related to the problematic branch points of the root functions giving the vertical wavenumber as a function of complex frequency. Along this line, the authors proposed a technique called imaginary frequency shift to assist in achieving this separation.

The inclusion of dissipative modes in a linearized model produces a numerical swamping for floating-point arithmetic (Maeda, 1985) in which certain descending modes grow so rapidly in the upward direction that numerical overflow occurs when the system of differential equation is subject to lower and upper boundary conditions. Several methods have been proposed to reduce numerical swamping.

1. Midgley and Liemohn (1966) used employed an iterative method that can be regarded as a Gauss–Seidel group iteration. For However, the Gauss–Seidel iteration to converge, it is essential that the gravity solutions are only minimally coupled with the dissipative solutions. However, this condition is violated at critical layers where the eigenvalues of the gravity solutions can be nearly identical to those of one or more dissipative solutions. The condition's failure, resulting in significant coupling, manifests at altitudes of around 200 km or higher (Volland, 1969a, b)may fail to converge in certain situations, in particular when gravity and dissipative modes become strongly coupled, as discussed in Volland (1969a, b). Klostermeyer (1980) avoids this problem difficulty by introducing the so called concept of a transfer matrix, which relates the amplitudes of the waves wave amplitudes at different altitude levels . The atmosphere is divided into rough layers, such that the critical level is approximately in the middle of a rough layer. The transfer matrix equations for the rough layers are solved by the Gauss–Seidel iteration, while the fine structure inside a rough layer is determined by a direct solution of the transfer matrix equations specific to that layerand provides a more robust framework for treating such coupling.

2. Volland (1969b) applied the scattering matrix formalism to a three-layer atmosphere assuming (i) abrupt changes in variables at the interfaces between the different layers and (ii) that certain background parameters remain constant in the lower and upper layers. Knight et al. (2019) also formulated the problem in terms of scattering matrices which are closely related to the reflection and transmission matrices appearing in seismology (Pérez-Álvarez and García-Moliner, 2004). However, in contrast to Volland, the authors used a more rigorous approach, i.e., a sequence of composed scattering matrices instead of just a single one stand-alone scattering matrix.

3. Maeda (1985) defined numerical swamping as the annihilation of linear independence among supposedly independent solutions. To address this challenge and to obtain a comprehensive set of special solutions that are linearly independent, he utilized a technique developed by Inoue and Horowitz (1966).

In radiative transfer, it is also necessary to solve a linear system of ordinary differential equations with constant coefficients. This arises by transforming the continuous dependence of radiance on direction directions into a dependence on a discrete set of direction. The standard methods for solving the linear system of ordinary differential equations are the discrete ordinate method (Stamnes, 1986; Wick, 1943; Chandrasekhar, 1950; Stamnes and Swanson, 1981) and the matrix operator method (Plass et al., 1973; Kattawar et al., 1973; van de Hulst, 1963; Nakajima and Tanaka, 1986). In the classical discrete ordinate method, the solution to these equations is expressed as a linear combination of characteristic solutions of the discretized problem. Conversely, the matrix operator method focuses on numerical computations of reflection and transmission matrices. Both methods can be formulated using the matrix exponential formalism. In the framework of the so called discrete ordinate method with matrix exponential, Doicu and Trautmann (2009a, b) designed stable numerical algorithms for computing the radiance field in a multi-layered atmosphere, while in the framework of the matrix operator method with matrix exponential, Budak et al. (2011, 2012) provided explicit and stable representations for the reflection and transmission matrices. A consistent overview of the matrix exponential description of radiative transfer can be found in (Efremenko et al., 2017; Efremenko and Kokhanovsky, 2021)Efremenko et al. (2017).

The main purpose of this article is to apply radiative transfer techniques to solve the linearized gravity-wave equations. As a prototype, we will consider the equations that describe gravity waves in the ionosphere, and that include viscosity, thermal conduction, and ion drag. In principle, a full wave model for the ionosphere comprises the hydrodynamic equations for the neutral atmosphere and the ionospheric equations. These two sets of equations are coupled through the ion drag, and should be solved together. However, in order to simplify the analysis, we will decouple the two sets of equations by employing an approximationwhich is due to Klostermeyer (1972). This approximation, which states that the ion velocity can be estimated by the air-dragged ion velocity, allows us to solve the neutral-atmosphere equations separatelyadopting a fast field-aligned diffusion approximation, which may be viewed as a generalization of an approximation originally proposed by Klostermeyer (1972).

Our paper is organized as follows. In Section 2we review the linearized neutral-atmosphere and ionospheric equations and describe the method of Klostermeyer for decoupling these two sets of equations. In Section 3 we , we present the derivation of the matrix exponential solution of the linearized equations, while in Section 4 we describe Section 3 describes stable numerical methods for computing this solution . Section 5the amplitudes of the characteristic solution in a stratified atmosphere. Section 4, which is completely largely inspired by the works of Knight et al. (2022, 2019, 2021), addresses Knight et al. (2019, 2021, 2022, 2024), addresses the computation of the perturbed quantities for both harmonic and non-harmonic source functions, that is, for single-frequency waves and time-dependent boundary conditions (source functions) when the linearized equations are solved in the frequency domain. The concept of causality , rigorously addressed in (Knight et al., 2022, 2019, 2021), will also be wave packets. The concepts of causality and the imaginary frequency shift, which are rigorously treated in Knight et al. (2019, 2021, 2022), are also briefly discussed. Aspects of the numerical implementation are addressed in Section 5, and representative simulation results are presented in Section 6. Additional theoretical issues are discussed in the appendices. Appendix A contains the linearized hydrodynamic equations for the neutral atmosphere and the derivation of the underlying system of differential equations. Appendix B outlines the linearized ionospheric equations and discusses the assumptions employed to decouple the hydrodynamic and ionospheric systems. Appendix C describes methods for computing grid-point values of the state vector in a stratified atmosphere. Appendix D addresses several implementation issues, including a practical, albeit heuristic, approach for determining the imaginary frequency shift.

2 Linearized Matrix exponential solution of the linearized equations

To design a full wave model for the ionosphere, we use the hydrodynamic equations for the neutral atmosphere and the ionospheric equations. In a linearized (perturbation) method, a quantity f is expressed as

$$f = f_0 + f', \tag{1}$$

where f_0 and f' are the unperturbed (background) and the perturbed quantity, respectively. The perturbations are assumed to be small so that it is justified to neglect all terms of higher than the first order.

Concretely, we need to solve solve the linearized hydrodynamic equations for the neutral atmosphere (e.g., (Midgley and Liemohn, 1966; Volland, 1969a)) together with the linearized ion continuity and momentum equations(Huba et al., 2000) and respectively, and the linearized electrically neutral equation

from TT to the check of above equations:a) For eq. (??): See Klostermeyer (1972), eqs. (7), (9) including the ion drag term $\nu(\mathbf{u}-\mathbf{u}_i)$, and by approximating $\mathbf{u}_i = (\mathbf{u}\cdot\widehat{\mathbf{b}})\widehat{\mathbf{b}}$. The resulting equation in Klostermeyer (1972) therefore is: The same expression can be found in Klostermeyer (1980), eq. (3), and Midgley and Liemohn (1966), eq. (2) – but there without ion drag force.

b) For the temperature equation, we find from Volland JAtmTerrPhys, 31, 1969, eq. (2): where $\beta = \sum_i \sum_k \sigma_{ik} \frac{\partial u_i}{\partial x_k}$ is the viscous heating, κ is the coefficient of heat conductivity (identical with our λ), and η is the coefficient of molecular viscosity. Volland defines the σ_{ik} as follows: $\sigma_{ik} = -\eta\left(\frac{\partial u_i}{\partial x_k} + \frac{\partial u_k}{\partial x_i} - \frac{2}{3}\delta_{ik}\nabla\cdot\mathbf{u}\right)$ Note that in other references σ_{ik} on its right side does not include the minus sign. In our eq. (10), we have the definition $P_{\mathrm{ID}} = \nu\rho(\mathbf{u}-\mathbf{u}_i)\cdot(\mathbf{u}-\mathbf{u}_i)$. In taking the linearization of the previous temperature evolution equation, we find term by term our expression eq. (??).

c) Our eq. (5) follows directly from the linearization of the equation of state $p = \rho\frac{R}{M}T$ for an ideal gas where R is the universal gas constant and M is the molar mass of the gas.

d) For (??): Please give a hint where this equation can be found. For example, it is not clear why the pressure p_i for the ion gas and the pressure p_e for the electron gas appears in this equation; actually, the sum of both pressures seems to appear, but not involving the pressure p_n of the neutral gas component. Huba and Joyce (2014), see , refer to a similar but not identical equation. Also Huba et al. (2000), JGR, 105, pp. 23035-23053 give an expression. Or is the reference from the SAMI2 or SAMI3 model? However, for the latter model developments, I could not find a full description of all equations to be solved.

In the neutral-atmosphere equations, ρ is the density, p the pressure, T the temperature, $\mathbf{u}$ the velocity, $\mathbf{g}$ the gravitational acceleration, c_{v} the specific heat at constant volume, λ the coefficient of thermal conductivity, $\overline{\boldsymbol{\sigma}}$ the viscous stress tensor, the ion-drag force per unit volume, the rate of work done by the ion drag force per unit volume, and ν_{ni} the neutral–ion collision frequency (the collision frequency between a neutral particle and all kind of ions). In the hydrodynamic equations, we neglected the Coriolis force, because we are interested in gravity waves with an angular frequency $\omega > 2\Omega$, where $\Omega = 7.3\times10^{-5}$ s^{-1} is the Earth's angular velocity. In the ionospheric equations, n_i, $\mathbf{u}_i$, $p_i = n_iKT_i$, T_i, and m_i are the number density, velocity, partial pressure, temperature and mass of ion i, respectively, n_e, $\mathbf{u}_e$, $p_e = n_eKT_e$, T_e, and m_e are the number density, velocity, partial pressure, temperature and mass of electrons, respectively, $\mathbf{B}$ is the magnetic induction, e the electron charge, c the speed of light, K the Boltzmann constant, P_i and $\mathcal{L}_i$ the ionization production rate and the loss rate due to chemical processes of ion i, respectively, ν_{in} the collision frequency between the ion i and the neutral n, ν_{ij} the collision frequency between the ions i and j, and $\nu_{\mathrm{in}} = \sum_n \nu_{i,n}$. Note that in the ionosphere, the neutral-ion collision frequency ν_{ni} is computed under the assumption that atomic oxygen O and O$^+$-ions are the main neutral and ionic constituents, that is, for $n = \mathrm{O}$ and $i = \mathrm{O}^+$. Also note that Eq. is in fact a linear combination of the ion and electron momentum equations (Huba et al., 2000).

. The linearized neutral-atmosphere and ionospheric equations are coupled through the ion-drag perturbations $\mathbf{f}'_{\mathrm{ID}}$ and P'_{ID}, given respectively, by where the neutral-ion collision frequency ν_{ni} depends on the ion number density n_i according to the relation $\nu_{ni} = (n_i/n_n)\nu_{in}$.

Klostermeyer (1972) proposed a simple method for solving the coupled systems of equations under the assumption that the ion velocity can be approximated by the air-dragged ion velocity, i.e., where $\widehat{\mathbf{b}}$ is a unit vector in the direction of the magnetic induction. Assumption (??), which was employed, for example, before by Volland (1969a) and later by Francis (1973), implies $\mathbf{u}_{0i} = (\mathbf{u}_0\cdot\widehat{\mathbf{b}})\widehat{\mathbf{b}}$ and $\mathbf{u}'_i = (\mathbf{u}'\cdot\widehat{\mathbf{b}})\widehat{\mathbf{b}}$ (a perturbation of $\widehat{\mathbf{b}}$ in the direction of the magnetic field is not considered), and eliminates the need of using the ion momentum equation (??). With $\mathbf{u}_i$ as in Eq. (??), Eqs. (??) and (??) become and their perturbed versions are, In fact, Klostermeyer solved the linearized neutral-atmosphere equations (??)–(??) together with the following ion continuity equation: where, as already mentioned, $\mathbf{u}_i' = (\mathbf{u}' \cdot \widehat{\mathbf{b}})\widehat{\mathbf{b}}$. The ion continuity equation (??) is a simplified version of Eq. (??), in which the term $\nabla \cdot (n_i' \mathbf{u}_{0i})$, as well as, the perturbed production and loss terms are neglected. Neglecting the term $\nabla \cdot (n_i' \mathbf{u}_{0i})$, where $\mathbf{u}_{0i} = (\mathbf{u}_0 \cdot \widehat{\mathbf{b}})\widehat{\mathbf{b}}$, means that in the continuity equation, the wind (background) velocity $\mathbf{u}_0$ is omitted. However, in Klostermeyer's formalism, this assumption is then relaxed, i.e., the ion-drag perturbations $\mathbf{f}_{\mathrm{ID}}'$ and P_{ID}' are computed by means of Eqs. (??)–(??), which still include the wind velocity. Adopting this solution method, we (i) use Eq. (??) to express n_i' in terms of $\mathbf{u}'$, (ii) assume that in the ionosphere, the atomic oxygen O and O^+-ions are the main neutral and ionic constituents, and compute ν_{0ni} and ν_{ni}' by means of the relations (Stubbe, 1968; Shibata, 1983) Here, I suggest that we make reference to physical units. Looking in Klostermeyer (1972), eq. (2), we find: Alternatively, from Figueroa and Hernandez (JAtmTerrPhys, 50, 1988), we have: As a consequence, the collision frequency then is in units of s^{-1}. Note that Figueroa and Hernandez define as reference temperature $T_r = (T_n + T_i)/2$. respectively, (iii) substitute these results into Eqs. (??) and (??), and (iv) solve the neutral-atmosphere equations (??)–(??) together with Eqs. (??)–(??) for $\mathbf{u}'$, ρ', p' and T'.

Some comments can be made here.

1. Shibata (1983) used a more precise representation for the ion velocity, that is, $\mathbf{u}_i = \mathbf{u}_{\mathrm{w}} + \mathbf{u}_{\mathrm{d}i} = (\mathbf{u} \cdot \widehat{\mathbf{b}})\widehat{\mathbf{b}} + \mathbf{u}_{\mathrm{d}i}$, where is the plasma diffusion velocity, $D_{\mathrm{a}} = 2KT/(m_i \nu_{in})$ the ambipolar diffusion coefficient, and b a coordinate along the magnetic induction. Under the assumption $T_i \approx T$, a perturbed version of Eq. (??) is solved together with (i) the ion continuity equation (??), in which the production and loss terms are neglected, and (ii) the linearized neutral-atmosphere equations (??)–(??). In the literature with one atomic gas O and one ion O^+, one often finds the reduced temperature $T_r = (T_n + T_i)/2$. If both temperatures are practically the same, we can set $T_i \approx T \approx T_n$, i.e. we do not allow for any differences in the temperatures of both species. I think, this would also imply, that the ion mass and the atomic (neutral) mass are practically identical, which is the case (since they are only one electron's mass apart from each other).

2. In the model that we designed, we use the assumption $\mathbf{u}_i = (\mathbf{u} \cdot \widehat{\mathbf{b}})\widehat{\mathbf{b}}$ and solve the neutral-atmosphere equations (??)–(??) as in Klostermeyer's model. A next step could be the one in which we revise the assumption on the ion velocity and use the wave-induced perturbations (obtained by solving Eqs. (??)–(??)) to compute the perturbed ion density n_i' and the perturbed ion velocity along the magnetic field line $u_{\mathrm{B}}' = \mathbf{u}_i' \cdot \widehat{\mathbf{b}}$ from the ionospheric equations (??)–(??). This topic will be discussed in more detail in the Conclusions.

3 General solution

The linearized neutral-atmosphere equations (??)–(??) are solved equations are solved under the following assumptions:

A1. The geographic and geomagnetic coordinates are identical.

A2. The wave propagates in the meridional direction plane (the x-coordinate is positive southwards while the z-coordinate is positive upwards), i.e.,

$$f = f(x, z, t). \tag{2}$$

A3. All background (unperturbed) quantities vary only in the z-direction, i.e.,

$$f_0 = f_0(z), \tag{3}$$

while all perturbations vary harmonically in time and the x-direction, i.e.,

$$f' = f'(x,z,t) = \overline{f}(z)\mathrm{e}^{\mathrm{j}(\omega t - k_{\mathrm{x}} x)}, \tag{4}$$

where ω is the angular frequency and k_{x} the horizontal wavenumber. Note that in some gravity-wave studies, the opposite sign convention for frequency and horizontal wavenumber is used (e.g. Knight et al. (2025)).

The linearization model is described in Appendix A. It provides a general framework that accounts for the altitude derivatives of the background velocity u_0, temperature T_0, density scale height H_ρ, and dynamic viscosity μ_0. Apart from the ion-drag terms, the formulation follows a structure similar to those employed by Vadas and Nicolls (2012) and Knight et al. (2024).

The computation of the ion-drag force and ion-drag heating is presented in Appendix B. The ion-drag terms are introduced in an approximate manner, with the explicit aim of decoupling the hydrodynamic and ion equation systems. To this end, we adopt the following assumptions:

A4.B1. **The atmosphere consists of a number of layers. In each layer, the dynamic (molecular) viscosity μ and the thermal conductivity λ are computed as (Dalgarno and Smith, 1962)**

In the previous equation I have corrected the power in the exponent (-7 to -4) of the right equation; and both equations are "marked" (all in MKS units). The exponent 10^{-4} in the expression for λ follows from Dalgarno and Smith (PlanetSpaceSci 9, 1962), valid for $100\,\mathrm{K} < T < 2000\,\mathrm{K}$: Thermal conductivity:$\lambda = 67.1\,T^{0.71}$ erg/(K cm s) $= 67.1 \times 10^{-7} \times 10^{2} T^{0.71}$ In Appendix ?? it is shown that under the above assumptions, the The linearized equations lead to a linear system of ordinary differential equations, written in matrix form as

$$\frac{1}{k_{\mathrm{x}}}\frac{\mathrm{d}\mathbf{e}}{\mathrm{d}z} = \mathrm{A}\mathbf{e}, \tag{5}$$

where

$$\mathbf{e} = [\widehat{u}, \widehat{w}, \widehat{T}, \widehat{\mathcal{U}}, \widehat{\mathcal{W}}, \widehat{\mathcal{T}}]^{\mathrm{T}} \tag{6}$$

is the unknown solution state vector, and A is the propagation matrix with altitude independent elements (whose expressions follow from Eqs. (??A41)–(??) of ??A46) of Appendix A). In general, the unknowns (the hat quantities in Eq. (6)) are defined through the relation

$$\overline{f}(z) = C(z)\widehat{f}(z), \tag{7}$$

where $\overline{f}$ is defined by Eq. (A324), and C is a known quantity that ensures that $\widehat{f}$ is dimensionless and that may or may not depend on altitude (here, we indicate that C depends depend on z). Specifically, for the background velocity $\mathbf{u}_0 = (u_0, 0, 0)$and , and the perturbed velocity $\mathbf{u}' = (u', 0, w')$, we have (cf. Eqs. (??) –(??) of ??) A39) and (A40) of Appendix A)

$$\overline{u}(z) = \frac{\omega_0}{k_{\mathrm{x}}}\widehat{u}(z), \tag{8}$$

$$\overline{w}(z) = \frac{\omega_0}{k_{\mathrm{x}}}\widehat{w}(z), \tag{9}$$

$$\overline{T}(z) = T_0(z)\widehat{T}(z), \tag{10}$$

and

$$\widehat{\mathcal{U}} = \frac{\mathrm{d}\widehat{u}}{\mathrm{d}z},\ \widehat{\mathcal{W}} = \frac{\mathrm{d}\widehat{w}}{\mathrm{d}z},\ \widehat{\mathcal{T}} = \frac{\mathrm{d}\widehat{T}}{\mathrm{d}z}.$$

where ω_0 is a reference frequency, and the dimensionless parameters η and ν are given by Eq. (**??**) of **??**. .

If $(\lambda_n, \mathbf{v}_n)$ is an eigenpair of the matrix A, i.e., $\mathrm{A}\mathbf{v}_n = \lambda_n \mathbf{v}_n$ for $n = 1, \ldots, N$, where $N = \dim(\mathbf{e})$, the general solution of Eq. (5) is a linear combination of the characteristic solutions $\exp(k_\mathrm{x}\lambda_n z)\mathbf{v}_n$$\exp(k_\mathrm{x}\lambda_n z)\mathbf{v}_n$, that is,

$$\begin{aligned}
\mathbf{e}(z) &= \sum_{n=1}^{N} a_n \mathrm{e}^{k_\mathrm{x}\lambda_n z}\mathbf{v}_n \\
&= [\mathbf{v}_1, \ldots \mathbf{v}_N] \begin{bmatrix} \mathrm{e}^{k_\mathrm{x}\lambda_1 z} & \cdots & 0 \\ \vdots & \ddots & \vdots \\ 0 & \cdots & \mathrm{e}^{k_\mathrm{x}\lambda_N z} \end{bmatrix} \begin{bmatrix} a_1 \\ \vdots \\ a_N \end{bmatrix} \\
&= \mathrm{V}\mathrm{diag}[\mathrm{e}^{k_\mathrm{x}\lambda_n z}]\mathbf{a},
\end{aligned} \tag{11}$$

where

$$\mathrm{V} = [\mathbf{v}_1, \ldots, \mathbf{v}_N],\ \mathrm{diag}[\mathrm{e}^{k_\mathrm{x}\lambda_n z}] = \begin{bmatrix} \mathrm{e}^{k_\mathrm{x}\lambda_1 z} & \cdots & 0 \\ \vdots & \ddots & \vdots \\ 0 & \cdots & \mathrm{e}^{k_\mathrm{x}\lambda_N z} \end{bmatrix}, \tag{12}$$

and $\mathbf{a} = [a_1, \ldots, a_N]^T$$\mathbf{a} = [a_1, \ldots, a_N]^\mathrm{T}$. At $z = 0$, we have $\mathbf{e}(0) = \mathrm{V}\mathbf{a}$; thus,

$$\mathbf{a} = \mathrm{V}^{-1}\mathbf{e}(0), \tag{13}$$

implying (cf. Eq. (11)),

$$\mathbf{e}(z) = \mathrm{V}\mathrm{diag}[\mathrm{e}^{k_\mathrm{x}\lambda_n z}]\mathrm{V}^{-1}\mathbf{e}(0) = \mathrm{e}^{k_\mathrm{x}\mathrm{A}z}\mathbf{e}(0), \tag{14}$$

and conversely,

$$\mathbf{e}(0) = \mathrm{V}\mathrm{diag}[\mathrm{e}^{-k_\mathrm{x}\lambda_n z}]\mathrm{V}^{-1}\mathbf{e}(z) = \mathrm{e}^{-k_\mathrm{x}\mathrm{A}z}\mathbf{e}(z). \tag{15}$$

From the theory of gravity waves within an isothermal, nondissipative atmosphere, it is generally known that the amplitude of an ascending mode increases like $\exp[z/(2H_\mathrm{a})]$modes increases like $\exp[z/(2H_\mathrm{a})]$, where H_a is the atmospheric scale height (Hines, 1960). This is necessary to keep the wave energy constant in an atmosphere where the pressure decreases exponentially with height. In this regard, we define the vertical wavenumber $k_{\mathrm{z}n}$ $k_{\mathrm{z}n}$ through the relation

$$\mathrm{diag}[\mathrm{e}^{k_\mathrm{x}\lambda_n z}] = \mathrm{diag}[\mathrm{e}^{z/(2H_\mathrm{a})}\mathrm{e}^{-\mathrm{j}k_{\mathrm{z}n}z}], \tag{16}$$

yielding

$$\lambda_n = -\frac{\mathrm{j}}{k_\mathrm{x}}k_{\mathrm{z}n} + \frac{1}{2}\alpha, \tag{17}$$

and conversely,

$$k_{zn} = \mathrm{j}k_{\mathrm{x}}\left(\lambda_n - \frac{1}{2}\alpha\right), \tag{18}$$

where $\alpha = 1/(k_{\mathrm{x}}H_{\mathrm{a}})\alpha = 1/(k_{\mathrm{x}}H_{\mathrm{a}})$. The characteristic equation $\det(\mathrm{A} - \lambda \mathrm{I}_N) = 0$ has $N = 6$ solutions. As shown in ??, in the case of an isothermal, homogeneous, and windless atmosphere, these solutions appear Appendix A, for a constant kinematic viscosity the solutions occur in pairs and correspond to (i) ascending and descending gravity-wave modes, (ii) ascending and descending viscosity-wave modes, and (iii) ascending and descending thermal conduction-wave modes . This thermal-conduction wave modes (Volland, 1969b; Francis, 1973). In that appendix, this pairing is explicitly demonstrated by deriving the dispersion relation for the special case of an isothermal (constant background temperature), homogeneous (constant kinematic viscosity), and windless atmosphere without ion drag. This solution classification is made according to the imaginary part of the vertical wavenumber $k_{zn}k_{zn}$. In the more realistic case of a constant background dynamic viscosity, it is generally not possible to define ascending and descending modes as corresponding pairs . (see Eq. (A52) in Appendix A). However, in our model we will use the same rule as in the case of an isothermal and a homogeneous atmosphere, even though the traditional concept of classifying waves in pairs is no longer applicable. Specifically, we compute k_{zn} k_{zn} for $n = 1, \ldots, N$ by means of Eq. (??18), and order the set $\{k_{zn}\}_{n=1}^{N}\{k_{zn}\}_{n=1}^{N}$, and accordingly, $\{\lambda_n\}_{n=1}^{N}$, such that

$$\mathrm{Im}(k_{z3}) < \mathrm{Im}(k_{z2}) < \mathrm{Im}(k_{z1}) < \mathrm{Im}(k_{z4}) < \mathrm{Im}(k_{z5}) < \mathrm{Im}(k_{z6}). \tag{19}$$

By convention, (i) the pairs $(k_{z1} = k_{z1}^{+}, \lambda_1 = \lambda_1^{+})$ and $(k_{z4} = k_{z1}^{-}, \lambda_4 = \lambda_1^{-})$ $(k_{z1} = k_{z1}^{+}, \lambda_1 = \lambda_1^{+})$ and $(k_{z4} = k_{z1}^{-}, \lambda_4 = \lambda_1^{-})$ will correspond to ascending and descending gravity-wave modes, respectively, (ii) the pairs $(k_{z2} = k_{z2}^{+}, \lambda_2 = \lambda_2^{+})$ and $(k_{z5} = k_{z2}^{-}, \lambda_5 = \lambda_2^{-})$ $(k_{z2} = k_{z2}^{+}, \lambda_2 = \lambda_2^{+})$ and $(k_{z5} = k_{z2}^{-}, \lambda_5 = \lambda_2^{-})$ to ascending and descending viscosity-wave modes, respectively, and (iii) the pairs $(k_{z3} = k_{z3}^{+}, \lambda_3 = \lambda_3^{+})$ and $(k_{z6} = k_{z3}^{-}, \lambda_6 = \lambda_3^{-})$ $(k_{z3} = k_{z3}^{+}, \lambda_3 = \lambda_3^{+})$ and $(k_{z6} = k_{z3}^{-}, \lambda_6 = \lambda_3^{-})$ to ascending and descending thermal conduction-wave modes, respectively. Thus, the vertical wavenumber is an auxiliary quantity that is used only to identify the different modes. According to the notation introduced above, $\{\lambda_m^{+}\}_{m=1}^{M}$, where $M = N/2$ is the number of modes, is the set of eigenvalues defining ascending modes, and $\{\lambda_m^{-}\}_{m=1}^{M}$ is the set of eigenvalues defining descending modes. Because $\mathrm{Re}(\lambda_n) = \mathrm{Im}(k_{zn})/k_{\mathrm{x}} + \alpha/2\mathrm{Re}(\lambda_n) = \mathrm{Im}(k_{zn})/k_{\mathrm{x}} + \alpha/2$, it is obvious that we can renounce on the put aside the concept of vertical wavenumber when identifying the different wave modes. We can simply order the set $\{\lambda_n\}_{n=1}^{N}$, such that

$$\mathrm{Re}(\lambda_3) < \mathrm{Re}(\lambda_2) < \mathrm{Re}(\lambda_1) < \mathrm{Re}(\lambda_4) < \mathrm{Re}(\lambda_5) < \mathrm{Re}(\lambda_6), \tag{20}$$

and use the same classification rule as above. Knight et al. (2019) employed this approach, providing a more intuitive explanation compared to the analogy with an isothermal and homogeneous atmosphere: For A commonly cited interpretation of condition (20) is that, for increasing z, the exponential term $\exp(k_{\mathrm{x}}\lambda_n z)$ $\exp(k_{\mathrm{x}}\lambda_n z)$ will tend to be damped more for ascending modes than for descending modes; conversely, for decreasing z, the roles of ascending and descending modes are reversed. However, such a classification of upgoing and downgoing roots (e.g., Volland (1969b) and related works) was primarily heuristic and lacked a rigorous theoretical justification. By contrast, the approach of Knight et al. (2019), which is discussed in Section 4, introduces additional constraints beyond condition (20) that are explicitly related to causality and is therefore grounded in theoretical considerations rather than heuristic arguments.

To highlight the different wave modes, we organize the solution state vector $\mathbf{e}(z)$ as

$$
\begin{aligned}
\mathbf{e}(z) &= \mathbf{e}_+(z) + \mathbf{e}_-(z) \\
&= \left(\sum_{m=1}^{M} a_m^+ \mathrm{e}^{k_x \lambda_m^+ z} \mathbf{v}_m^+ \right) + \left(\sum_{m=1}^{M} a_m^- \mathrm{e}^{k_x \lambda_m^- z} \mathbf{v}_m^- \right) \\
&= [\mathrm{V}_+, \mathrm{V}_-] \begin{bmatrix} \mathrm{diag}[\mathrm{e}^{k_x \lambda_m^+ z}] & 0_M \\ 0_M & \mathrm{diag}[\mathrm{e}^{k_x \lambda_m^- z}] \end{bmatrix} \begin{bmatrix} \mathbf{a}_+ \\ \mathbf{a}_- \end{bmatrix},
\end{aligned} \tag{21}
$$

where the eigenvector $\mathbf{v}_m^\pm$ corresponds to the eigenvalue $\lambda_m^\pm$,

$$
\mathrm{V} = [\mathrm{V}_+, \mathrm{V}_-], \ \mathrm{V}_\pm = [\mathbf{v}_1^\pm, \ldots, \mathbf{v}_M^\pm], \tag{22}
$$

$$
\mathbf{a} = \begin{bmatrix} \mathbf{a}_+ \\ \mathbf{a}_- \end{bmatrix}, \ \mathbf{a}_\pm = \begin{bmatrix} a_1^\pm \\ \vdots \\ a_M^\pm \end{bmatrix}, \tag{23}
$$

and O_M 0_M is the zero matrix of dimension $M \times M$. Some useful relations are listed below

1. From Eq. (13), we find

$$
\mathbf{a}_+ = [\mathrm{I}_M, 0_M]\mathbf{a} = [\mathrm{I}_M, 0_M]\mathrm{V}^{-1}\mathbf{e}(0), \tag{24}
$$

$$
\mathbf{a}_- = [0_M, \mathrm{I}_M]\mathbf{a} = [0_M, \mathrm{I}_M]\mathrm{V}^{-1}\mathbf{e}(0), \tag{25}
$$

   where I_M is the identity matrix of dimension $M \times M$.

2. From Eq. (21), that is,

$$
\mathbf{e}_\pm(z) = \sum_{m=1}^{M} a_m^\pm \mathrm{e}^{k_x \lambda_m^\pm z} \mathbf{v}_m^\pm = \mathrm{V}_\pm \mathrm{diag}[\mathrm{e}^{k_x \lambda_m^\pm z}]\mathbf{a}_\pm, \tag{26}
$$

   we deduce that

$$
\mathbf{e}_\pm(0) = \mathrm{V}_\pm \mathbf{a}_\pm. \tag{27}
$$

3. From Eq. (14), we obtain

$$
\mathbf{e}_+(z) = \mathrm{T}_+ \mathbf{e}(0), \tag{28}
$$

   where

$$
\mathrm{T}_+ = \mathrm{V} \begin{bmatrix} \mathrm{diag}[\mathrm{e}^{k_x \lambda_m^+ z}] & 0_M \\ 0_M & 0_M \end{bmatrix} \mathrm{V}^{-1}, \tag{29}
$$

while from Eq. (15), we find

$$\mathbf{e}_{-}(0) = \mathrm{T}_{-}\mathbf{e}(z), \tag{30}$$

where

$$\mathrm{T}_{-} = \mathrm{V}\begin{bmatrix} 0_M & 0_M \\ 0_M & \mathrm{diag}[\mathrm{e}^{-k_x\lambda_m^{-}z}] \end{bmatrix}\mathrm{V}^{-1}. \tag{31}$$

3 Solution of the linearized equations for a stratified atmosphere

Consider an equidistant discretization of the atmosphere, i.e., $\widehat{z}_i = z_{\min} + (i-1)\Delta\widehat{z}$ for $i = 1,...,2L+1$. A layer l, where $l = 1,\ldots,L$ and L is the number of layers, is bounded from below and from above by the grid points $z_l = \widehat{z}_{2l-1}$ and $z_{l+1} = \widehat{z}_{2l+1}$, respectively, and its center is located at the grid point $\overline{z}_l = \widehat{z}_{2l}$. The atmosphere extends from $z_{\min} = z_1 = \widehat{z}_1$ to $z_{\max} = z_{L+1} = \widehat{z}_{2L+1} = z_{\min} + L(2\Delta\widehat{z})$. We adopt a nonstandard multilayer method (Klostermeyer, 1972)numerical multilayer method (Klostermeyer, 1972; Knight et al., 2022, 2019), and approximate the altitude dependent matrix A in each layer l by its value at the layer center, i.e., $\mathrm{A}_l = \mathrm{A}(\overline{z}_l)$. The eigenpairs of the propagation matrix A_l are denoted denote by $(\lambda_{nl}, \mathbf{v}_{nl})$ for $n = 1,\ldots,N$. The matrix differential equation (5) can be solved for either (i) in terms of the amplitudes $\mathbf{a}_l$, $l = 1,\ldots,L$ of the characteristic solutions, or (ii) the discrete in terms of the grid-point values $\mathbf{e}_l = \mathbf{e}(z_l)$, $l = 1,\ldots,L$ of the solution state vector $\mathbf{e}(z)$. In the following we present the method based on the amplitude of the characteristic solutions, whereas the second method is described in Appendix C.

3.1 Amplitudes of the characteristic solutions

In the layers l and $l+1$, the solutions are given by (cf. Eq. (11))

$$\mathbf{e}_l(z) = \mathrm{V}_l\mathrm{diag}[\mathrm{e}^{k_x\lambda_{nl}(z-z_l)}]\mathbf{a}_l,\ z_l \le z \le z_{l+1}, \tag{32}$$

and

$$\mathbf{e}_{l+1}(z) = \mathrm{V}_{l+1}\mathrm{diag}[\mathrm{e}^{k_x\lambda_{n,l+1}(z-z_{l+1})}]\mathbf{a}_{l+1},\ z_{l+1} \le z \le z_l, \tag{33}$$

respectively. The continuity condition at the interface $z = z_{l+1}$,

$$\mathbf{e}_l(z_{l+1}) = \mathbf{e}_{l+1}(z_{l+1}), \tag{34}$$

gives

$$\mathrm{V}_l^{-1}\mathrm{V}_{l+1}\mathbf{a}_{l+1} = \mathrm{diag}[\mathrm{e}^{k_x\lambda_{n,l}\Delta_l}]\mathbf{a}_l, \tag{35}$$

where $\Delta_l = z_{l+1} - z_l$. To obtain a stable system of equations, we define a scaling matrix S_l^1 with entries K_l^1 with entries

$$[\mathrm{K}_l^1]_{nn} = \begin{cases} \mathrm{e}^{-k_x\lambda_{nl}\Delta_l}, & \mathrm{Re}(\lambda_{nl}) > 0 \\ 1, & \mathrm{Re}(\lambda_{nl}) \le 0 \end{cases}, \tag{36}$$

and a scaling matrix S_l^0 by second scaling matrix K_l^0 by

$$\mathrm{K}_l^0 = \mathrm{K}_l^1 \mathrm{diag}[\mathrm{e}^{k_\mathrm{x}\lambda_{nl}\Delta_l}], \text{ i.e., } [\mathrm{K}_l^0]_{nn} = \begin{cases} 1, & \mathrm{Re}(\lambda_{nl}) > 0 \\ \\ \mathrm{e}^{k_\mathrm{x}\lambda_{nl}\Delta_l}, & \mathrm{Re}(\lambda_{nl}) \leq 0 \end{cases}. \tag{37}$$

Multiplying Eq. (35) from the left with S_l^1 gives K_l^1 yields the continuity equation

$$\mathbb{A}_{l,l+1}^1 \mathbf{a}_{l+1} - \mathbb{A}_{l,l+1}^0 \mathbf{a}_l = \mathbf{0}_{2M}, \; l = 1, ..., L-1, \tag{38}$$

where $\mathbf{0}_{2M}$ is the $2M$-dimensional zero vector, and

$$\mathbb{A}_{l,l+1}^1 = \mathrm{K}_l^1 (\mathrm{V}_l^{-1} \mathrm{V}_{l+1}), \tag{39}$$

$$\mathbb{A}_{l,l+1}^0 = \mathrm{K}_l^0. \tag{40}$$

The scaling matrices K_l^1 and K_l^0 prevent a possible blow-up of the exponential terms for $\mathrm{Re}(\lambda_{nl}) > 0$ and $\mathrm{Re}(\lambda_{nl}) \leq 0$, respectively. Such scaling techniques are standard in radiative transfer theory and are commonly used to obtain stable numerical algorithms for computing the radiance field in multilayered atmospheres (Doicu and Trautmann, 2009a, b).

Actually, we have $L-1$ continuity equations imposed at the levels $z_2, \ldots, z_L$ for the L unknowns $\mathbf{a}_1, \ldots, \mathbf{a}_L$. The two missing equations are obtained from the lower and upper boundary conditions.

1. At the lower boundary, i.e., at $z = z_1 (= z_{\min})$, we assume that only the ascending wave modes transport energy upward. In this regard, we impose that in the layer $l = 1$, we have $a_{1,l=1}^+ = s =$ finite, and that the rest of $a_{m,l=1}^+$ are zero, that is, $a_{m,l=1}^+ = 0$ for $m \neq 1$ (Klostermeyer, 1972). Note that $a_{1,l=1}^+$ is the amplitude of the ascending gravity-wave modes, while the condition $a_{m,l=1}^+ = 0$ for $m \neq 1$ means that the amplitudes of the ascending viscosity-wave and thermal conduction-wave modes are assumed to be zero. In this case, the boundary condition for ascending modes is

$$\mathbf{e}_{l=1}^+(z_1) = \begin{bmatrix} \widehat{u}_{l=1}^+(z_1) \\ \widehat{w}_{l=1}^+(z_1) \\ \widehat{T}_{l=1}^+(z_1) \\ \widehat{\mathcal{U}}_{l=1}^+(z_1) \\ \widehat{\mathcal{W}}_{l=1}^+(z_1) \\ \widehat{\mathcal{T}}_{l=1}^+(z_1) \end{bmatrix} = \sum_{m=1}^{M} a_{m,l=1}^+ \mathbf{v}_{m,l=1}^+ = s\mathbf{v}_{1,l=1}^+. \tag{41}$$

Excluding for the moment the scale factor s, we express the boundary condition for amplitudes,

$$\mathbf{a}_{l=1}^+ = \begin{bmatrix} a_{1,l=1}^+ \\ a_{2,l=1}^+ \\ \vdots \\ a_{M,l=1}^+ \end{bmatrix} = \mathbf{i}_1 \text{ with } \mathbf{i}_1 = \begin{bmatrix} 1 \\ 0 \\ \vdots \\ 0 \end{bmatrix}, \tag{42}$$

in matrix form as

$$[\mathrm{I}_M, 0_M]\mathbf{a}_1 = [\mathrm{I}_M, 0_M]\begin{bmatrix}\mathbf{a}_1^+\\ \mathbf{a}_1^-\end{bmatrix} = \mathbf{i}_1, \tag{43}$$

where in general, $\mathbf{a}_{l_0}^{\pm} = \mathbf{a}_{l=l_0}^{\pm}$, for $l_0 = 1, \ldots, L$. The boundary condition (41) is a modal (eigenvector-based) boundary condition, which imposes that the state at z_1 is exactly aligned with a chosen eigenmode. In this way, a pure normal mode is injected into the system.

2. A reasonable upper boundary condition is that there is no downgoing energy at great altitudes, so that the amplitudes of all descending wave modes must be zero at the upper boundary (Klostermeyer, 1972). In this regard, we impose $a_{m,l=L}^- = 0$ for all $m = 1, \ldots, M$, in which case, in the layer L, the boundary condition for descending modes is

$$\mathbf{e}_{l=L}^-(z) = \sum_{m=1}^{M} a_{m,l=L}^- \mathrm{e}^{k_x \lambda_{m,l=L}^- z} \mathbf{v}_{m,l=L}^- = \mathbf{0}_{2M} \tag{44}$$

$$\mathbf{e}_{l=L}^-(z) = \sum_{m=1}^{M} a_{m,l=L}^- \mathrm{e}^{k_x \lambda_{m,l=L}^- z} \mathbf{v}_{m,l=L}^- = \mathbf{0}_{2M} \tag{45}$$

for all $z_L \leq z \leq z_{L+1}$. In matrix form, the boundary condition for amplitudes

$$\mathbf{a}_{l=L}^- = \begin{bmatrix} a_{1,l=L}^- \\ a_{2,l=L}^- \\ \vdots \\ a_{M,l=L}^- \end{bmatrix} = \mathbf{0}_M \tag{46}$$

is written as

$$[0_M, \mathrm{I}_M]\mathbf{a}_L = [0_M, \mathrm{I}_M]\begin{bmatrix}\mathbf{a}_L^+\\ \mathbf{a}_L^-\end{bmatrix} = \mathbf{0}_M. \tag{47}$$

Comments.

1. The scaling matrices defined by Eqs. (36) and (37) do not take into account a classification of the wave modes as ascending and descending (as defined by Eq. (20)). Consequently, the continuity equations (38) do not account for this classification, and the only equations in which it is necessary to distinguish between ascending and descending modes are the boundary condition equations (43) and (47). From this point of view, the method is similar to finite-difference methods (Lindzen and Kuo, 1969; Hickey et al., 1998, 2009). For the continuity equations and the boundary condition equations to be consistent (for both to rely on a categorization of wave modes as ascending or descending), we may define the scaling matrices as and

2. Knight et al. (2022, 2019) specified the An alternative type of lower boundary condition was proposed by Knight et al. (2022, 2019). In this approach, the lower boundary condition for ascending modes is prescribed in terms of M values $b_{1,k}$, $k =$

$1,\ldots,M$, as according to (compare with Eq. (41))

$$\left[\frac{\mathrm{d}^{k-1}\mathbf{e}^{+}_{l=1}}{\mathrm{d}z^{k-1}}(z_1)\right]_q = b_{1,k},\ k=1,...,M, \tag{48}$$

where as before, s is a scale factor, and the notation $[\mathbf{x}]_q$ stands for denotes the qth component of the vector $\mathbf{x}$. In the present context, this refers to the first M components, corresponding to $\widehat{u}$ $(q=1)$, $\widehat{w}$ $(q=2)$, and $\widehat{T}$ $(q=3)$. In Eq. (48), k denotes the derivative order, and in the case $M=3$, we have explicitly,

$$\left[\mathbf{e}^{+}_{l=1}(z_1)\right]_q = b_{1,1},\ \left[\frac{\mathrm{d}\mathbf{e}^{+}_{l=1}}{\mathrm{d}z}(z_1)\right]_q = b_{1,2},\ \left[\frac{\mathrm{d}^2\mathbf{e}^{+}_{l=1}}{\mathrm{d}z^2}(z_1)\right]_q = b_{1,3}. \tag{49}$$

Note that Eq. (48) generalizes Eq. (2.19) in Knight et al. (2022), which is formulated for the first state variable rather than for an arbitrary state variable. Using the relations

$$\frac{\mathrm{d}^{k-1}\mathbf{e}^{+}_{l=1}}{\mathrm{d}z^{k-1}}(z_1) = \sum_{m=1}^{M} a^{+}_{m,l=1}(k_{\mathrm{x}}\lambda^{+}_{m,l=1})^{k-1}\mathbf{v}^{+}_{m,l=1},\ k=1,\ldots,M, \tag{50}$$

and

$$\left[\frac{\mathrm{d}^{k-1}\mathbf{e}^{+}_{l=1}}{\mathrm{d}z^{k-1}}(z_1)\right]_q = \widehat{\mathbf{i}}_q^{\mathrm{T}}\frac{\mathrm{d}^{k-1}\mathbf{e}^{+}_{l=1}}{\mathrm{d}z^{k-1}}(z_1) = \sum_{m=1}^{M} a^{+}_{m,l=1}(k_{\mathrm{x}}\lambda^{+}_{m,l=1})^{k-1}\widehat{\mathbf{i}}_q^{\mathrm{T}}\mathbf{v}^{+}_{m,l=1}, \tag{51}$$

where $\widehat{\mathbf{i}}_q$ is a $2M$-dimensional vector with components (compare with Eq. (42))

$$[\widehat{\mathbf{i}}_q]_k = \begin{cases} 1,\ k=q \\ 0,\ k\neq q \end{cases},\ k=1,\ldots,2M, \tag{52}$$

we find

$$\sum_{m=1}^{M}[\mathsf{B}]_{mk}a^{+}_{m,l=1} = b_{1,k},\ k=1,...M, \tag{53}$$

where A B is a matrix with entries

$$[\mathsf{B}]_{mk} = (k_{\mathrm{x}}\lambda^{+}_{m,l=1})^{k-1}\widehat{\mathbf{i}}_q^{\mathrm{T}}\mathbf{v}^{+}_{m,l=1},\ m,k=1,\ldots,M. \tag{54}$$

Setting $\mathbf{b}_1=[b_{1,1},\ldots,b_{1,M}]^T$, and omitting the scale factor s, $\mathbf{b}_1=[b_{1,1},\ldots,b_{1,M}]^{\mathrm{T}}$, we consider the boundary condition for amplitudes

$$\mathbf{a}_1^{+} = \mathsf{B}^{-1}\mathbf{b}_1, \tag{55}$$

that is (compare with Eq. (43))

$$[\mathrm{I}_M, 0_M]\mathbf{a}_1 = \mathsf{B}^{-1}\mathbf{b}_1. \tag{56}$$

For the choice $b_{1,k} = 0$ with $k \geq 2$, the first component of the boundary-value vector $\mathbf{b}_1$ can be identified with the scale factor s, that is, $s = b_{1,1}$. Consequently, for a unit scale factor and $M = 3$, we have $\mathbf{b}_1 = [1, 0, 0]^{\mathrm{T}}$. The boundary condition (49) is a localized condition that prescribes the value of a single state variable while enforcing vanishing slope and curvature at the boundary. It effectively acts as an external driver applied to one variable and is appropriate for non-harmonic source functions. Note that this form of the lower boundary condition is used in the statement of Theorem 1 in Knight et al. (2019). For causality considerations, boundary conditions must be expressed in terms of state variables rather than modal amplitudes, since modes are defined in the frequency domain.

3. The eigenvectors are not uniquely defined and may be scaled by an arbitrary nonzero complex factor. When the LAPACK routine ZGEEV is used, the eigenvectors are returned with a built-in normalization, namely unit Euclidean norm together with a fixed phase convention. In the present work, we follow Knight et al. (2022, 2019) and apply a component-wise normalization, i.e.,

$$[\mathbf{v}_n]_j = \frac{1}{|[\mathbf{v}_n]_q|}[\mathbf{v}_n]_j, \; j = 1, \ldots, N,$$

in which each eigenvector is rescaled such that a selected reference component has unit magnitude ($|[\mathbf{v}_n]_q| = 1$). This reference component is chosen to correspond to a boundary value, thereby fixing the overall amplitude of the eigenmode in a manner consistent with the imposed boundary conditions.

Starting from the continuity equation (38), we will determine the amplitudes $\mathbf{a}_l$ by using two solution methods, namely, (i) the so-called global matrix method with matrix exponential and (ii) the scattering matrix method.

3.0.1 Global matrix method with matrix exponential

3.1 Global matrix method with matrix exponential

The continuity equations (38), and the boundary conditions (43) and (47) for a unit scale factor, are assembled into a system of equations for the stratified atmosphere, i.e.,

$$\mathbb{A}\mathbf{a} = \mathbf{b}, \tag{57}$$

where

$$
\mathbb{A}=\begin{bmatrix} [0_M, \mathrm{I}_M] & 0 & \dots & 0 & 0 \\ \mathbb{A}^1_{L-1,L} & -\mathbb{A}^0_{L-1,L} & \dots & 0 & 0 \\ \vdots & \vdots & \ddots & \vdots & \vdots \\ 0 & 0 & \dots & \mathbb{A}^1_{12} & -\mathbb{A}^0_{12} \\ 0 & 0 & \dots & 0 & [\mathrm{I}_M, 0_M] \end{bmatrix}, \tag{58}
$$

$$
\mathbf{a}=\begin{bmatrix} \mathbf{a}_L \\ \mathbf{a}_{L-1} \\ \vdots \\ \mathbf{a}_2 \\ \mathbf{a}_1 \end{bmatrix}, \text{ and } \mathbf{b}=\begin{bmatrix} \mathbf{0}_M \\ \mathbf{0}_{2M} \\ \vdots \\ \mathbf{0}_{2M} \\ \mathbf{i}_1 \end{bmatrix}. \tag{59}
$$

For the lower boundary condition (56), $\mathbf{i}_1$ in Eq. (59) should be replaced by $\mathrm{A}^{-1}\mathbf{b}_1 \mathrm{B}^{-1}\mathbf{b}_1$, where, for a unit scale factor, $\mathbf{b}_1=[1,0,0]^{\mathrm{T}}$. The matrix $\mathbb{A}$ has $3M-1$ sub- and super-diagonals and it can be compressed into band-storage and inverted using standard methods. From Eq. (58), we see that the scale factor s determines the solution, and can be interpreted as a source term. For this reason, in Eq. (57) we were more precise and showed that the vector of amplitudes depends on the source term s. In what follows, when we want to show that a quantity depends on the source term we will use the index s; when the index s is omitted, it will be understood that $s=1$ (according to this convention, $\mathbf{e}^{+}_{l=1}$ in Eqs. (41) and (48) should also depend on the index s). superdiagonals (excluding the main diagonal) and can therefore be stored in banded form and treated using standard band-matrix techniques. To solve the resulting banded system of linear equations, we employed the LAPACK routines ZGBTRF and ZGBTRS. The routine ZGBTRF performs an LU factorization with partial pivoting of the complex band matrix, and ZGBTRS subsequently uses this factorization to solve the linear system for the prescribed right-hand side. In this approach, the inverse of the full system matrix is not computed explicitly, which improves the computational efficiency.

After solving Eq. (57), we compute the solution state vector as

$$
\mathbf{e}_l=\mathbf{e}(z_l)=\begin{bmatrix} \widehat{u}(z_l) \\ \widehat{w}(z_l) \\ \widehat{T}(z_l) \\ \widehat{\mathcal{U}}(z_l) \\ \widehat{\mathcal{W}}(z_l) \\ \widehat{\mathcal{T}}(z_l) \end{bmatrix}=\mathrm{V}_l\mathbf{a}_l,\ l=1,\dots,L, \tag{60}
$$

and the wave amplitudes by means of the relation

$$
\overline{f}(z)=C(z)\widehat{f}(z), \tag{61}
$$

where f stands for u, w, p, and T. The ascending and descending solution modes are computed by using Eq. (27), that is,

$$
\mathbf{e}^{\pm}_l=\mathrm{V}^{\pm}_l\mathbf{a}^{\pm}_l, l=1,\dots,L. \tag{62}
$$

According to the basic requirement of a linearization method, we can compute s by imposing that the perturbed quantities are a small fraction of their unperturbed values. For example, we can impose, or where δ_{T} and δ_{u} are prescribed tolerances. Alternatively, we can impose a value for the vertical energy flux at the lowest level $z_1 = z_{\min}$ as in (Hickey and Cole, 1988). In Section **??** s will be assumed to be some time dependent source function as in (Knight et al., 2022, 2019, 2021).

3.2 Scattering matrix method

3.2.1 Scattering matrix method

We consider the continuity equation (38) and partition the matrices $\mathbb{A}^{0(1)}_{l,l+1}$ as $\mathbb{A}^{i}_{l,l+1}$, with $i = 0, 1$, as

$$\mathbb{A}^{i}_{l,l+1} = \begin{bmatrix} [\mathbb{A}^{i}_{l,l+1}]_{11} & [\mathbb{A}^{i}_{l,l+1}]_{12} \\ [\mathbb{A}^{i}_{l,l+1}]_{21} & [\mathbb{A}^{i}_{l,l+1}]_{22} \end{bmatrix}. \tag{63}$$

Further, we define the scattering matrix at the interface between the layers l and $l+1$ (in fact, at the layer grid point z_{l+1}), $\mathrm{S}_{l,l+1}$ through the relation

$$\begin{bmatrix} \mathbf{a}^{-}_{l} \\ \mathbf{a}^{+}_{l+1} \end{bmatrix} = \mathrm{S}_{l,l+1} \begin{bmatrix} \mathbf{a}^{+}_{l} \\ \mathbf{a}^{-}_{l+1} \end{bmatrix}, \tag{64}$$

where

$$\mathrm{S}_{l,l+1} = \begin{bmatrix} \mathrm{R}^{+}_{l,l+1} & \mathrm{T}^{-}_{l,l+1} \\ \mathrm{T}^{+}_{l,l+1} & \mathrm{R}^{-}_{l,l+1} \end{bmatrix}, \tag{65}$$

and $\mathrm{R}^{\pm}_{l,l+1}$ and $\mathrm{T}^{\pm}_{l,l+1}$ with $\dim(\mathrm{R}^{\pm}_{l,l+1}) = \dim(\mathrm{T}^{\pm}_{l,l+1}) = M \times M$, are the reflection and transmission matrices, respectively. In analogy with radiative transfer theory (e.g., Budak et al. (2011, 2012)), Eq. (64) is the so-called referred to as the interaction principle equation at the interface $(l, l+1)$, and it is apparent . It shows that the scattering matrix $\mathrm{S}_{l,l+1}$ relates the amplitudes $\mathbf{a}^{-}_{l}$ and $\mathbf{a}^{+}_{l+1}$ of the waves leaving the interface with the amplitudes $\mathbf{a}^{+}_{l}$ and $\mathbf{a}^{-}_{l+1}$ of the waves entering the interface. Starting with EqFrom Eqs. (38) , inserting the partitioning of the matrices $\mathbb{A}^{0(1)}_{l,l+1}$ as given by Eq. (63), using $\mathbf{a}_{l(l+1)} = [\mathbf{a}^{+}_{l(l+1)}, \mathbf{a}^{-}_{l(l+1)}]^{T}$, and rearranging the resulting equation in a fashion as given by Eq. and (64), we find

$$\begin{bmatrix} \mathrm{R}^{+}_{l,l+1} & \mathrm{T}^{-}_{l,l+1} \\ \mathrm{T}^{+}_{l,l+1} & \mathrm{R}^{-}_{l,l+1} \end{bmatrix} = \begin{bmatrix} [\mathbb{A}^{0}_{l,l+1}]_{12} & -[\mathbb{A}^{1}_{l,l+1}]_{11} \\ [\mathbb{A}^{0}_{l,l+1}]_{22} & -[\mathbb{A}^{1}_{l,l+1}]_{21} \end{bmatrix}^{-1} \begin{bmatrix} -[\mathbb{A}^{0}_{l,l+1}]_{11} & [\mathbb{A}^{1}_{l,l+1}]_{12} \\ -[\mathbb{A}^{0}_{l,l+1}]_{21} & [\mathbb{A}^{1}_{l,l+1}]_{22} \end{bmatrix}. \tag{66}$$

Starting with Eq. (38), inserting the partitioning of the matrices $\mathbb{A}^{0(1)}_{l,l+1}$ as given by Eq. (63), using $\mathbf{a}_{l(l+1)} = [\mathbf{a}^{+}_{l(l+1)}, \mathbf{a}^{-}_{l(l+1)}]^{T}$, and rearranging the resulting equation in a fashion as given by Eq. 64, we find ...

We organize the computational process as an upward recurrence using the concept of a “stack”. The stack $\mathcal{S}_{l_0 l}$ with $l_0 < l$, is a group of interfaces characterized by the interaction principle equation

$$\begin{bmatrix} \mathbf{a}^{-}_{l_0} \\ \mathbf{a}^{+}_{l} \end{bmatrix} = \begin{bmatrix} \mathcal{R}^{+}_{l_0 l} & \mathcal{T}^{-}_{l_0 l} \\ \mathcal{T}^{+}_{l_0 l} & \mathcal{R}^{-}_{l_0 l} \end{bmatrix} \begin{bmatrix} \mathbf{a}^{+}_{l_0} \\ \mathbf{a}^{-}_{l} \end{bmatrix}, \tag{67}$$

where the matrices $\mathcal{R}^{\pm}_{l_0 l}$ and $\mathcal{T}^{\pm}_{l_0 l}$ are obtained through a successive application of the interaction principle equation at the interfaces (l_0, l_0+1), (l_0+1, l_0+2),...,$(l-1, l)$. Adding a new layer $l+1$, and taking into account that at the interface $(l, l+1)$, the reflection and transmission matrices are $\mathrm{R}^{\pm}_{l,l+1}$ and $\mathrm{T}^{\pm}_{l,l+1}$, respectively, we find that the interaction principle equation for the stack $\mathcal{S}_{l_0,l+1}$, is

$$\begin{bmatrix} \mathbf{a}^{-}_{l_0} \\ \mathbf{a}^{+}_{l+1} \end{bmatrix} = \begin{bmatrix} \mathcal{R}^{+}_{l_0,l+1} & \mathcal{T}^{-}_{l_0,l+1} \\ \mathcal{T}^{+}_{l_0.l+1} & \mathcal{R}^{-}_{l_0.l+1} \end{bmatrix} \begin{bmatrix} \mathbf{a}^{+}_{l_0} \\ \mathbf{a}^{-}_{l+1} \end{bmatrix}, \tag{68}$$

where $\mathcal{R}^{\pm}_{l_0,l+1}$ and $\mathcal{T}^{\pm}_{l_0,l+1}$ are computed recursively by using of the “adding formulas”

$$\mathcal{R}^{+}_{l_0,l+1} = \mathcal{R}^{+}_{l_0 l} + \mathcal{T}^{-}_{l_0 l}(\mathrm{I} - \mathrm{R}^{+}_{l,l+1}\mathcal{R}^{-}_{l_0 l})^{-1}\mathrm{R}^{+}_{l,l+1}\mathcal{T}^{+}_{l_0 l}, \tag{69}$$

$$\mathcal{T}^{-}_{l_0,l+1} = \mathcal{T}^{-}_{l_0 l}(\mathrm{I} - \mathrm{R}^{+}_{l,l+1}\mathcal{R}^{-}_{l_0 l})^{-1}\mathrm{T}^{-}_{l,l+1}, \tag{70}$$

$$\mathcal{T}^{+}_{l_0,l+1} = \mathrm{T}^{+}_{l,l+1}(\mathrm{I} - \mathcal{R}^{-}_{l_0 l}\mathrm{R}^{+}_{l,l+1})^{-1}\mathcal{T}^{+}_{l_0 l}, \tag{71}$$

$$\mathcal{R}^{-}_{l_0,l+1} = \mathrm{R}^{-}_{l,l+1} + \mathrm{T}^{+}_{l,l+1}(\mathrm{I} - \mathcal{R}^{-}_{l_0 l}\mathrm{R}^{+}_{l,l+1})^{-1}\mathcal{R}^{-}_{l_0 l}\mathrm{T}^{-}_{l,l+1}, \tag{72}$$

for $l = l_0+1, ..., L-1$. Note that Eqs. (69)–(72) are mathematically equivalent to Eqs. (4.30)–(4.33) in Knight et al. (2019). The procedure is initialized with $\mathcal{R}^{\pm}_{l_0,l_0+1} = \mathrm{R}^{\pm}_{l_0,l_0+1}$ and $\mathcal{T}^{\pm}_{l_0,l_0+1} = \mathrm{T}^{\pm}_{l_0,l_0+1}$, and is repeated until the last interface is added to the stack. For the stack $\mathcal{S}_{1L}$, the interaction principle equation is

$$\begin{bmatrix} \mathbf{a}^{-}_{1} \\ \mathbf{a}^{+}_{L} \end{bmatrix} = \begin{bmatrix} \mathcal{R}^{+}_{1L} & \mathcal{T}^{-}_{1L} \\ \mathcal{T}^{+}_{1L} & \mathcal{R}^{-}_{1L} \end{bmatrix} \begin{bmatrix} \mathbf{a}^{+}_{1} \\ \mathbf{a}^{-}_{L} \end{bmatrix}, \tag{73}$$

and from the boundary conditions for amplitudes (42) and (46), that is, from the relations $\mathbf{a}^{+}_{1} = \mathbf{i}_1$ and $\mathbf{a}^{-}_{L} = \mathbf{0}_M$, respectively, we find

$$\mathbf{a}^{-}_{1} = \mathcal{R}^{+}_{1L}\mathbf{a}^{+}_{1} \text{ and } \mathbf{a}^{+}_{L} = \mathcal{T}^{+}_{1L}\mathbf{a}^{+}_{1}. \tag{74}$$

For the lower boundary condition (56), $\mathbf{a}^{+}_{1}$ in Eq. (74) is given by $\mathbf{a}^{+}_{1} = \mathrm{B}^{-1}\mathbf{b}_1$, where, for a unit scale factor, $\mathbf{b}_1 = [1, 0, 0]^{\mathrm{T}}$. To restore the entire set of amplitude vectors $\mathbf{a}_l$, we consider the interaction principle equations for the stacks $\mathcal{S}_{1l}$ and $\mathcal{S}_{lL}$, yielding

$$\mathbf{a}^{+}_{l} = (I - \mathcal{R}^{-}_{1l}\mathcal{R}^{+}_{lL})^{-1}\mathcal{T}^{+}_{1l}\mathbf{a}^{+}_{1}, \tag{75}$$

$$\mathbf{a}^{-}_{l} = \mathcal{R}^{+}_{lL}\mathbf{a}^{+}_{l}, \tag{76}$$

for $l = L-1, ..., 1$. The solution state vector and the wave amplitudes are then computed by using Eqs. (60) and (61), respectively. In contrast to the previous method, this approach requires a clear differentiation between ascending and descending modes as defined by Eq. (20).

3.3 Discrete values of the solution vector

In this section, the global matrix method with matrix exponential and the scattering matrix method will be formulated for the discrete values of the solution vector .

3.2.1 Global matrix method with matrix exponential

In the layer l, with boundaries z_l and z_{l+1}, the discrete values $\mathbf{e}_{l+1} = \mathbf{e}(z_{l+1})$ and $\mathbf{e}_l = \mathbf{e}(z_l)$ are related through the relation (cf. Eq. (14)) or equivalently, Taking into account that by Eq. (14), we have $\mathbf{e}_l = \mathrm{V}_l \mathbf{a}_l$ and $\mathbf{e}_{l+1} = \mathrm{V}_{l+1}\mathbf{a}_{l+1}$, we see that Eq. (35) and (C2) are completely equivalent. Multiplying Eq. (C2) with the scaling matrix S_l^1, we obtain the layer equation whereand S_l^1 and S_l^0, are given by Eqs. (36) and (37), respectively. Essentially, we have $L-1$ equations imposed on layers $1,\ldots,L-1$ for the L unknowns $\mathbf{e}_1,\ldots,\mathbf{e}_L$. On the layer $l=1$, the boundary condition (cf. Eq. (42)) $\mathbf{a}_1^+ = \mathbf{i}_1$, translates into (cf. Eq. (24)) while on

4 Source function

In the derivation so far, the amplitude vector is uniquely defined up to a multiplicative factor, namely the scale factor s. Accordingly, the layer $l = L$, the boundary condition general solution can be written as $\mathbf{a}_\mathrm{s} = s\mathbf{a}$, where, here and it what follows, the subscript s indicates the dependence on s. Since $\mathbf{a}_\mathrm{s}$ satisfies the equation $\mathbb{A}\mathbf{a}_\mathrm{s} = s\mathbf{b}$ (cf. Eq. (46))$\mathbf{a}_L^- = \mathbf{0}_M$ translates into (cf. Eq. (25))

As before, the layer equations (C3) together with the boundary conditions (C6) and (C7) are assembled into a system of equations for the stratified atmosphere, i. e., where After solving Eq. (C8) for $s=1$, we compute the wave amplitudes by using Eq. (61).

Comments. The ascending and descending solution modes can be derived by using the upward and downward recurrence relations (cf. Eqs. (28) –(31), (41) and (45)) respectively, where Obviously, the relation $\mathbf{e}_l = \mathbf{e}_l^+ + \mathbf{e}_l^-$ 57)), $l = 1,\ldots,L$, can be used to verify the numerical algorithm. If we assume that the ascending modes are the dominant modes, i.e., $\mathbf{e}_l \approx \mathbf{e}_l^+$ for $l = 1,\ldots,L$, we may compute the solution vector by means of the upward recurrence relation (cf. Eq. (C11))

4.0.1 Global matrix method with the Padé approximation to the matrix exponential

The layer equation (C3) was derived from the solution representation (C1). In fact, this equation is simply the matrix-exponential representation of the solution, i.e., where the matrix exponential is calculated using an eigendecomposition of the propagation matrix A_l, i.e., $\mathrm{A}_l = \mathrm{V}_l \mathrm{diag}[\lambda_{nl}]\mathrm{V}_l^{-1}$. However, instead of an eigendecomposition method, we can use the Padé approximation to compute the matrix exponential (Doicu and Trautmann, 2009a, b). This method is presumably more efficient than the eigendecomposition method.

the scale factor can be interpreted as a source factor. The nth diagonal Padé approximation to the matrix exponential is where $\mathrm{D}(x\mathrm{A})$ source factor is constant in the case of a harmonic (monochromatic) source function, corresponding to a single-frequency wave, but is time dependent for a non-harmonic source function, corresponding to a time-dependent wave packet. In this section, we describe the computation of the perturbed quantities for both harmonic and non-harmonic source functions. We also present a brief overview of the causality condition and the imaginary frequency shift introduced by Knight et al. (2019), and $\mathrm{N}(x\mathrm{A})$ are polynomials in $\mathrm{A}x$ of degree n given respectively, by The coefficients c_k are defined by and can be computed recursively by means of the relation with the initial value $c_0 = 1$. The layer equation (**??**) then becomes that is where Now, the layer equations (C17) together with the boundary conditions (C6) and (C7) are assembled into a system of equations for the stratified atmosphere, which is then solved by standard methods for band matrices. Taking into account that the boundary conditions (C6) and (C7) are expressed in terms of the eigenvector matrix, we see that in this approach, the eigendecomposition method must only be used in the lower and upper layers, i.e., for $l = 1$ and $l = L$, while in the rest of the layers, the Padé approximation is used. latter extended and applied in Knight et al. (2021, 2022, 2024, 2025). Although it would be sufficient to simply refer to these works, we include a short discussion here because the underlying mathematical structure provides valuable insight into the method.

Comments.

1. The first-order Padé approximation is equivalent with the finite-difference scheme
2. Considering the Taylor series approximation to the matrix exponential, we deduce that for $k = 1$, we have which, when used in Eq. (??), is equivalent with the forward finite-difference scheme

4.1 Non-harmonic source (time-dependent wave packet)

4.1.1 Scattering matrix method

The scattering matrix method can also be formulated in terms of the discrete values of the solution vector. Starting from the interaction principle equation (48), using Eq. (27), i.e., $\mathbf{e}_l^{\pm} = \mathrm{V}_l^{\pm}\mathbf{a}_l^{\pm}$, and Eqs. (24)–(25), i.e., (here we use the more precise notation $(\mathrm{V}_l)^{-1}$ instead of V_l^{-1}) we find that for the stack $\mathcal{S}_{l_0 l}$, the interaction principle equation involving the discrete values of the solution vector is where $\dim(\mathscr{R}_{l_0 l}^{\pm}) = \dim(\mathscr{T}_{l_0 l}^{\pm}) = 2M \times 2M$, and with The boundary values of the solution vector $\mathbf{e}_1^-$ and $\mathbf{e}_L^+$ are computed from Eqs. (74) with $\mathbf{e}_1^+ = \mathbf{v}_1^+$ and $\mathbf{e}_L^- = \mathbf{0}_{2M}$, while the rest of the discrete values $\mathbf{e}_l^+$ and $\mathbf{e}_l^-$ are obtained from Eqs. (75) and (76) with $\mathbf{e}$ replacing $\mathbf{a}$, respectively. Because the dimensions of the matrices $\mathscr{R}_{l_0 l}^{\pm}$ and $\mathscr{T}_{l_0 l}^{\pm}$ are twice as large as those of the matrices $\mathcal{R}_{l_0 l}^{\pm}$ and $\mathcal{T}_{l_0 l}^{\pm}$, the computation time will be higher. The computation time can be somewhat reduced, if the Neumann series representation $(\mathrm{I}_{4M} - \mathrm{A})^{-1}\mathrm{A} = \sum_{n=1}^{\infty} \mathrm{A}^n$ is used (this expansion is valid for $\|\mathrm{A}\| < 1$, where $\|\cdot\|$ is some matrix norm).

5 Time dependent source function

If the source term is time-dependent (or more precisely, if it lacks a temporal dependence in the form of $\exp(\mathrm{j}\omega t)$)not purely harmonic in time (i.e., it cannot be written as a single factor $\exp(\mathrm{j}\omega t)$), the perturbed quantity $f'(x,z,t)$ is not a single-frequency wave with a specified angular frequency ω(a single-frequency wave). In this case, the equations should be are treated in the frequency domain by considering the Fourier transform in time (Knight et al., 2022, 2019, 2021)(Knight et al., 2019, 2021, 2022). This is defined by

$$F'(x,z,\omega) = \int_{-\infty}^{\infty} f'(x,z,t)\mathrm{e}^{-\mathrm{j}\omega t}\mathrm{d}t = \mathcal{F}[f'(x,z,t)](x,z,\omega) \tag{77}$$

and its inverse by

$$f'(x,z,t) = \frac{1}{2\pi}\int_{-\infty}^{\infty} F'(x,z,\omega)\mathrm{e}^{\mathrm{j}\omega t}\mathrm{d}\omega = \mathcal{F}^{-1}[F'(x,z,\omega)](x,z,t). \tag{78}$$

Applying the Fourier transform to the linearized equations (??A29)–(??A31) of Appendix AA, using the result

$$\mathcal{F}\left[\frac{\partial f'}{\partial t}(x,z,t)\right](x,z,\omega) = \mathrm{j}\omega F'(x,z,\omega), \tag{79}$$

and setting

$$F'(x,z,\omega) = \overline{F}(z,\omega)\mathrm{e}^{-\mathrm{j}k_x x} \tag{80}$$

as the counterpart of Eq. (A32) (in which the exponential term $\exp(\mathrm{j}\omega t)$ is absorbed into the expression of $\overline{f}(z)$), and together with

$$\overline{F}(z,\omega) = C(z)\widehat{F}(z,\omega) \tag{81}$$

as the counterpart of Eq. (7), we are led to the system of differential equations (??A41)–(??A46) of Appendix A A (or equivalently, to the matrix differential equation (5)), but with $\widetilde{\widehat{f}}(z,\omega)$ $\widehat{F}(z,\omega)$ replacing $\widehat{f}(z)$. In the frequency domain, the lower boundary conditions (41)and (48)for a unit source function become

At the lower boundary z_1, we consider the localized boundary conditions

$$f'_{\mathrm{s}q_0}(x,z_1,t) = C_{q_0}(z_1)s(x,t),\ \frac{\partial f'_{\mathrm{s}q_0}}{\partial z}(x,z_1,t) = 0,\ \frac{\partial^2 f'_{\mathrm{s}q_0}}{\partial z^2}(x,z_1,t) = 0, \tag{82}$$

for $a^+_{m,l=1}(\omega) = \delta_{m1}$, where δ_{m1} is the Kronecker delta, and q_0 takes the values 1, 2, and 3 for the horizontal velocity, vertical velocity, and temperature, respectively. In Eq. (82), the source function is given by

$$s(x,t) = As(t)\mathrm{e}^{-\mathrm{j}k_{\mathrm{x}}x}, \tag{83}$$

respectively. As in Section ??, with $\widetilde{\widehat{f}}(z,\omega)$ being A denoting the scalar source amplitude and $s(t)$ its prescribed time dependence. In our implementation, the time-dependent part of the source function is chosen as

$$s(t) = \mathrm{e}^{\mathrm{j}\omega_0(t-t_0)}\mathrm{e}^{-\dfrac{(t-t_0)^2}{2\sigma_{\mathrm{t}}^2}} \tag{84}$$

with the Fourier transform

$$S(\omega) = \frac{\sqrt{2\pi}}{\sigma_\omega}\mathrm{e}^{-\mathrm{j}\omega t_0}\mathrm{e}^{-\dfrac{(\omega-\omega_0)^2}{2\sigma_\omega^2}}, \tag{85}$$

where ω_0 is the reference frequency (the central frequency in the Fourier spectrum), t_0 is the time at which the source function is maximum, and σ_{t} and $\sigma_\omega = 1/\sigma_{\mathrm{t}}$ are the standard deviations in the time and frequency domains, respectively. The amplitude of the source function A is specified by imposing the normalization condition:

$$|\mathrm{Re}\{f'_{\mathrm{s}q_0}(x=0,z_1,t_0)\}| = f_{\mathrm{b}q_0}, \tag{86}$$

for some prescribed boundary value $f_{\mathrm{b}q_0} > 0$. For example, in the case $q_0 = 1$, $f_{\mathrm{b}q_0}$ may be chosen as a fraction of the maximum horizontal velocity of neutrals in the south direction over the altitude range, whereas in the case $q_0 = 3$, $f_{\mathrm{b}q_0}$ may be chosen as a fraction of the maximum temperature of neutrals over the altitude range.

Applying the Fourier transform to Eq. (82) and using Eqs. (80) and (81), we obtain the following boundary conditions in the frequency domain (note that $AS(\omega)$ is the Fourier transform of $As(t)$):

$$\widehat{F}_{\mathrm{s}q_0}(z_1,\omega) = AS(\omega),\ \frac{\partial \widehat{F}_{\mathrm{s}q_0}}{\partial z}(z_1,\omega) = 0,\ \frac{\partial^2 \widehat{F}_{\mathrm{s}q_0}}{\partial z^2}(z_1,\omega) = 0. \tag{87}$$

Comparing Eqs. (87) and (49), we see that the latter corresponds to the choice $b_{1,2} = b_{1,3} = 0$. In this case, the source factor $s = b_{1,1}$ can be identified with $AS(\omega)$. Therefore, as in Section 3, we define $\widehat{F}_q(z,\omega) = [\mathbf{e}(z,\omega)]_q$, $q = 1,2,3$, where

$\mathbf{e}(z,\omega)$ denotes the solution of the differential equation (5) for a unitsource function (source factor in the frequency domain), we compute the perturbed quantity $f'_s(x,z,t)$ by taking (i.e., for $\mathbf{b}_1 = [1,0,0]^{\mathrm{T}}$). The perturbed quantity $f'_{\mathrm{s}q}(x,z,t)$ is then obtained by applying the inverse transform (78) with to

$$F'_{\mathrm{s}q}(x,z,\omega) = AS(\omega)\mathrm{e}^{-\mathrm{j}k_{\mathrm{x}}x}C_q(z)\widehat{F}_q(z,\omega), \tag{88}$$

that is,

$$f'_{\mathrm{s}q}(x,z,t) = \frac{1}{2\pi}\int_{-\infty}^{\infty} F'_{\mathrm{s}q}(x,z,\omega)\mathrm{e}^{\mathrm{j}\omega t}\mathrm{d}\omega = A\overline{f}_q(z,t)\mathrm{e}^{-\mathrm{j}k_{\mathrm{x}}x}, \tag{89}$$

where $\widetilde{s}(\omega)$ is the Fourier transform of some source function $s(t)$, i.e., $\widetilde{s} = \mathcal{F}[s]$.

$$\overline{f}_q(z,t) = \frac{C_q(z)}{2\pi}\int_{-\infty}^{\infty} S(\omega)\widehat{F}_q(z,\omega)\mathrm{e}^{\mathrm{j}\omega t}\mathrm{d}\omega. \tag{90}$$

For $S(\omega)$ as above, $\overline{f}_q(z,t)$ can be written as

$$\overline{f}_q(z,t) = \frac{C_q(z)}{2\pi}\int_{-\infty}^{\infty} \mathscr{S}(\omega)\widehat{F}_q(z,\omega)\mathrm{e}^{\mathrm{j}\omega(t-t_0)}\mathrm{d}\omega, \tag{91}$$

with

$$\mathscr{S}(\omega) = \frac{\sqrt{2\pi}}{\sigma_\omega}\mathrm{e}^{-\dfrac{(\omega-\omega_0)^2}{2\sigma_\omega^2}}. \tag{92}$$

The computation of $\widetilde{f}(z,\omega)$ $\widehat{F}_q(z,\omega)$ can be performed without any limitations using any of the methods presented in Section 4. Note that the most general situation is when the source function depends on time and the horizontal coordinate, that is , $s = s(x,t)$. In this case , we have to consider the two-dimensional Fourier transform in time and space. However, a simplification occurs in case that the variables are separable, i. e., $s = s_t(t)s_x(x)$; in this case, 3. The computed quantity is $\overline{f}_q(z,t)$, the amplitude $A > 0$, is determined from the normalization condition (86) as

$$A = \frac{f_{\mathrm{b}q_0}}{|\mathrm{Re}\{\overline{f}_{q_0}(z_1,t_0)\}|}, \tag{93}$$

and the perturbed quantity $f'_{\mathrm{s}q}(x,z,t)$ is computed from Eq. (89).

4.1 Monochromatic source (single-frequency wave)

The case of a monochromatic source is obtained as a special case of the above approach by choosing

$$s(t) = \mathrm{e}^{\mathrm{j}\omega_0 t}, \tag{94}$$

whose Fourier transform is

$$S(\omega) = \int_{-\infty}^{\infty} s(t)\,\mathrm{e}^{-\mathrm{j}\omega t}\,\mathrm{d}t = \int_{-\infty}^{\infty} \mathrm{e}^{-\mathrm{j}(\omega-\omega_0)t}\,\mathrm{d}t = 2\pi\delta(\omega-\omega_0), \tag{95}$$

where the equality is understood in the sense of distributions.

The lower boundary conditions in the time domain are specified as

$$f'_{\mathrm{s}q_0}(x,z_1,t) = \frac{1}{2\pi} C_{q_0}(z_1)\, s(x,t), \;\; \frac{\partial f'_{\mathrm{s}q_0}}{\partial z}(x,z_1,t) = 0, \;\; \frac{\partial^2 f'_{\mathrm{s}q_0}}{\partial z^2}(x,z_1,t) = 0, \tag{96}$$

with

$$s(x,t) = A s(t)\mathrm{e}^{-\mathrm{j}k_{\mathrm{x}}x} = A\mathrm{e}^{\mathrm{j}(\omega_0 t - k_{\mathrm{x}}x)}. \tag{97}$$

Applying the Fourier transform with respect to time yields

$$\widehat{F}_{\mathrm{s}q_0}(z_1,\omega) = A\,\delta(\omega - \omega_0). \tag{98}$$

Since the forcing is monochromatic, the frequency-domain problem is solved only at the excitation frequency $\omega = \omega_0$. Accordingly, the term $\widetilde{s}(\omega)\exp(-\mathrm{j}k_{\mathrm{x}}x)$ in localized boundary conditions are imposed directly on the harmonic amplitudes at ω_0, namely

$$\widehat{F}_{\mathrm{s}q_0}(z_1,\omega_0) = A, \;\; \frac{\partial \widehat{F}_{\mathrm{s}q_0}}{\partial z}(z_1,\omega_0) = 0, \;\; \frac{\partial^2 \widehat{F}_{\mathrm{s}q_0}}{\partial z^2}(z_1,\omega_0) = 0. \tag{99}$$

Again, by comparing Eqs. (99) and (49), we see that the source factor $s = b_{1,1}$ can be identified with A. In this regard, let $\widehat{F}_q(z,\omega_0) = \left[\mathbf{e}(z,\omega_0)\right]_q$, $q = 1,2,3$, where $\mathbf{e}(z,\omega_0)$ denotes the solution of the differential equation (5) for a unit source factor in the frequency domain. The perturbed quantity $f'_{\mathrm{s}q}(x,z,t)$ is then obtained by the inverse Fourier transform (78) of $F'_{\mathrm{s}q}(x,z,\omega)$ (cf. Eq. (88)should be replaced by the product of one-dimensional Fourier transforms $\widetilde{s}_t(\omega)\widetilde{s}_x(k_{\mathrm{x}})$), and the result is

$$f'_{\mathrm{s}q}(x,z,t) = A\,\overline{f}_{\mathrm{s}q}(z)\mathrm{e}^{\mathrm{j}(\omega_0 t - k_{\mathrm{x}}x)}, \tag{100}$$

where

$$\overline{f}_{\mathrm{s}q}(z) = C_q(z)\,\widehat{F}_q(z,\omega_0). \tag{101}$$

Thus, the computed quantity is $\overline{f}_{\mathrm{s}q}(z)$, and the amplitude A is determined from the normalization condition

$$|\mathrm{Re}\{f'_{\mathrm{s}q_0}(x=0,z_1,t=0)\}| = f_{\mathrm{b}q_0}, \tag{102}$$

which yields

$$A = \frac{f_{\mathrm{b}q_0}}{|\mathrm{Re}\{\overline{f}_{\mathrm{s}q}(z_1)\}|}. \tag{103}$$

Note that for a monochromatic source, the modal boundary condition (41) can be used instead of the localized boundary condition (99).

We conclude this section with a comment related to causality as discussed in (Knight et al., 2019).

4.2 Causality and imaginary frequency shifting

Causality means that a the wave field in response to any source function can never cannot be nonzero prior to the earliest time at which the source function is nonzero. According to the classification rule (20), we have

$$\mathrm{Re}[\lambda_{1l}^{+}(\omega)] < \mathrm{Re}[\lambda_{1l}^{-}(\omega)], \tag{104}$$

for any layer $l = 1, \ldots, L$ and any real frequency ω. However, as shown by Knight et al. (2019), to To preserve causality in solutions of two-point boundary value problems, a much stronger condition should be met. This condition is stronger condition is required, namely

$$\max_{l=1,\ldots,L} \mathrm{Re}[\lambda_{1l}^{+}(\omega)] < \min_{l=1,\ldots,L} \mathrm{Re}[\lambda_{1l}^{-}(\omega)] \tag{105}$$

for all $\varpi = \mathrm{Re}(\varpi) + \mathrm{j}\mathrm{Im}(\varpi) \in \overline{U}_{\delta}$, where for any $\delta \geq 0$, $\overline{U}_{\delta}$ is the closed lower half-plane $\mathrm{Im}(\varpi) \leq -\delta$. Eq. (**??**) states that the upper altitude bound of the real part of the eigenvalues for ascending modes should be smaller than the lower altitude bound of the same values for descending modes. In some situation, condition(**??**) is not satisfied for $\delta = 0$, but it is satisfied for some $\delta > 0$. If so, an imaginary frequency shifting, i. e., $\omega \rightarrow \omega - \mathrm{j}\delta$ is required to preserve causality (Knight et al., 2019). To summarize this approach $\omega \in \mathbb{R}$. Equivalently, this condition requires that there exists a single real constant σ, such that

$$\mathrm{Re}[\lambda_{1l}^{+}(\omega)] < \sigma < \mathrm{Re}[\lambda_{1l}^{-}(\omega)], \tag{106}$$

for all l and all $\omega \in \mathbb{R}$.

In some situations, condition (106) is not satisfied on the real frequency axis but can be enforced by introducing an imaginary frequency shift $\omega \rightarrow \omega - \mathrm{j}\delta$. Following Knight et al. (2019), we impose a causality requirement, which we refer to as the Global Causality (GC) condition. This condition demands that there exists a single real constant σ, such that

$$\mathrm{Re}[\lambda_{1l}^{+}(\omega - \mathrm{j}\delta)] < \sigma < \mathrm{Re}[\lambda_{1l}^{-}(\omega - \mathrm{j}\delta)], \tag{107}$$

for all l and all $\omega \in \mathbb{R}$.

Knight et al. (2024) subsequently relaxed the requirement that (107) hold for all layers l for a fixed σ. The new condition, which we refer to as the Layerwise Causality (LC) condition, requires that at each layer l there is a σ_l such that

$$\mathrm{Re}[\lambda_{1l}^{+}(\omega - \mathrm{j}\delta)] < \sigma_l < \mathrm{Re}[\lambda_{1l}^{-}(\omega - \mathrm{j}\delta)], \tag{108}$$

for all $\omega \in \mathbb{R}$. Equivalently, if at each layer l, we consider the shifted source function in the frequency domain

$$d_l(\omega) = \mathrm{Re}[\lambda_{1l}^{-}(\omega - \mathrm{j}\delta)] - \mathrm{Re}[\lambda_{1l}^{+}(\omega - \mathrm{j}\delta)] > 0, \tag{109}$$

and let for all $\omega \in \mathbb{R}$, then the multilayer algorithm will still preserve causality. The LC condition requires a strict separation between the two eigenvalue families within each layer, but it does not require that the same separator works for all layers. Thus, each layer may have its own separating value σ_l. Equivalently, $d_l(\omega) > 0$ means that, in layer l, the real parts of the eigenvalues associated with the ascending and descending gravity waves remain separated (and therefore do not cross) as functions of the real frequency ω after the shift.

To summarize the approach for computing $f'_{sq}(x,z,t)$ in the case of imaginary frequency shifting, we introduce the shifted spectrum

$$S_\delta(\omega) = S(\omega - \mathrm{j}\delta) = \int\limits_{-\infty}^{\infty} s(t)\mathrm{e}^{-\mathrm{j}(\omega-\mathrm{j}\delta)t}\mathrm{d}t = \int\limits_{-\infty}^{\infty} \left[s(t)\mathrm{e}^{-\delta t}\right]\mathrm{e}^{-\mathrm{j}\omega t}\mathrm{d}t, \tag{110}$$

which can be viewed as the analytic continuation of $S(\omega)$ to complex frequencies. Note that the shift $\omega \to \omega - \mathrm{j}\delta$ corresponds in the time domain to multiplication by $\exp(-\delta t)$. Let

$$F'_{\delta\mathrm{s}q}(x,z,\omega) = AS(\omega-\mathrm{j}\delta)C_q(z)\widehat{F}_q(z,\omega-\mathrm{j}\delta)\mathrm{e}^{-\mathrm{j}k_\mathrm{x}x} \tag{111}$$

be the Fourier transform (in time) of the perturbed quantity with frequency shifting $f'_{s\delta}(x,z,t)$, i.e., $\widetilde{f'_{s\delta}} = \mathcal{F}[f'_{s\delta}]$, $f'_{\delta\mathrm{s}q}(x,z,t)$, where as usual, $\widetilde{\widetilde{f}}(z,\omega-\mathrm{j}\delta)$ $\widehat{F}_q(z,\omega-\mathrm{j}\delta) = [\mathbf{e}(z,\omega-\mathrm{j}\delta)]_q$ is solution of the differential equation (5) for a unit source function. By Cauchytheorem it can be shown that the perturbed quantity with frequency shifting computes as factor in the frequency domain. Under the usual analyticity and decay assumptions (so that contour shifting is permitted), Cauchy's theorem yields the shift relation

$$f'_{\delta\mathrm{s}q}(x,z,t) = \frac{1}{2\pi}\int\limits_{-\infty}^{\infty} F'_{\delta\mathrm{s}q}(x,z,\omega)\mathrm{e}^{\mathrm{j}\omega t}\mathrm{d}\omega = \mathrm{e}^{-\delta t}f'_{\mathrm{s}q}(x,z,t), \tag{112}$$

where f'_s $f'_{\mathrm{s}q}$ is the perturbed quantity without frequency shifting given by Eq. (89). As a result, we obtain the so called Equivalently, this implies the shift-invariance property of the solution, i.e.,

$$f'_{\mathrm{s}q}(x,z,t) = \mathrm{e}^{\delta t}f'_{\delta\mathrm{s}q}(x,z,t). \tag{113}$$

Summarizing, in the frequency shifting approach we (i) compute $\widetilde{\widetilde{f}}(z,\omega-\mathrm{j}\delta)$ as

Summarizing, the computational steps for the frequency-shifting approach are as follows:

1. Compute $\mathbf{e}(z,\omega-\mathrm{j}\delta)$ as the solution of the differential equation (5) for a unit source function, (ii) calculate $\widetilde{f'_{s\delta}}$ factor, and set $\widehat{F}_q(z,\omega-\mathrm{j}\delta) = [\mathbf{e}(z,\omega-\mathrm{j}\delta)]_q$.

2. Calculate $F'_{\delta\mathrm{s}q}$ by means of Eq. (111) , (iii)determine $f'_{s\delta}$ as $f'_{s\delta} = \mathcal{F}[\widetilde{f'_{s\delta}}]$, with $S(\omega)$ replaced by $S(\omega-\mathrm{j}\delta)$ and (iv)compute f'_s from the $\widehat{F}_q(z,\omega)$ replaced by $\widehat{F}_q(z,\omega-\mathrm{j}\delta)$.

3. Compute $f'_{\delta\mathrm{s}q}$ by inverse Fourier transform

$$f'_{\delta\mathrm{s}q}(x,z,t) = A\mathrm{e}^{-\mathrm{j}k_\mathrm{x}x}\frac{C_q(z)}{2\pi}\int\limits_{-\infty}^{\infty} S(\omega-\mathrm{j}\delta)\widehat{F}_q(z,\omega-\mathrm{j}\delta)\mathrm{e}^{\mathrm{j}\omega t}\mathrm{d}\omega. \tag{114}$$

4. Recover $f'_{\mathrm{s}q}$ from the shift-invariance property (113). An issue that may arise

For $S(\omega)$ as in Eq. (85), it is convenient to write the recovered solution in the form

$$f'_{\mathrm{s}q}(x,z,t) = A\overline{f}_{\delta q}(z,t)\mathrm{e}^{-\mathrm{j}k_{\mathrm{x}}x}, \tag{115}$$

where (compare with Eq. (91))

$$\overline{f}_{\delta q}(z,t) = \mathrm{e}^{\delta(t-t_0)}\frac{C_q(z)}{2\pi}\int\limits_{-\infty}^{\infty}\mathscr{S}(\omega-\mathrm{j}\delta)\widehat{F}_q(z,\omega-\mathrm{j}\delta)\mathrm{e}^{\mathrm{j}\omega(t-t_0)}\mathrm{d}\omega, \tag{116}$$

and $\mathscr{S}$ is given by Eq. (92). The computed quantity is $\overline{f}_{\delta q}(z,t)$, the amplitude $A > 0$ is determined from the normalization condition (86) as

$$A = \frac{f_{\mathrm{b}q_0}}{|\mathrm{Re}\{\overline{f}_{\delta q}(z_1,t_0)\}|}, \tag{117}$$

and the perturbed quantity $f'_{\mathrm{s}q}(x,z,t)$ is computed from Eq. (115). The Fourier integral in Eq. (116) is evaluated using a direct discrete Fourier transform (FT) rather than a fast Fourier transform (FFT). The frequency and time discretization used in the Fourier transform are discussed in Appendix D.

A potential numerical issue with this approach is that the interaction between a large frequency shift δ(which ensures , while ensuring the causality condition(**??**)) and the rounding errors in computing a small $f'_{s\delta}$, , may amplify rounding errors when recovering $f'_{\mathrm{s}q}$ from $f'_{\delta\mathrm{s}q}$ through the exponential term $\exp(\delta t)$, can cause the left-hand $\exp[\delta(t-t_0)]$. For large t, this may lead to an uncontrolled growth of the right-hand side of Eq. (113)to explode for large t. Since this problem appears frequently in our simulations, we decided to renounce on the causality condition (**??**) (in other words, on the frequency shifting), and to compute f'_s directly by using Eq. (89). Parenthetically we note that instead of condition (**??**) we can give another condition that preserves causality. From Eqs. (111) –(113), we find where Assume that the source function $s(t)$ is applied at $t = 0$, and in view of Eq. (**??**) 116). Therefore, care is required in selecting δ: it must be large enough to ensure the layerwise causality condition , consider the convolution integral Further, assume that In this case, for $t \le T$ and $t_1 \ge 0$, we have $\tau = t - t_1 \le T$, implying $\widehat{f}_\delta(z,\tau = t-t_1) = 0$. Consequently, for $t \le T$, we have $I(z,t) = 0$, and we conclude that the effect (reaction) $I(z,t)$ appears at $t > T$, while the cause (action) $s(t)$ appears at $t = 0$. Thus, in the new formulation, condition (**??**) is the analogue of condition (**??**). The problem arising here is that in practice, condition (**??**) should be verified for all z within the considered but not significantly larger than that. Rigorous methods for determining the minimum sufficient δ were described by Knight et al. (2019, 2021, 2022), while the numerical blow-up associated with the exponential growth term was discussed in Appendix B of Knight et al. (2021). In our implementation we employ a heuristic approach that combines (i) the Layerwise Causality (LC) condition applied at selected altitude levels, and (ii) a Source-Function Reconstruction (SFR) test. First, an admissible interval $[\delta_{\min}, \delta_{\max}]$ is constructed by enforcing the SFR criterion, and within this interval, the LC condition is applied at selected altitude levels to obtain a refined lower bound $\delta_{\min}$. In the final selection step, a discrete set of candidate shifts is evaluated, and for each candidate the LC condition is checked over the entire altitude range. However, if we decide not to be so strict in verifying causality , we can determine the pair $(z_0,t_0) = \arg\max_{z,t}\widehat{f}_\delta(z,t)$ and then compare $s(t)$ with $\widehat{f}_\delta(z_0,t)$. Among all shifts that satisfy causality at all altitudes, the algorithm selects the one whose maximum-amplitude vector is closest to the center of mass of the admissible solutions. A detailed description of this approach is provided in Appendix D.

Table 1. Geographic locations and heights of the IRI data sets

Location
Jicamarca (Peru)
Arecibo (Puerto Rico)
Millstone Hill (USA)
Saint-Santin (France)
EISCAT TromsMethod 5:ø Scattering matrix method for the discrete values of the solution vector. The main difference between global and scattering matrix methods is that the former with t
Svalbard archipelago (Norway)

5 Numerical simulationsimplementation

We designed a numerical model for solving the ionospheric linearized gravity-wave equations. The solution methods included in the model are the following. An implementation of the method is freely available as an open-source code at https://github.com/AlexandruDoicu/Gravity-Waves. The code uses as input the data file produced by the International Reference Ionosphere (IRI) code available at https://ccmc.gsfc.nasa.gov/models/IRI~2016/ is used. From these date, we read

1. Method 1:Global matrix method with matrix exponential for the amplitudes of the characteristic solutions; the date (year, month, and day) and the time,
2. Method 2:Scattering matrix method for the amplitudes of the characteristic solutions; the geographic latitude and longitude,
3. Method 3:Global matrix method with matrix exponential for the discrete values of the solution vector; the magnetic dip angle,
4. Method 4:Global matrix method with the Padé approximation to the matrix exponential for the discrete values of the solution vector; the solar radio flux f10.7 and its 81-day average,
5. the number density of O^+ ions as a function of altitude.

In its present implementation, the IRI data files correspond to the locations summarized in Table 1. The altitude grid extends from $z_{\mathrm{min}} = 80$ km to $z_{\mathrm{max}} = 500$ km with a step size of $\mathrm{d}z = 1.0$ km. Users may generate custom data files by running the IRI code and specifying the corresponding file names in the input namelist.

The input parameters of the numerical model are the background quantities ρ_0, T_0, u_0 and n_{0i}. These are delivered by the IRI data are subsequently used in a manner analogous to that in the SAMI2 model of the Naval Research Lab (Huba et al., 2000), while the derivatives $\mathrm{d}T_0/\mathrm{d}z$, $\mathrm{d}u_0/\mathrm{d}z$, and $\mathrm{d}n_{0i}/\mathrm{d}z$ are computed by finite-differences. Note that in Laboratory (https://github.com/NRL-Plasma-Physics-Division/SAMI2). In the present implementation, the ionospheric equations follow the SAMI2 framework originally developed by Huba et al. (2000) and described in detail by Huba (2023). In SAMI2, the neutral atmosphere is atmospheric parameters–namely the neutral number density, total mass density, and temperature–are specified using the Mass Spectrometer Incoherent Scatter model (MSIS) (Hedin, 1987), and MSIS family of models. In this study, these parameters are based on the MSIS formulation of Hedin (1987), while we note that more recent updates are provided by the NRLMSIS 2.0 model of Emmert et al. (2021). The meridional and zonal winds are specified using the Horizontal Wind Model(HWM) (Hedin et al., 1991). The background quantities T_0, u_0 and n_{0i}, as well as their derivatives are illustrated in Fig. ??. . In the present implementation, we follow the formulation of Hedin et al. (1991), while more recent updates are described by Drob et al. (2015).

Background quantities T_0, u_0 and n_{0i} ($i = \mathrm{O}^+$) delivered by SAMI2 (upper panels), and their height derivatives (lower panels).

In our numerical analysis, we consider two types of source functions, namely and where ω_0 is the reference frequency (the central frequency in the Fourier spectrum), t_0 is the time at which the source function is maximum, σ_t and $\sigma_\omega = 1/\sigma_t$ are The derivatives of the standard deviations in the time and frequency domains, respectively, and s_0 is the amplitude of the source function (computed from Eq. (**??**) with $\delta_{\mathrm{T}} = 0.1$) . The first type of source function leads to a single-frequency solution with frequency ω_0, that is, while the second type corresponds to a time wavepacket (with a Gaussian pulse function as envelope). The reference frequency used in the definitions (8) and (9) of $\widehat{u}$ and $\widehat{w}$, respectively, is ω_0. The quantities of interest (which will be calculated and analyzed) are the perturbations in the first case, and in the second case.

The numerical analysis is performed under the following assumptions. background parameters are computed using central finite differences. Prior to applying the finite-difference calculations, the background parameters are smoothed by means of cubic spline interpolation with regularization.

Other features of the model are summarized as follows:

1. The atmosphere extends from $z_{\min} = 50\,\mathrm{km}$ to $z_{\max} = 500\,\mathrm{km}$, the number of layers is $L = 400$, the number of grid points is $2L+1 = 801$, the altitude discretization step is $\Delta\widehat{z} = 0.56\,\mathrm{km}$, and the layer thickness is $2\Delta\widehat{z} = 1.12\,\mathrm{km}$.

2. Unless stated otherwise, we assume non-zero height derivatives for background temperature and wind velocity, as well as a constant background dynamic viscosity in each layer (in other words, we assume the layer conditions (**??**)). Two linearization models are included in the code:

   (a) We choose $\omega_0 = \kappa_\omega \max_z \nu_{0ni}(z)$ with $0.6 \le \kappa_\omega \le 1$, where ν_{0ni} is the background neutral-ion collision frequency given by Eq. (**??**) . For κ_ω ranging from 0.6 to 1.0, ω_0 varies between $1.25 \times 10^{-3}\,\mathrm{s}^{-1}$ and $2.10 \times 10^{-3}\,\mathrm{s}^{-1}$, and correspondingly, the time period $T_0 = 2\pi/\omega_0$ varies between $50\,\mathrm{min}$ and $83\,\mathrm{min}$. a general model that accounts for the altitude derivatives of the background velocity, temperature, density scale height, and dynamic viscosity; and

   (b) For the first type of source function, we analyze $\overline{f}_s(z)$ in the spatial frequency domain by applying a nonuniform Fourier Transform (FT) with $N_k = 256$ points. The sampling wavenumber is $\Delta k_z = k_{z0}/20$, a simplified model for an isothermal, homogeneous, and windless atmosphere without ion drag.

3. The methods for solving the linearized equations based on the matrix exponential formalism comprise:

   (a) the Global Matrix Method for the Amplitudes (GMMA) of the characteristic solutions;

   (b) the Scattering Matrix Method for the Amplitudes (SMMA) of the characteristic solutions; and

   (c) the Global Matrix Method for the Nodal (grid-point) values (GMMN) of the state vector.

4. At the lower boundary, we impose that a selected component of the state vector is finite and that its first and second derivatives with respect to height vanish. At the upper boundary, we assume that there is no downward energy propagation, i.e., the amplitudes of all descending wave modes are set to zero.

5. The code first computes the wave parameters for a single-frequency wave and then for a time-dependent wave packet.

6. Typical values of the horizontal wavelength lie in the range 300–700 km.

7. The algorithm computes lower and upper bounds for the wave period by solving the inviscid dispersion equation for two prescribed minimum and maximum values of the vertical wavelength. The computational procedure is described in Appendix D. The user then selects an appropriate value within this range.

8. For a single-frequency wave, the output quantity of interest is $A\overline{f}_{sq}(z)$, where $k_{z0} = 2\pi/\lambda_{z0}$ $\overline{f}_{sq}(z)$ and A are given by Eqs. (101) and (103), respectively, whereas for a time-dependent wave packet the corresponding output quantity is $A\overline{f}_{\delta q}(z,t)$, where $\overline{f}_{\delta q}(z,t)$ and $\lambda_{z0} = 50$ km. The Fourier spectrum is smoothed using cubic smoothing spline, while for a better comparison, the FT-amplitudes are normalized by their maximum values.

9. For the second type of source function, we choose $\sigma_\omega = \omega_0/30$, and $t_0 = \kappa_t\sigma_t$ with $\kappa_t = 4$ A are given by Eqs. (116) and $\sigma_t = 1/\sigma_\omega$, so that with a good approximation, $s(t) \approx 0$ for $t \leq 0$ and $t \geq 2\kappa_t\sigma_t$. Thus, the time domain is $t_{\min} = 0$ and $t_{\max} = 2\kappa_t\sigma_t$, while the frequency domain is $\omega_{\min} = \omega_0 - \kappa_t\sigma_\omega$ and $\omega_{\max} = \omega_0 + \kappa_t\sigma_\omega$. We perform a nonuniform Fourier transform with $N_t = N_\omega = 512$ points; accordingly, the sampling time is $\Delta t = (t_{\max} - t_{\min})/(N_t - 1)$ and the sampling frequency is $\Delta\omega = (\omega_{\max} - \omega_{\min})/(N_\omega - 1)$.

10. If not stated otherwise, we use Method 1 as solution method and set the frequency parameter κ_ω to 0.8. (117), respectively.

5.1 Single-frequency waves

Our numerical analysis is organized as follows. In a first step, we test the numerical model, and in a second step, we evaluate the accuracy and efficiency of the proposed solution methods.Further, we discuss the significance of the vertical wavenumber, and analyze the pairwise classification of ascending and descending modes, as well as, the influence of the ion drag, lower boundary condition, and lower altitude level on the results. Finally, we calculate the ascending and descending wave modes by using Methods 1

6 Numerical simulations

The simulations are performed using, as input, an IRI data file corresponding to the EISCAT Tromsø (auroral) location on 11 February 2012 at 10:00. The solar zenith angle is 84.2 °, the magnetic inclination angle is 78.28 °, the daily solar radio flux F10.7 is 109.4 sfu, and 3.

Model testing. To test the numerical model we compare the results obtained by solving (see Appendix A) the linearized equations (**??**)–(**??**) for an isothermal, homogeneous, and windless atmosphere, i.e., for the layer conditions the 81-day averaged solar radio flux is 116.9 sfu, where $1\,\mathrm{sfu} = 10^{-22}\ \mathrm{Wm^{-2}Hz^{-1}}$. In the simulations, the Prandtl number is 0.66, the magnetic index is 7.0, and the horizontal wind model 14 implemented in SAMI2 is used. The altitude grid extends from 80 km to 500 km and contains 801 grid points. The lower boundary can, in principle, be set to smaller altitudes (e.g., 50 km), but we choose 80 km because this level is typically adopted as the lower boundary for ionospheric equations. Unless stated otherwise, the horizontal wavelength is $\lambda_\mathrm{x} = 400$ km, the wave period is $\lambda_\mathrm{t} = 40$ min, and the linearized equations (**??**)–(**??**). In this simulation, the altitude range is from $z_{\min} = 125\,\mathrm{km}$ to $z_{\max} = 450\,\mathrm{km}$. The results in Fig. **??** show that there are no visible differences in the altitude profiles of temperature $\overline{T}_s$, vertical velocity $\overline{w}_s$, and horizontal velocity $\overline{u}_s$the imaginary frequency shift for a single-frequency wave is $10^{-6}\ \mathrm{s}^{-1}$. The lower boundary conditions are imposed on the vertical velocity with $f_{\mathrm{b}2} = 5 \times 10^{-2}\,\mathrm{ms}^{-1}$ in Eqs. (86) and (102).

Altitude profiles of the perturbed temperature $\overline{T}_s$, vertical velocity $\overline{w}_s$, and horizontal velocity $\overline{u}_s$ computed by solving the linearized equations (**??**)–(**??**) (a) and (**??**)–(**??**) (b) of Appendix A.

Accuracy and efficiency of the solution methods. To test the accuracy of the solution methods, we choose Method 1 Taking the global matrix method for amplitudes as a reference, and calculate the relative root-mean square error of a method as In Fig. **??** we plot the relative root-mean square error we find that the relative root-mean-square errors in the perturbed temperature, vertical velocity, and horizontal velocity versus the frequency parameters κ_ω. The results were obtained using Method 4 with the second- and third-order Padé approximations, and Method 5 with a third-order Neumann series approximation for matrix inversion. We present only these errors, because the errors for Methods 2 and 3 obtained with the other two solution methods are smaller than 10^{-6}. The elapsed time (wall time) of all solution methods are shown in Fig. **??**. The following conclusions can be drawn. The relative root-mean square errors of the third-order Padé approximation are generally smaller than 5×10^{-3}. In contrast, the errors of the second-order Padé approximation can reach values of 5×10^{-2}. Excluding an outlier, the relative root-mean square errors of Method 5 are of about 3×10^{-2}. These large errors may be due to the fact that the rounding errors may affect the calculation of the reflection and transmission matrices of a stack (these matrices have larger dimensions and require more matrix inversion operations than in Method 2). The scattering matrix methods (Methods 2 and 5) are more time consuming Thus, all methods exhibit comparable accuracy. On the other hand, we find that the scattering matrix method is more time-consuming than the global matrix methods(Methods 1, 3, and 4), particularly for time-dependent wave packets. This is because scattering matrix methods necessitate many matrix operations per layer, while the scattering matrix approach requires numerous matrix operations in each layer, whereas solving a system of equations compressed into band-storage is not so time expensive. The conclusion of this simulation is that Method 1 is not only the most accurate but also the most efficient. band storage is computationally less expensive.

Relative root-mean square error in the perturbed temperature, vertical velocity, and horizontal velocity. The results are computed by Method 4 with the second-order Padé approximation (a) and the third-order Padé approximation (b), and by Method 5 (c).

Elapsed time of all solution methods. Method 4A corresponds to the second-order Padé approximation, while Method 4B corresponds to the third-order Padé approximation.

Vertical wavelength. In Fig. **??**, we illustrate the altitude profiles of the perturbed temperature$\overline{T}_s$, vertical velocity $\overline{w}_s$, and horizontal velocity$\overline{u}_s$, as well as, their Fourier spectra in the spatial frequency domain. The calculation is done for three value of the frequency parameter κ_ω, namely, 1.0, 0.8, and 0.6. The variation of the vertical wavelength $\lambda_{\mathrm{z}0}$, corresponding to the maximum FT-amplitudes of the perturbed temperature, vertical velocity, and horizontal velocity, with respect to the frequency parameter κ_ω is depicted in Fig. **??**. The results reveal that when the contribution of the ion drag increases (i.e., the frequency parameters κ_ω decreases)

1. the widths of the Fourier spectra increases,

2. the vertical wavelength $\lambda_{\mathrm{z}0}$, corresponding to the maximum FT-amplitude, decreases, and

3. the wave is more absorbed (a wave with a larger vertical wavelength penetrates deeper into the atmosphere).

What appears to be problematic for our further analysis is the fact that for a fixed κ_ω, we cannot associate a unique vertical wavelength to the wave (the λ_{z0} determined by analyzing the temperature *Background atmospheric parameters*. The code provides altitude-dependent profiles of the input parameters used in the numerical model. These include the temperature, vertical velocity, and horizontal velocity Fourier spectra are different). Solving this problem requires more effort in the futuremass density, pressure, southward horizontal velocity, atmospheric scale height, density scale height, specific heat capacity, ratio of specific heats, sound speed, number density of O^+ ions, neutral–ion collision frequency, ion–neutral collision frequency, and the diffusion velocity. In addition, altitude derivatives of the temperature, horizontal velocity, mass density, pressure, density scale height, and ion number density are also provided. As an illustrative example, Fig. 1 shows the background temperature T_0, horizontal velocity u_0 and the ion number density n_{i0}, together with their corresponding altitude derivatives.

Pairwise classification of ascending and descending modes. In the upper and middle panels of Fig. 2, we plot the imaginary part of the vertical wavenumber k_{zn}, $n = 1, \ldots, 6$ for the layer conditions (**??**) and (**??**). As expected, the for ascending (k_{z1}) and descending (k_{z4}) gravity waves, computed using the general and the simplified models, respectively. The plots demonstrate that only in the second case , latter case do the vertical wavenumbers appear in pairs. In the first case, the former case, a problematic altitude range for gravity waves seems to be from 50 km to 120 km, is observed between 80 km and 120 km, where the imaginary parts of the wavenumber for vertical wavenumbers for the ascending and descending modes are nearly identical, either positive or negative. Although the vertical wavenumbers do not appear in pairs, being either both positive or both negative. In the lower panel of Fig. 2, we show the imaginary part of the vertical wavenumber k_z for all wave types $(k_{zn}, n = 1, \ldots, 6)$, computed using the results obtained using both (i) global matrix methods with the scaling matrices (36) and (37), general model. The plots reveal a clear distinction between gravity waves and viscosity- and (ii) scattering matrix methods with classification rule (19) exhibit very close agreement. Furthermore, thermal-conduction waves. However, the viscosity and thermal-conduction waves are very close to each other. In the upper panel of Fig. 2, we also compare the imaginary part of the use of global matrix methods with the scaling matrices (**??**) and (**??**) (which take into account the classification of modes as ascending and descending) does not produce a significant change in the results (although not shown here, the relative errors are less than 10^{-5}). On the other hand, because vertical wavenumber computed with and without ion drag. No pronounced effect of ion drag on the vertical wavenumber is observed. A small effect appears in the altitude range from 50 to 120 km, the amplitudes of the waves are small, categorizing wave modes into pairs seems not to be essential. Parenthetically, we note thatthe wave modes almost appear in pairs for

1. the layer conditions that is, for a zero height derivative of the wind velocity, and
2. the layer conditions (**??**) but with the altitude z ranging from $z_{\min} = 125$ km to $z_{\max} = 450$ km.

This can be seen in the lower panels of Fig. 2. 180 to 300 km, where the ion number density is relatively high. This finding is consistent with the results of Shibata (1983), who showed that, for gravity waves, plasma diffusion is of minor importance with respect to the vertical wavenumber, which is mainly controlled by dissipation due to viscosity and thermal conduction in the neutral gas.

General and 5 to ascending and descending viscosity-wave modessimplified models. The altitude profiles of the perturbed temperature, respectivelyvertical velocity, and 3 horizontal velocity computed using the general and simplified models are shown in Fig. 3. The plots show that, in the altitude range 150–300 km, the amplitudes obtained with the general model are larger than

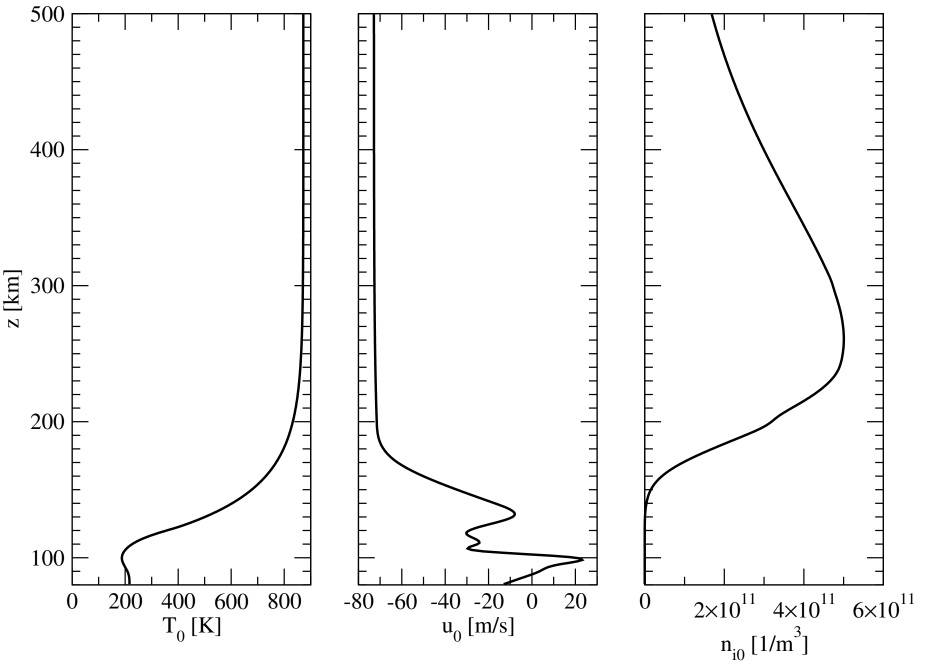

i

Altitude profiles of the perturbed temperature $\overline{T}_s$, vertical velocity $\overline{w}_s$, and horizontal velocity $\overline{u}_s$(upper panels), and their normalized FT-amplitudes in the spatial frequency domain (lower panels). The results correspond to $\kappa_\omega = 1$ (a), $\kappa_\omega = 0.8$ (b), and $\kappa_\omega = 0.6$ (c).

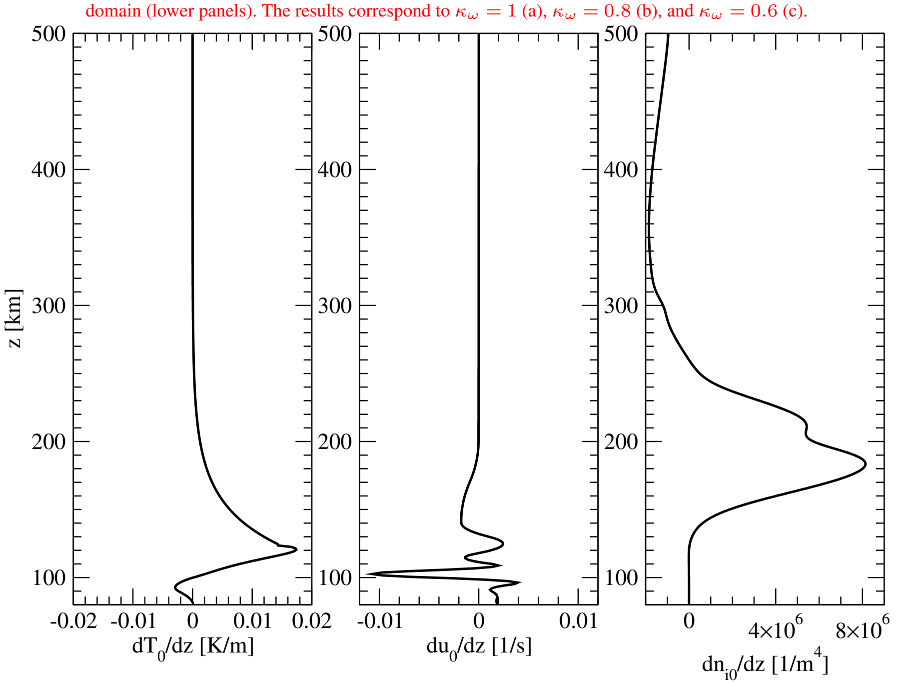

Figure 1. Vertical wavelengths, corresponding to the maximum FT-amplitudes, versus the frequency parameter κ_ω. The results are obtained by analyzing the Fourier spectra of the perturbed Background temperature (a)T_0, vertical horizontal velocity u_0 and ion number density n_{i0} (b$i = \mathrm{O}^+$) (upper panels), and horizontal velocity their height derivatives (clower panels).

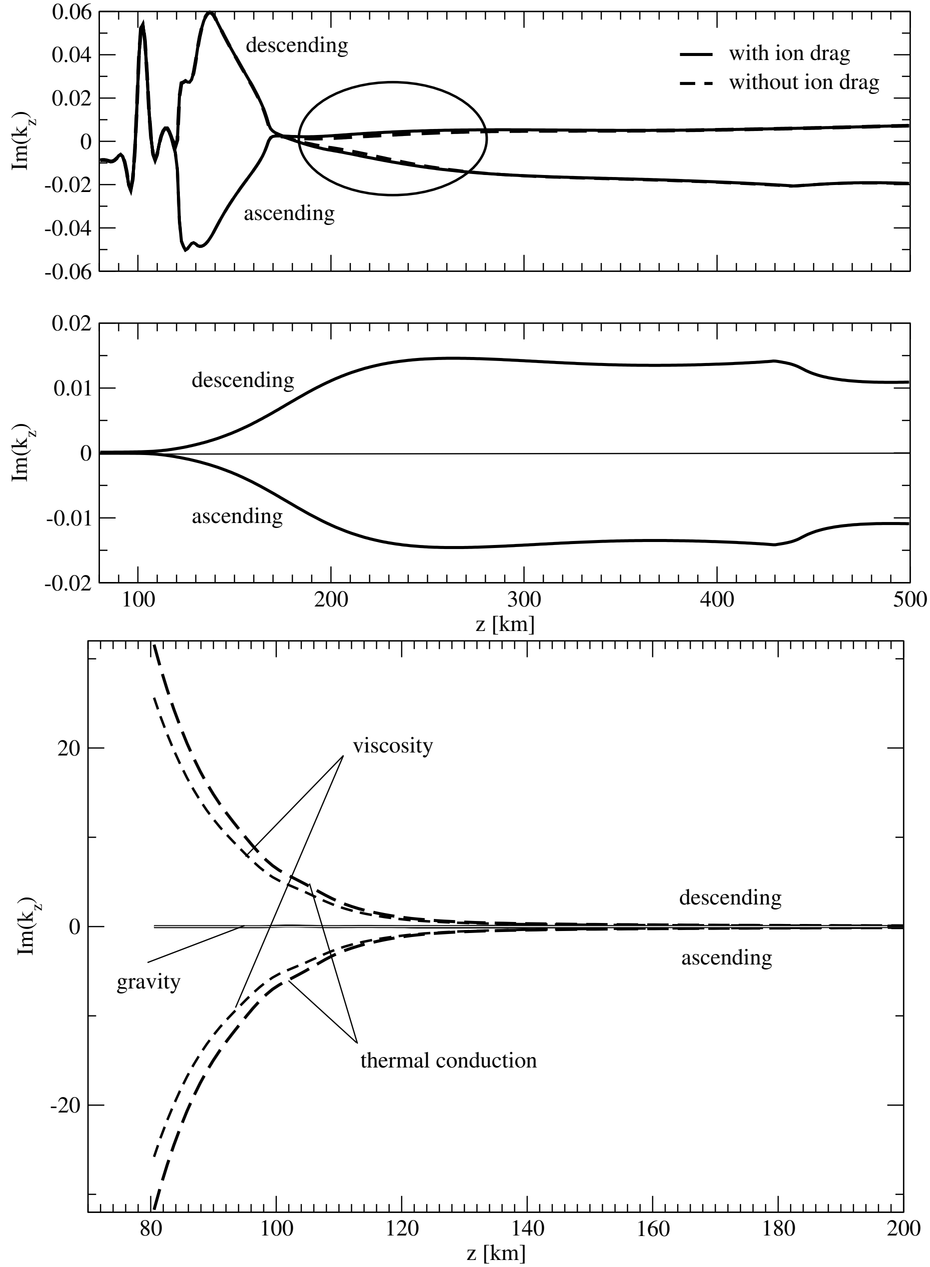

Figure 2. Upper panelspanel: The imaginary part of the vertical wavenumber $k_{zn}, n = 1, \ldots, 6$ $k_{\rm z}$ for the layer conditions ascending (**??**) (left)$k_{\rm z1}$) and descending ($k_{\rm z4}$) gravity waves, with and without ion drag, computed using the general model. Middle panel: The imaginary part of the vertical wavenumber $k_{\rm z}$ for ascending (**??**) $k_{\rm z1}$) and descending (right)$k_{\rm z4}$) gravity waves, computed using the simplified model. Lower panelspanel: The imaginary part of the vertical wavenumber $k_{zn}, n = 1, \ldots, 6$ $k_{\rm z}$ for the layer conditions all types of waves (**??**) (left)$k_{zn}, n = 1, \ldots, 6$), and (**??**) with $z_{\min} = 125$ km and $z_{\max} = 450$ km (right)computed using the general model. The labels 1 and 4 results correspond to ascending $\lambda_{\rm x} = 400$ km and descending gravity-wave modes, respectively, 2 $\lambda_{\rm t} = 40$ min

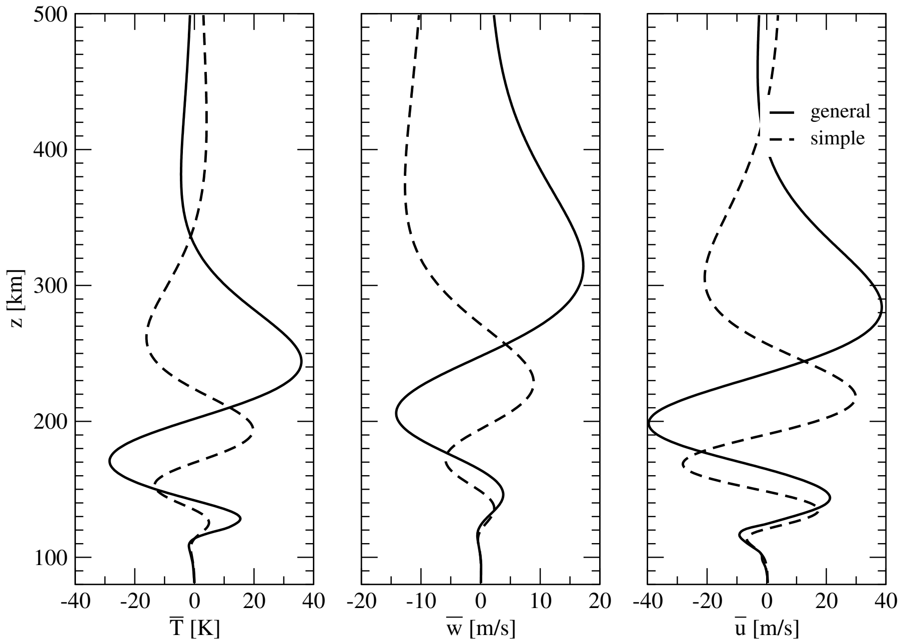

Figure 3. Altitude profiles of the perturbed temperature $\overline{T}$, vertical velocity $\overline{w}_s\overline{w}$, and horizontal velocity $\overline{u}_s$. The simulations are performed when the ion drag is excluded in the linearized equations, and when it is included; in the second case, the frequency parameter κ_ω is chosen as 1.2 $\overline{u}$ for the general and 0.8. The results in Fig. 4, show a complete agreement between the cases (i) ion-drag excluded and (ii) ion-drag included with $\kappa_\omega = 1.2$.simplified models. The results correspond to $\lambda_{\mathrm{x}} = 400$ km and $\lambda_{\mathrm{t}} = 40$ min

those obtained with the simplified model. If the imaginary parts of the vertical wavenumber for ascending gravity waves computed with the general and simplified models were plotted on the same graph (i.e. by merging the lower and 6 middle panels of Fig. 2), it would be seen that the imaginary part of the vertical wavenumber corresponding to the general model is negative but larger (i.e., less negative) than that obtained with the simplified model. As a consequence, the exponential attenuation with altitude is weaker in the general model, leading to systematically larger wave amplitudes in this region. This difference reflects the modified balance between wave propagation and dissipation introduced by the inclusion of altitude-dependent background properties and by relaxing the assumption of constant kinematic viscosity in the general model, which reduces the effective vertical damping compared to ascending and descending thermal conduction-wave modes, respectivelythe simplified, homogeneous approximation.

Ion drag. The ion-drag is important for time frequencies ω_0 that are smaller than the neutral-ion collision frequency ν_{0ni}. To verify this result, we analyze the influence of the ion-drag on the perturbed temperature$\overline{T}_s$

Ion Drag. The effect of ion drag on the perturbed temperature, vertical velocity, and horizontal velocity is illustrated in Fig. 4. A moderate attenuation is observed in the altitude range from 180 to 350 km, where the ion number density is relatively high. When $\mathbf{E} \times \mathbf{B}$ drifts are not included, ion drag does not exhibit the classical regime in which auroral convection strongly drives the neutral atmosphere. Instead, ion drag mainly arises from diffusion- and pressure-gradient-driven ion

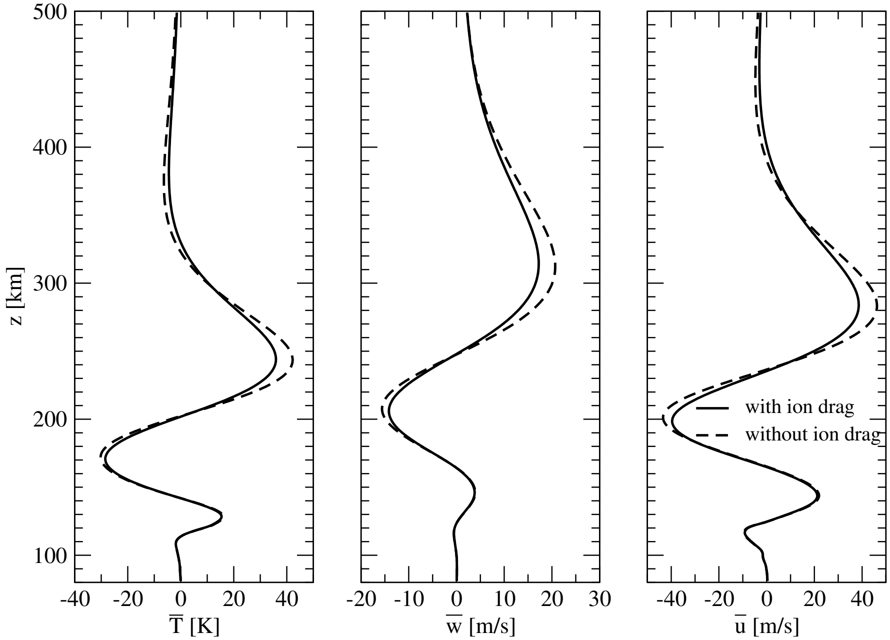

Altitude profiles of the perturbed temperature $\overline{T}_s$, vertical velocity $\overline{w}_s$, and horizontal velocity $\overline{u}_s$ when the ion drag is excluded in the linearized equations (a), and when it is included; in the latter case, the frequency parameter κ_ω is 1.2 (b) and 0.8 (c).

Figure 4. Altitude profiles of the perturbed temperature $\overline{T}$, vertical velocity $\overline{w}$, and horizontal velocity $\overline{u}$ for the general model, with and without ion drag. The results correspond to $\lambda_{\mathrm{x}} = 400$ km and $\lambda_{\mathrm{t}} = 40$ min

motion along the magnetic field, as well as from any relative ion–neutral motion induced by neutral winds. Consequently, ion drag does not constitute the dominant forcing mechanism for the neutral perturbations in this configuration.

Lower Boundary Condition. In Fig. **??** we show the results for the lower boundary conditions (43) and (56) with $\mathbf{b}_1 = [1, 0, \ldots, 0]^T$. The boundary condition (56)is imposed on the horizontal velocity $\widehat{u}_1^+$ $(q = 1)$ and the vertical velocity $\widehat{w}_1^+$ $(q = 2)$. In all cases, the amplitude s_0 in Eq. (**??**) is computed from Eq. (**??**) with $\delta_{\mathrm{T}} = 0.1$. Small differences are visible in the case (56) with $q = 2$, compared to *Horizontal wavelength and time period.* The influence of the other two cases.

horizontal wavelength λ_{x} and the wave period λ_{t} on the perturbed quantities is shown in Fig. 6. These plots indicate that the wave amplitude decreases with increasing λ_{x} and λ_{t}. The underlying reasons are as follows:

1. Horizontal wavelength. As the horizontal wavelength increases, horizontal pressure gradients become weaker, which reduces the driving of the wave motion. This also weakens the coupling between horizontal and vertical motions, resulting in smaller gravity-wave amplitudes.

2. Wave period. As the wave period increases, the buoyancy restoring force acts more slowly, leading to weaker oscillations for a given forcing. In addition, dissipative processes such as viscosity and thermal diffusion act more effectively on low-frequency waves, further reducing their amplitudes.

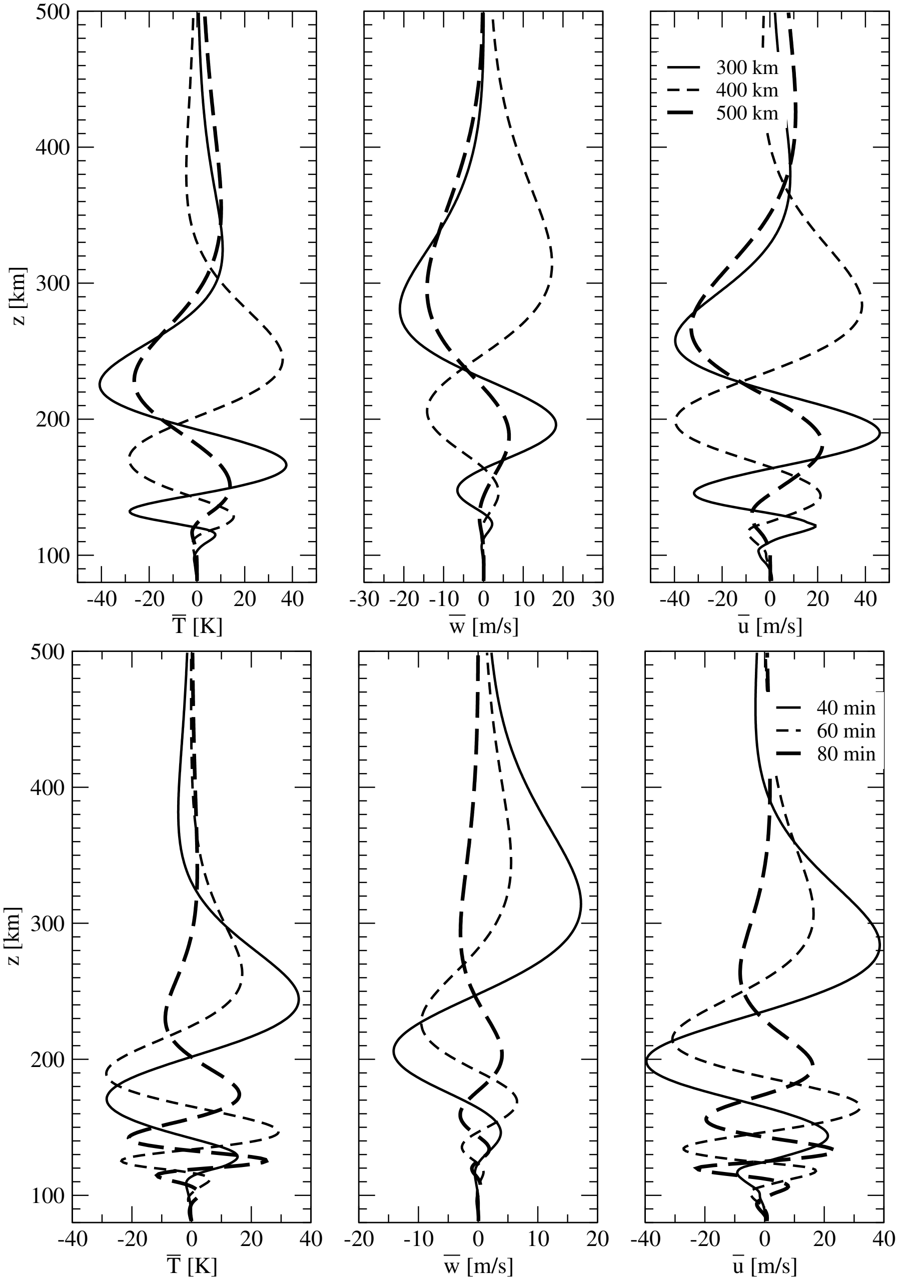

Lower altitude level. To model waves in the ionosphere, The results correspond to the lower altitude level was chosen by Volland (1969b), Klostermeyer (1972), and Shibata (1983) at 150 km, by Hickey and Cole (1988) at 120 km, and by Maeda (1985) at 100 km. Our choice $z_{\min} = 50$ km corresponds to that of Knight et al. (2019). It is interesting to see what is the effect of the lower altitude level on the results. In Fig. **??**, we plot the perturbed temperature altitude profile and its Fourier spectrum for $z_{\min} = 50$ km and $z_{\min} = 70$ km. In the two cases, the Fourier spectrum is practically unchanged, which makes us conclude that modifying the lower altitude level roughly causes a shift in the wave phase.

Perturbed temperature altitude profile and its Fourier spectrum for $z_{\min} = 50$ km (a) and $z_{\min} = 70$ km (b)general model with ion drag.

Lower altitude level. To model waves in the ionosphere, The results correspond to the lower altitude level was chosen by Volland (1969b), Klostermeyer (1972), and Shibata (1983) at 150 km, by Hickey and Cole (1988) at 120 km, and by Maeda (1985) at 100 km. Our choice $z_{\min} = 50$ km corresponds to that of Knight et al. (2019). It is interesting to see what is the effect of the lower altitude level on the results. In Fig. **??**, we plot the perturbed temperature altitude profile and its Fourier spectrum for $z_{\min} = 50$ km and $z_{\min} = 70$ km. In the two cases, the Fourier spectrum is practically unchanged, which makes us conclude that modifying the lower altitude level roughly causes a shift in the

Computing ascending and descending wave modes. The ascending and descending modes solution modes in layer l, denoted by $\mathbf{e}_l^+$ and $\mathbf{e}_l^-$, respectively, can be computed with Method 1 by using using the GMMA through Eq. (62) , or with Method 3 by using the or using the GMMN via the recurrence relations (C11) and (C12). The results in Fig. ?? demonstrate that (i) both methods yield almost the same results, and total solution mode $\mathbf{e}_l$, obtained from Eq. (ii) the dominant wave mode is the ascending mode. Encouraged by this result, we calculated the solution vector by using the recurrence relation (C15). The plots in Fig. ?? suggest that the approximation 60) in the GMMA formulation and by solving Eq. (C8) in the GMMN formulation, should satisfy the relation $\mathbf{e}_l = \mathbf{e}_l^+ + \mathbf{e}_l^-$. In all our simulations, this identity is satisfied. Furthermore, the results shown in Fig. 6 indicate that the ascending mode is dominant, except in the altitude range between 120 km and 180 km in the case of the general model. This finding, which is consistent with the results presented by Knight et al. (2019) (see their Fig. 6), suggests that in a simplified model one may assume the ascending modes to be dominant at altitudes above 200 km, that is, $\mathbf{e}_l \approx \mathbf{e}_l^+$ for $l = 1, \ldots, L$, does look quite reasonable; visible differences appear at high altitudes , say, at $z \geq 350\,\mathrm{km}$. Because this method is very efficient, it can be used to obtain quickly a primary information about the gravity wave$l = 1, \ldots, L$. Under this assumption, the state vector can be computed using the upward recurrence relation (C11). In Knight et al. (2019), this approach was referred to as the transmission-only approximation, whereas in Knight et al. (2021) a related single-mode approximation was introduced.

6.1 Time wavepacket

Time-dependent wave packet. For the source function (??), we plot in Fig. ??, the time dependent 83)–(84), Fig. 7 shows the perturbed temperature and vertical velocity profiles $\overline{T}_s(z,t)$ and $\overline{w}_s(z,t)$, respectively. For each perturbed temperature profile, we determine the pair $(z_0, t_0) = \arg\max_{z,t} \overline{T}_s(z,t)$, as functions of time and altitude. Note the different time intervals used for each horizontal wavelength λ_x in these plots. The maximum values of the perturbed temperature are 32.21 K, 31.15 K, and 32.73 K for the horizontal wavelengths 300 km, 500 km, and 700 km, respectively, whereas the corresponding maximum values of the vertical velocity are $21.40\,\mathrm{ms}^{-1}$, $16.21\,\mathrm{ms}^{-1}$, and depict in Fig. ??, the Gaussian envelope of the source function, still denoted by $s(t)$, together with the perturbation $\overline{T}_s(z_0,t)$. The plots reveal

1. a stronger attenuation of the waves in the case $\kappa_\omega = 0.6$;

2. a positive time shift between the maxima of the wave and source function envelops; the time shift is (i) $168\,\mathrm{mins}$ for $\kappa_\omega = 1$, (ii) $219\,\mathrm{mins}$ for $\kappa_\omega = 0.8$, and (iii) $376\,\mathrm{mins}$ for $\kappa_\omega = 0.6$.

Note that the computation time was $25\,\mathrm{s}$ for Method 1 and $1530\,\mathrm{s}$ for Method 2. If in the case of a pulse source function, we interpret causality in terms of the occurrence of maximum values, we can conclude that this is preserved. $12.08\,\mathrm{ms}^{-1}$.

To understand the link between causality and imaginary frequency shifting, we plot in the upper panels of Fig. ?? the real part of the eigenvalue λ_n, $n = 1, \ldots, 6$ without and with an imaginary frequency shifting δ, that is, for $\delta = 0$ and $\delta = 5 \times 10^{-3}$. The results show that the causality condition (??)is not satisfied in the case $\delta = 0$, but is almost satisfied in the case $\delta = 5 \times 10^{-3}$. Coming to the causality condition (??), we illustrate in the lower panels of Fig. ??, the Gaussian envelope of the source function $s(t)$ together with the perturbations $\widehat{T}(z_0,t) = \widehat{T}_{\delta=0}(z_0,t)$ and $\widehat{T}_\delta(z_0,t)$ with $\delta = 5 \times 10^{-3}$. The plots highlight the fact that $\widehat{T}(z_0,t)$ has small oscillations around 0 for $t \leq 0$, *Imaginary frequency shift.* For the time-dependent wave packet, we choose the minimum and maximum values of the imaginary frequency shift as $\delta_\mathrm{min} = 10^{-6}\ \mathrm{s}^{-1}$ and $\delta_\mathrm{max} = 10^{-4}\ \mathrm{s}^{-1}$, respectively, and set the discrete step to $\Delta\delta = \delta_\mathrm{min}$. Referring

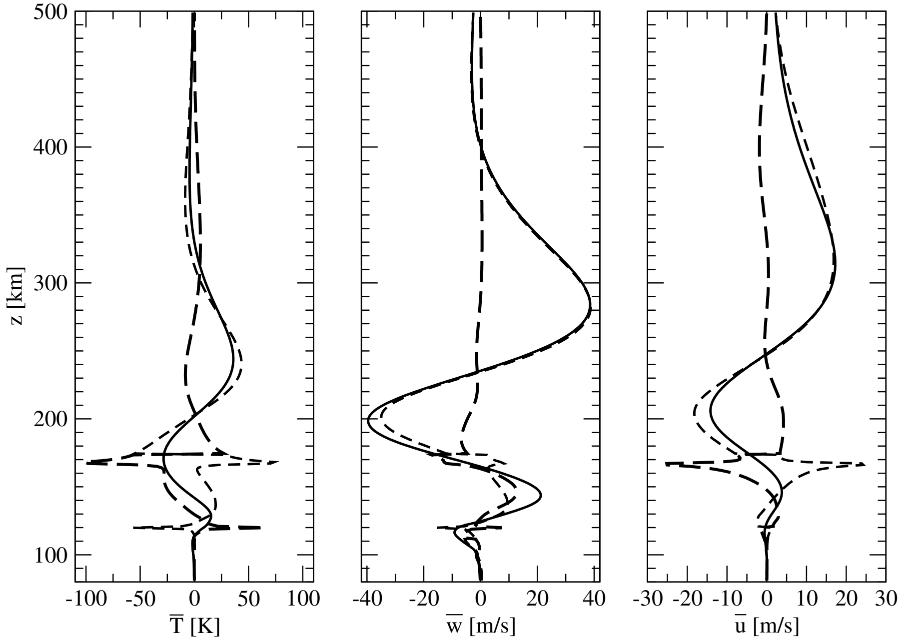

Upper panels: Altitude profiles of the perturbed temperature $\overline{T}_s$ corresponding to ascending and descending modes and being computed with Method 1 (a) and Method 3 (b).

Lower panels: Altitude profiles of the perturbed temperature $\overline{T}_s$, vertical velocity $\overline{w}_s$, and horizontal velocity $\overline{u}_s$ corresponding to the total wave mode (a), ascending mode (b), and descending mode (c). The results are computed with Method 1.

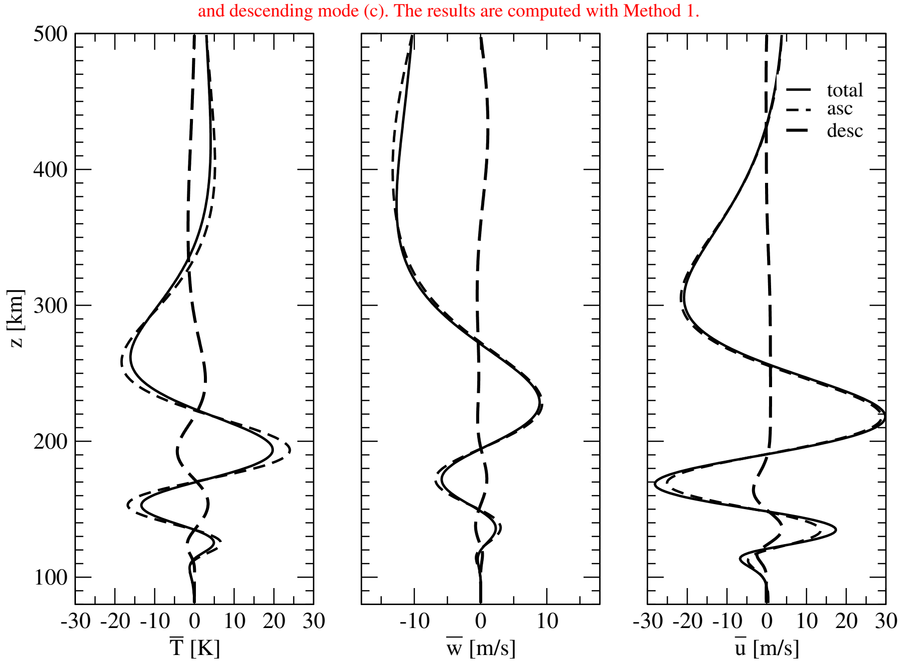

Figure 6. Altitude profiles of the perturbed temperature $\overline{T}_s\overline{T}$, vertical velocity $\overline{w}_s\overline{w}$, and horizontal velocity $\overline{u}_s$ computed with Method 1 $\overline{u}$ for the total mode (a$\mathbf{e}_l = \mathbf{e}_l^+ + \mathbf{e}_l^-$ in layer l), and by using the recurrence relation ascending mode (C15$\mathbf{e}_l^+$), and the descending mode (b$\mathbf{e}_l^-$). The upper panels correspond to the general model, and the lower panels to the simplified model. The horizontal wavelength is $\lambda_x = 400$ km and the wave period is $\lambda_t = 40$ min

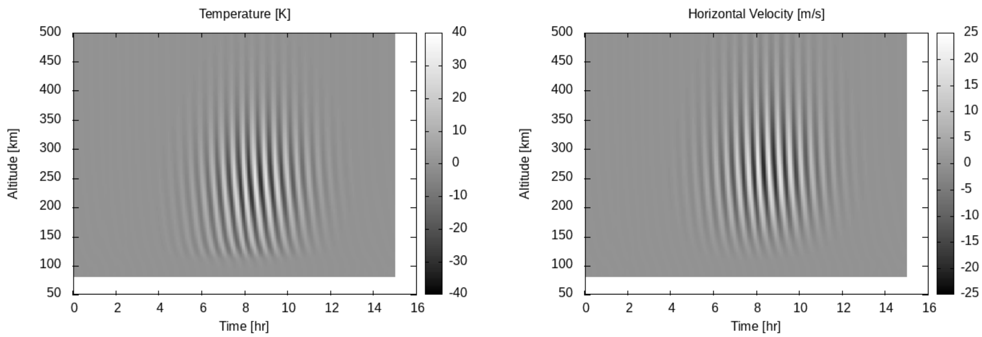

Perturbed temperature (left panels) and vertical velocity (right panels) as functions of time and altitude. The upper panels correspond to the frequency parameter $\kappa_\omega = 1$, the middle panels to $\kappa_\omega = 0.8$, and the lower panels to $\kappa_\omega = 0.6$.

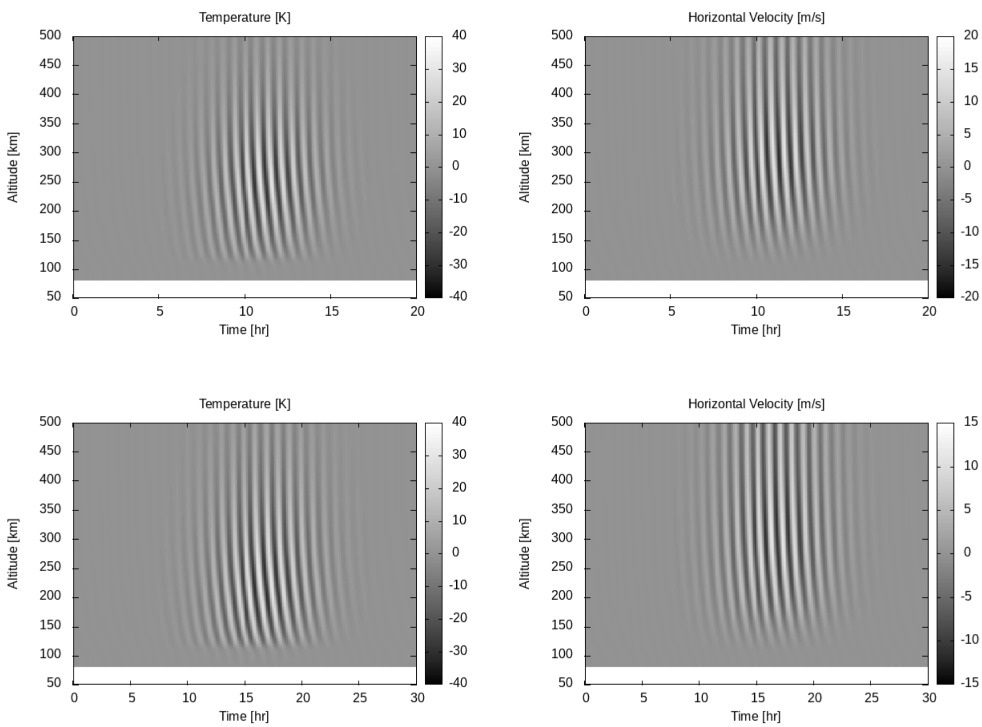

The Gaussian envelope of the source function s together with the perturbation $\overline{T}_s(z_0,\cdot)$. The results correspond to the frequency parameter $\kappa_\omega = 1$ (a), $\kappa_\omega = 0.8$ (b), and $\kappa_\omega = 0.6$ (c).

Figure 7. Perturbed temperature (left panels) and vertical velocity (right panels) as functions of time and altitude. The upper panels correspond to $\lambda_x = 300$ km and $\lambda_t = 30$ min, the middle panels to $\lambda_x = 500$ km and $\lambda_t = 40$ min, and the lower panels to $\lambda_x = 700$ km and $\lambda_t = 60$ min

Table 2. Maximum values of the perturbed horizontal velocity ($\overline{u}_{\max}$), vertical velocity ($\overline{w}_{\max}$), and temperature ($\overline{T}_{\max}$) for different values of the imaginary frequency shift δ

$\delta\,[10^{-6}\mathrm{s}^{-1}]$	$\overline{u}_{\max}$ $[\mathrm{ms}^{-1}]$	$\overline{w}_{\max}$ $[\mathrm{ms}^{-1}]$	$\overline{T}_{\max}$ [K]
32.24	38.084	16.210	31.153
24.43	38.115	16.224	31.132
16.62	38.079	16.210	31.158
8.81	38.110	16.225	31.186
1.00	38.017	16.186	31.113

to Appendix D, the results obtained with the imaginary frequency shift approach for $\lambda_\mathrm{x} = 500$ km and $\lambda_\mathrm{t} = 40$ min are summarized as follows:

- In the first step, the input value $\delta_{\min} = 10^{-6}\ \mathrm{s}^{-1}$ passes the Source-Function Reconstruction (SFR) test.
- In the second step, the SFR test reduces the input value $\delta_{\max} = 10^{-4}\ \mathrm{s}^{-1}$ to $\delta_{\max} = 32.24 \times 10^{-6}\ \mathrm{s}^{-1}$.
- In the third step, it is found the the interval $[\delta_{\min}, \delta_{\max}]$ contains a sufficient number of internal grid points, spaced by $\Delta\delta$, to be used in the subsequent step.
- In the fourth step, the Layerwise Causality (LC) condition is evaluated at 10 altitude starting at 80 km with a spacing of 20 km. It is found to be satisfied for $\delta_{\mathrm{LC}} = \delta_{\min}$, and that these oscillations become smaller, in the case of $\widehat{T}_\delta(z_0, t)$. However, if we are not so strict in defining causality, we can accept the solution without imaginary frequency shifting as realistic. therefore for all $\delta \in [\delta_{\min}, \delta_{\max}]$, for which the SFR test also holds.
- In the fifth step, five equidistant frequency shifts in $[\delta_{\min}, \delta_{\max}]$ are considered; for each, the wave parameters and their maximum values are computed and the layerwise causality condition is verified over the full altitude range. All five frequency shifts satisfy this condition and yield very similar maximum amplitudes (Table 2). The final solution is selected as the one whose maximum-amplitude vector is closest to the center of mass in the space of perturbed horizontal velocity, vertical velocity, and temperature, corresponding to $\delta = 16.62 \times 10^{-6}\ \mathrm{s}^{-1}$. The maxima occur at 11.06 hr and 248.00 km for the horizontal velocity, 10.98 hr and 303.64 km for the vertical velocity, and 10.90 hr and 257.45 km for the temperature.

Upper panels: The real part of the eigenvalue λ_n, $n = 1, \ldots, 6$ for $\delta = 0$ (left) and $\delta = 5 \times 10^{-3}$ (right). The upper bound for ascending modes (AM) is indicated by a solid line, while the lower bound for descending modes (DM) is indicated by a dashed line. Lower panels: The Gaussian envelope of the source function s together with the perturbation $\widehat{T}(z_0, \cdot) = \widehat{T}_{\delta=0}(z_0, \cdot)$ and $\widehat{T}_\delta(z_0, \cdot)$ with $\delta = 5 \times 10^{-3}$.

7 Conclusions

We designed a numerical model for solving the linearized gravity-wave equations by using a multilayer method. The numerical model employs the following solution methods: , which is freely available as open-source code at https://github.com/AlexandruDoicu/Gravity-Waves. To decouple the hydrodynamic equations for the neutral atmosphere from the ionospheric equations, which are coupled through ion drag, we adopt a fast field-aligned diffusion approximation. This approximation may be viewed as a generalization of an approach originally proposed by Klostermeyer (1972).

To solve the linearized equations, we employ (i) global matrix methods using matrix exponentials , based on matrix exponentials and (ii) scattering matrix methods for determining either (ito determine either (a) the amplitudes of the characteristic solutions or (ii) the discrete b) the grid-point values of the solution state vector. Ascending and descending wave modes are identified according to the rule criterion that the real parts of the eigenvalues of the characteristic equation for ascending modes are smaller than those for descending modes (orequivalently, , equivalently, that the imaginary parts of the vertical wavenumbers are smaller). Global matrix methods with using the scaling matrices (36) and (37) , require defining require the classification of ascending and descending modes only at the upper and lower boundaries, while the use of the scaling matrices (??) and (??) requires a classification of modes as ascending and descending in each layer. Scattering matrix methods also lower and upper boundaries, whereas scattering matrix methods require an explicit determination of the mode type at every altitude. The model includes two types of lower boundary condition, namely, (43) and (56). is devoted to solving the linearized equations including viscosity, thermal conduction, and ion drag. A simplified model, corresponding to an isothermal, homogeneous atmosphere with constant kinematic viscosity, no background wind, and no ion drag, is also considered.

Depending on the type form of the source function, either single-frequency waves or time wavepackets time-dependent wave packets can be analyzed. The amplitude of the source function can be computed by imposing an upper bound for the perturbed temperature (??), or the horizontal wind velocity (??). The model is devoted to the solution of the linearized equations with viscosity, thermal conduction, and ion drag included. According to Eqs. (??) –(??), it can be simplified to an isothermal atmosphere with constant wind velocity, a homogeneous atmosphere, and an atmosphere without ion dragA heuristic approach for determining the imaginary frequency shift introduced by Knight et al. (2019) is also considered. This approach is based on (i) a layerwise causality condition applied at selected altitude levels, and (ii) a source-function reconstruction test.

Numerical simulations demonstrate that both global matrix and scattering matrix methods achieve comparable accuraciesaccuracy. However, the former exhibit significantly greater efficiency are significantly more efficient than the latter, especially noticeable particularly in simulations involving time wavepackets. Within time-dependent wave packets. Among the global matrix methods, the approach that solves based on solving for the amplitudes of the characteristic solutions appears to offer provide the highest efficiency and accuracy.

The linearized equations on which the solution methods were tested correspond to the ionosphere. In fact, the final ionospheric conditions. The ultimate goal of our research is to design a complete develop a comprehensive model for analyzing ionospheric gravity waves from satellite limb using satellite measurements. The approach presented in this paper represents only the first component of this complete model. Our strategyinvolves a two-step process: first , to solve such a model. Two options are envisaged for extending it to a more complete formulation.

1. Fully coupled neutral–ion model. The linearized hydrodynamic equations would be solved together with the ion equations. In this case, the ion continuity equation would include perturbed production and loss terms, whereas ion inertia and ion–ion collisions would continue to be neglected in the ion momentum equation, and only transport parallel to the magnetic field lines would be retained. The state vector would then be augmented by two additional components, namely the perturbed ion number density and the ion diffusion velocity.

2. Two-step coupling strategy. In the first step, the neutral-atmosphere equations using Klostermeyer's approximation, and then, in are solved using the fast field-aligned diffusion approximation. In the second step, to use the wave-induced perturbations from the initial step obtained from the neutral solution are used as input to solve the ionospheric equations for the perturbed density of O^+ -ions and to calculate the volume emission rate of a line with a wavelength of 630.0 nmion density. The ionospheric equations will may be solved using the SAMI2 model (Huba et al., 2000) . Thus, our strategyis to prioritize for low latitudes, where the $\mathbf{E}\times\mathbf{B}$ drift is neglected, or the SAMI3 model (Huba et al., 2008) at higher altitudes, where the $\mathbf{E}\times\mathbf{B}$ drift is included and the electric field is determined from the solution of a two-dimensional potential equation. In this strategy, priority is given to the ionospheric equations of the SAMI2 model, and to manage the SAMI framework, while wave-induced perturbations using the present approximate approach . The final goal we proposed also explains some of the approximations we made. First, we use a linearized model for faster processing of the measurements made by the satellite instrument. Second, we consider a two-dimensional geometry because for limb measurements, it is much easier in this case to account for the curvature of the atmosphere through a series of approximations, such as the shallow-atmosphere approximation and an order-of-magnitude approximation. A comprehensive description of this complete model are handled using the approximate approach developed in the present study. Along similar lines, Knight et al. (2025) solved the neutral-atmosphere equations without ion drag in a first step, and subsequently addressed the ionospheric response using the Field-Line Interhemispheric Plasma (FLIP) model (Richards and Peterson, 2008).

The development and application of these complete models will be addressed in a future paperfuture papers.

Appendix A: The linearized hydrodynamic equations for Derivation of the neutral atmospherelinear system of ordinary differential equations

In this appendixwe present a general model for the hydrodynamic equations including viscosity, thermal conduction, and ion drag, together with some simplified models, which are frequently found in the literature, we derive the explicit representation of the linear system of ordinary differential equations (5).

A1. General model

A1 Hydrodynamic equations

To solve the linearized The hydrodynamic equations for the neutral atmosphere , we use assumptions A1–A4, consist in the continuity, momentum, heat, and ideal gas equations (e.g., Midgley and Liemohn (1966); Volland (1969a))

$$\frac{\mathrm{D}\rho}{\mathrm{D}t} = -\rho\nabla\cdot\mathbf{u}, \tag{A1}$$

$$\rho\frac{\mathrm{D}\mathbf{u}}{\mathrm{D}t} = -\nabla p + \rho\mathbf{g} + \nabla\cdot\overline{\boldsymbol{\sigma}} - \mathbf{f}_{\mathrm{ID}}, \tag{A2}$$

$$\rho c_{\mathrm{v}}\frac{\mathrm{D}T}{\mathrm{D}t} = -p\nabla\cdot\mathbf{u} + \overline{\boldsymbol{\sigma}}:\nabla\mathbf{u} + \nabla\cdot(\Lambda\nabla T) - q_{\mathrm{ID}}, \tag{A3}$$

$$p = \rho R_{\mathrm{M}} T, \tag{A4}$$

where ρ is the density, p the pressure, T the temperature, $\mathbf{u}$ the velocity, $\mathrm{D}/\mathrm{D}t = \partial/\partial t + \mathbf{u}\cdot\nabla$ the material (substantial) derivative, c_{v} the specific heat at constant volume, Λ the coefficient of thermal conductivity, R_{M} the specific gas constant, and $\overline{\boldsymbol{\sigma}}$ the viscous stress tensor. The quantities $\mathbf{f}_{\mathrm{ID}}$ and let q_{ID} denote the ion-drag force exerted by neutrals on ions per unit volume, and the frictional heating rate per unit volume arising from ion–neutral collisions, respectively. In a Cartesian coordinate system (x_1, x_2, x_3), the components of the viscous stress tensor are given by

$$\sigma_{ij} = \mu\left(\frac{\partial u_i}{\partial x_j} + \frac{\partial u_j}{\partial x_i} - \frac{2}{3}\delta_{ij}\nabla\cdot\mathbf{u}\right), \tag{A5}$$

where I the geomagnetic inclination (being positive in the northern hemisphere) . For μ is the dynamic viscosity and δ_{ij} the Kroneker delta. Accordingly, the double dot product of $\overline{\boldsymbol{\sigma}} = \sum_{ij}\sigma_{ij}\widehat{\mathbf{x}}_i\otimes\widehat{\mathbf{x}}_j$ with $\nabla\mathbf{u} = \sum_{ij}\partial u_i/\partial x_j\widehat{\mathbf{x}}_i\otimes\widehat{\mathbf{x}}_j$ is

$$\overline{\boldsymbol{\sigma}}:\nabla\mathbf{u} = \sum_{ij}\sigma_{ij}\frac{\partial u_i}{\partial x_j}. \tag{A6}$$

that is , and the linearized equations (??)–(??) Using the ideal-gas law $p = \rho R_{\mathrm{M}} T$ so that $\nabla p = \rho R_{\mathrm{M}}\nabla T + R_{\mathrm{M}} T\nabla\rho$, the momentum equation can be written in component form as as

$$\frac{\partial\mathbf{u}}{\partial t} = -\frac{R_{\mathrm{M}} T}{\rho}\nabla\rho - R_{\mathrm{M}}\nabla T - (\mathbf{u}\cdot\nabla)\mathbf{u} + \mathbf{g} + \frac{1}{\rho}\nabla\cdot\overline{\boldsymbol{\sigma}} - \frac{1}{\rho}\mathbf{f}_{\mathrm{ID}}. \tag{A7}$$

Moreover, using

$$c_{\mathrm{p}} = c_{\mathrm{v}} + R_{\mathrm{M}},\ \gamma = \frac{c_{\mathrm{p}}}{c_{\mathrm{v}}},\ \Lambda = \frac{c_{\mathrm{p}}\mu}{\mathrm{Pr}}, \tag{A8}$$

where c_{p} is the specific heat at constant pressure, γ the ratio of specific heats, and Pr the Prandtl number, and assuming that c_{p} and Pr are constant, the heat equation becomes

$$\frac{\partial T}{\partial t} = -(\gamma-1)T\nabla\cdot\mathbf{u} - \mathbf{u}\cdot\nabla T + \frac{1}{\rho c_{\mathrm{v}}}\overline{\boldsymbol{\sigma}}:\nabla\mathbf{u} + \frac{\gamma}{\rho\mathrm{Pr}}\nabla\cdot(\mu\nabla T) - \frac{1}{\rho c_{\mathrm{v}}}q_{\mathrm{ID}}. \tag{A9}$$

and

In the momentum and heat equations, the ion-drag force and the corresponding heating per unit mass are given by

$$\frac{1}{\rho}\mathbf{f}_{\mathrm{ID}} = \nu_{ni}(\mathbf{u} - \mathbf{u}_i), \tag{A10}$$

$$\frac{1}{\rho}q_{\mathrm{ID}} = \frac{1}{\rho}\mathbf{f}_{\mathrm{ID}}\cdot(\mathbf{u} - \mathbf{u}_i) = \nu_{ni}|\mathbf{u} - \mathbf{u}_i|^2, \tag{A11}$$

In the above equations, $\mathbf{f}'_{\mathrm{ID}} = (f'_{\mathrm{IDx}}, 0, f'_{\mathrm{IDz}})$, μ_0 and λ_0 are computed by using the relations (cf. Eq. (??)) where ν_{ni} is the neutral-ion collision frequency (the collision frequency between a neutral particle and all kind of ions).

We choose a rectangular coordinate system such that the x-axis is directed to the geographic south, the y-axis to the east and the z-axis upward. The wave propagates in the meridional plane, i.e., in the (x,z) plane. The viscous terms per unit mass in the momentum equation are then given by

$$\frac{1}{\rho}(\nabla\cdot\overline{\boldsymbol{\sigma}})_{\mathrm{x}} = \mu_{\mathrm{k}}\left[\left(\frac{\partial^2 u}{\partial x^2}+\frac{\partial^2 u}{\partial z^2}\right)+\frac{1}{3}\left(\frac{\partial^2 u}{\partial x^2}+\frac{\partial^2 w}{\partial x\partial z}\right)\right]+\frac{1}{\rho}\frac{\partial\mu}{\partial z}\left(\frac{\partial u}{\partial z}+\frac{\partial w}{\partial x}\right), \tag{A12}$$

$$\frac{1}{\rho}(\nabla\cdot\overline{\boldsymbol{\sigma}})_{\mathrm{z}} = \mu_{\mathrm{k}}\left[\left(\frac{\partial^2 w}{\partial x^2}+\frac{\partial^2 w}{\partial z^2}\right)+\frac{1}{3}\left(\frac{\partial^2 u}{\partial x\partial z}+\frac{\partial^2 w}{\partial z^2}\right)\right]+\frac{1}{\rho}\frac{\partial\mu}{\partial z}\left(\frac{4}{3}\frac{\partial w}{\partial z}-\frac{2}{3}\frac{\partial u}{\partial x}\right), \tag{A13}$$

respectively, while the quantities V_{T}, V_{dT}, C_{T}, C_{dT}, W_{u}, and W_{T} are given respectively, by viscous dissipation term per unit mass appearing in the heat equation is

$$\begin{aligned}\frac{1}{\rho}\overline{\boldsymbol{\sigma}}:\nabla\mathbf{u} = {}& \frac{4}{3}\mu_{\mathrm{k}}\left(\frac{\partial u}{\partial x}\right)^2-\frac{4}{3}\mu_{\mathrm{k}}\frac{\partial u}{\partial x}\frac{\partial w}{\partial z}+\frac{4}{3}\mu_{\mathrm{k}}\left(\frac{\partial w}{\partial z}\right)^2\\ &+\mu_{\mathrm{k}}\left(\frac{\partial u}{\partial z}\right)^2+2\mu_{\mathrm{k}}\frac{\partial u}{\partial z}\frac{\partial w}{\partial x}+\mu_{\mathrm{k}}\left(\frac{\partial w}{\partial x}\right)^2.\end{aligned} \tag{A14}$$

Here, $\mu_{\mathrm{k}} = \mu/\rho$ is the kinematic viscosity, and we have assumed that the viscosity depends only on altitude, so that

$$\frac{\partial\mu}{\partial x} = 0. \tag{A15}$$

In a second step, we use Eq. (??) to eliminate the mass density perturbation ρ' in Using Eqs. (??A12)–(??) , and in a third step, we assume the plane wave solutions A14) together with assumption (A15), we express the hydrodynamic equations as

$$\begin{aligned}\frac{\partial u}{\partial t} = {}& -\frac{R_{\mathrm{M}}T}{\rho}\frac{\partial\rho}{\partial x}-R_{\mathrm{M}}\frac{\partial T}{\partial x}-\left(u\frac{\partial u}{\partial x}+w\frac{\partial u}{\partial z}\right)\\ &+\mu_{\mathrm{k}}\left[\left(\frac{\partial^2 u}{\partial x^2}+\frac{\partial^2 u}{\partial z^2}\right)+\frac{1}{3}\left(\frac{\partial^2 u}{\partial x^2}+\frac{\partial^2 w}{\partial x\partial z}\right)\right]\\ &+\frac{1}{\rho}\frac{\partial\mu}{\partial z}\left(\frac{\partial u}{\partial z}+\frac{\partial w}{\partial x}\right)-\frac{1}{\rho}f_{\mathrm{IDx}},\end{aligned} \tag{A16}$$

$$\begin{aligned}\frac{\partial w}{\partial t} = {}& -\frac{R_{\mathrm{M}}T}{\rho}\frac{\partial\rho}{\partial z}-R_{\mathrm{M}}\frac{\partial T}{\partial z}-\left(u\frac{\partial w}{\partial x}+w\frac{\partial w}{\partial z}\right)-g\\ &+\mu_{\mathrm{k}}\left[\left(\frac{\partial^2 w}{\partial x^2}+\frac{\partial^2 w}{\partial z^2}\right)+\frac{1}{3}\left(\frac{\partial^2 u}{\partial x\partial z}+\frac{\partial^2 w}{\partial z^2}\right)\right]\\ &+\frac{1}{\rho}\frac{\partial\mu}{\partial z}\left(\frac{4}{3}\frac{\partial w}{\partial z}-\frac{2}{3}\frac{\partial u}{\partial x}\right)-\frac{1}{\rho}f_{\mathrm{IDz}},\end{aligned} \tag{A17}$$

$$\frac{\partial T}{\partial t} = -(\gamma-1)T\left(\frac{\partial u}{\partial x}+\frac{\partial w}{\partial z}\right) - \left(u\frac{\partial T}{\partial x}+w\frac{\partial T}{\partial z}\right)$$
$$+\frac{1}{c_{\mathrm{v}}}\left[\frac{4}{3}\mu_{\mathrm{k}}\left(\frac{\partial u}{\partial x}\right)^2 - \frac{4}{3}\mu_{\mathrm{k}}\frac{\partial u}{\partial x}\frac{\partial w}{\partial z}+\frac{4}{3}\mu_{\mathrm{k}}\left(\frac{\partial w}{\partial z}\right)^2\right.$$
$$\left.+\mu_{\mathrm{k}}\left(\frac{\partial u}{\partial z}\right)^2+2\mu_{\mathrm{k}}\frac{\partial u}{\partial z}\frac{\partial w}{\partial x}+\mu_{\mathrm{k}}\left(\frac{\partial w}{\partial x}\right)^2\right]$$
$$+\frac{\mu_{\mathrm{k}}\gamma}{\mathrm{Pr}}\left(\frac{\partial^2 T}{\partial x^2}+\frac{\partial^2 T}{\partial z^2}\right)+\frac{\gamma}{\rho \mathrm{Pr}}\frac{\partial \mu}{\partial z}\frac{\partial T}{\partial z}-\frac{1}{c_v\rho}q_{\mathrm{ID}}, \tag{A18}$$

where f_{IDx} and f_{IDz} are the components of the ion drag force $\mathbf{f}_{\mathrm{ID}}$ on the x- and z-axis, respectively.

In the above hydrodynamic equations, the Coriolis force has been neglected. For a two-dimensional wave geometry in which both the background flow and the perturbation velocities are confined to the vertical (x,z) plane and all variables are independent of the transverse horizontal coordinate y, the Coriolis acceleration associated with the Earth's rotation is directed entirely along the transverse direction and therefore does not enter the momentum equations considered here. More precisely, for $\mathbf{u}=(u,0,w)$ and $\mathbf{\Omega}=(-\Omega\cos\phi,0,\Omega\sin\phi)$, where f stands for u, w, p, T, and n_i. Under assumption (**??**), the linearized equations (**??**)–(**??**) transform into a linear system of ordinary differential equations. This system of ordinary differential equationswill be expressed in terms of the dimensionless quantities $\widehat{u}$, $\widehat{w}$, $\widehat{p}$, and $\widehat{T}$, defined through the relations ϕ is the geographic latitude and $\Omega = 7.29\times10^{-5}\,\mathrm{s}^{-1}$ the Earth's angular velocity, the Coriolis force per unit mass is $\mathbf{f}_{\mathrm{C}} = -2\mathbf{\Omega}\times\mathbf{u} = (0, 2\Omega(\cos\phi w+\sin\phi u), 0)$. Thus, the Coriolis acceleration is directed entirely along the transverse horizontal direction y and does not affect the two-dimensional (x,z) momentum equations.

and of the derivatives $\widehat{\mathcal{U}}$ and $\widehat{\mathcal{T}}$, defined through the relations

A2 Linearized equations

To linearize the hydrodynamic equations, we assume that all background (unperturbed) quantities vary only in the z-direction and write

$$f(x,z,t) = f_0(z)+f'(x,z,t),$$

where ω_0 is a reference frequency, and f denotes any state variable. In particular, we assume

$$\mathbf{u}_0(z) = (u_0(z),0,w_0(z)=0),\ \rho_0=\rho_0(z),\ T_0=T_0(z). \tag{A19}$$

are dimensionless parameters. The linear system of ordinary differential equationsconsist of six equations. These are:

Furthermore, we neglect the second derivative of the background horizontal wind and background temperature,

$$\frac{\mathrm{d}^2u_0}{\mathrm{d}z^2}=0,\ \frac{\mathrm{d}^2T_0}{\mathrm{d}z^2}=0, \tag{A20}$$

1. The linearized continuity equation is

$$\frac{\partial \rho'}{\partial t} = -u_0\frac{\partial \rho'}{\partial x}+\frac{\rho_0}{H_\rho}w'-\rho_0\left(\frac{\partial u'}{\partial x}+\frac{\partial w'}{\partial z}\right). \tag{A21}$$

2. The linearized momentum equations are

$$\frac{\partial u'}{\partial t} = -\frac{\mathrm{d}u_0}{\mathrm{d}z}w' - u_0\frac{\partial u'}{\partial x} - \frac{c_\mathrm{s}^2}{\gamma\rho_0}\frac{\partial \rho'}{\partial x} - \frac{c_\mathrm{s}^2}{\gamma T_0}\frac{\partial T'}{\partial x}
+ \mu_{\mathrm{k}0}\left[\left(\frac{\partial^2 u'}{\partial x^2} + \frac{\partial^2 u'}{\partial z^2}\right) + \frac{1}{3}\left(\frac{\partial^2 u'}{\partial x^2} + \frac{\partial^2 w'}{\partial x \partial z}\right)\right]
+ \frac{1}{\rho_0}\frac{\mathrm{d}\mu_0}{\mathrm{d}z}\left(\frac{\partial u'}{\partial z} + \frac{\partial w'}{\partial x}\right) + \frac{1}{\rho_0}\frac{\mathrm{d}u_0}{\mathrm{d}z}\frac{\partial \mu'}{\partial z} - \frac{1}{\rho_0}\frac{\mathrm{d}\mu_0}{\mathrm{d}z}\frac{\mathrm{d}u_0}{\mathrm{d}z}\frac{\rho'}{\rho_0} - \left(\frac{1}{\rho}f_{\mathrm{IDx}}\right)' \tag{A22}$$

and

$$\frac{\partial w'}{\partial t} = -\frac{c_\mathrm{s}^2}{\gamma\rho_0}\frac{\partial \rho'}{\partial z} + \frac{c_\mathrm{s}^2}{\gamma H_\rho}\left(\frac{T'}{T_0} - \frac{\rho'}{\rho_0}\right) - \frac{c_\mathrm{s}^2}{\gamma T_0}\frac{\partial T'}{\partial z} - u_0\frac{\partial w'}{\partial x}
+ \mu_{\mathrm{k}0}\left[\left(\frac{\partial^2 w'}{\partial x^2} + \frac{\partial^2 w'}{\partial z^2}\right) + \frac{1}{3}\left(\frac{\partial^2 u'}{\partial x \partial z} + \frac{\partial^2 w'}{\partial z^2}\right)\right]
+ \frac{1}{\rho_0}\frac{\mathrm{d}\mu_0}{\mathrm{d}z}\left(\frac{4}{3}\frac{\partial w'}{\partial z} - \frac{2}{3}\frac{\partial u'}{\partial x}\right) - \left(\frac{1}{\rho}f_{\mathrm{IDz}}\right)', \tag{A23}$$

where

$$c_\mathrm{s} = \sqrt{\gamma R_\mathrm{M} T_0} \tag{A24}$$

is the speed of sound and H_ρ is the density scale height defined by

$$\frac{\mathrm{d}\rho_0}{\mathrm{d}z} = -\frac{\rho_0}{H_\rho}. \tag{A25}$$

Here, $(f_{\mathrm{IDx}}/\rho)'$ and $(f_{\mathrm{IDz}}/\rho)'$ denote the perturbations of the x- and z-components, respectively, of the ion-drag force per unit mass f_{IDx}/ρ and f_{IDz}/ρ.

3. The linearized heat equation is

$$\frac{\partial T'}{\partial t} = -(\gamma-1)T_0\left(\frac{\partial u'}{\partial x} + \frac{\partial w'}{\partial z}\right) - \left(u_0\frac{\partial T'}{\partial x} + \frac{\mathrm{d}T_0}{\mathrm{d}z}w'\right)
+ \frac{2\mu_{\mathrm{k}0}}{c_\mathrm{v}}\frac{\mathrm{d}u_0}{\mathrm{d}z}\left(\frac{\partial u'}{\partial z} + \frac{\partial w'}{\partial x}\right) + \frac{\mu_0}{c_\mathrm{v}\rho_0}\left(\frac{\mathrm{d}u_0}{\mathrm{d}z}\right)^2\left(\frac{\mu'}{\mu_0} - \frac{\rho'}{\rho_0}\right)
+ \frac{\mu_{\mathrm{k}0}\gamma}{\mathrm{Pr}}\left(\frac{\partial^2 T'}{\partial x^2} + \frac{\partial^2 T'}{\partial z^2}\right) + \frac{\gamma}{\rho_0 \mathrm{Pr}}\left(\frac{\mathrm{d}\mu_0}{\mathrm{d}z}\frac{\partial T'}{\partial z} + \frac{\mathrm{d}T_0}{\mathrm{d}z}\frac{\partial \mu'}{\partial z}\right) - \frac{1}{c_\mathrm{v}}\left(\frac{1}{\rho}q_{\mathrm{ID}}\right)', \tag{A26}$$

where $(q_{\mathrm{ID}}/\rho)'$ denotes the perturbation of the ion-drag heating per unit mass.

The linearized equations (A21), (A22), (A23), and (A26) are structurally consistent with Eqs. (7), (4), (5), and (6) in Vadas and Nicolls (2012), respectively, when only the terms in black and blue are considered (the terms indicated in red are not included). They are likewise related to Eqs. (3.5), (3.1), (3.3), and (3.4) in Knight et al. (2024), when only the terms indicated in black are considered (the additional contributions indicated in red and blue are not included).

and

Using the following representation for the dynamic viscosity μ (Dalgarno and Smith, 1962)

$$\mu = 3.34\times 10^{-7} T^{0.71}, \tag{A27}$$

In Eqs. (**??**)–(**??**), we obtain

$$\mu' = 0.71\mu_0 \frac{T'}{T_0},\ \frac{\partial \mu'}{\partial z} = 0.71\frac{\mathrm{d}\mu_0}{\mathrm{d}z}\left(\frac{T'}{T_0}\right) + 0.71\mu_0\frac{\partial}{\partial z}\left(\frac{T'}{T_0}\right). \tag{A28}$$

With these relations, the linearized equations can be written as follows:

1. A_u, A_w, and A_p are given respectively, by x-momentum equation

$$\begin{aligned}\frac{\partial u'}{\partial t} =& -\frac{\mathrm{d}u_0}{\mathrm{d}z}w' - u_0\frac{\partial u'}{\partial x} - \frac{c_\mathrm{s}^2}{\gamma\rho_0}\frac{\partial \rho'}{\partial x} - \frac{c_\mathrm{s}^2}{\gamma T_0}\frac{\partial T'}{\partial x}\\ &+\mu_{\mathrm{k}0}\left[\left(\frac{\partial^2 u'}{\partial x^2} + \frac{\partial^2 u'}{\partial z^2}\right) + \frac{1}{3}\left(\frac{\partial^2 u'}{\partial x^2} + \frac{\partial^2 w'}{\partial x\partial z}\right)\right]\\ &+\frac{1}{\rho_0}\frac{\mathrm{d}\mu_0}{\mathrm{d}z}\left(\frac{\partial u'}{\partial z} + \frac{\partial w'}{\partial x}\right) + \frac{1}{\rho_0}\frac{\mathrm{d}u_0}{\mathrm{d}z}\left[0.71\frac{\mathrm{d}\mu_0}{\mathrm{d}z}\frac{T'}{T_0} + 0.71\mu_0\frac{\partial}{\partial z}\left(\frac{T'}{T_0}\right)\right]\\ &-\frac{1}{\rho_0}\frac{\mathrm{d}\mu_0}{\mathrm{d}z}\frac{\mathrm{d}u_0}{\mathrm{d}z}\frac{\rho'}{\rho_0} - \left(\frac{1}{\rho}f_{\mathrm{IDx}}\right)',\end{aligned} \tag{A29}$$

where $\widehat{\omega} = \omega - k_\mathrm{x}u_0$ is the intrinsic frequency,

2. the specific heat at constant volume is computed as $c_\mathrm{v} = R_\mathrm{M}/(\gamma-1)$, where $\gamma = 1.4$ is the ratio of specific heats and $R_\mathrm{M} = 287\,\mathrm{J/kg\,K}$ the specific gas constant,

3. the background neutral-ion collision frequency ν_{0ni} is calculated from Eq. (**??**),

4. the ion-drag terms in Eqs. (**??**)and (**??**)are given by z-momentum equation

$$\begin{aligned}\frac{\partial w'}{\partial t} =& -\frac{c_\mathrm{s}^2}{\gamma\rho_0}\frac{\partial \rho'}{\partial z} + \frac{c_\mathrm{s}^2}{\gamma H_\rho}\left(\frac{T'}{T_0} - \frac{\rho'}{\rho_0}\right) - \frac{c_\mathrm{s}^2}{\gamma T_0}\frac{\partial T'}{\partial z} - u_0\frac{\partial w'}{\partial x}\\ &+\mu_{\mathrm{k}0}\left[\left(\frac{\partial^2 w'}{\partial x^2} + \frac{\partial^2 w'}{\partial z^2}\right) + \frac{1}{3}\left(\frac{\partial^2 u'}{\partial x\partial z} + \frac{\partial^2 w'}{\partial z^2}\right)\right]\\ &+\frac{1}{\rho_0}\frac{\mathrm{d}\mu_0}{\mathrm{d}z}\left(\frac{4}{3}\frac{\partial w'}{\partial z} - \frac{2}{3}\frac{\partial u'}{\partial x}\right) - \left(\frac{1}{\rho}f_{\mathrm{IDz}}\right)',\end{aligned} \tag{A30}$$

and

5. heat equation

$$\begin{aligned}\frac{\partial T'}{\partial t} =& -(\gamma-1)T_0\left(\frac{\partial u'}{\partial x} + \frac{\partial w'}{\partial z}\right) - \left(u_0\frac{\partial T'}{\partial x} + \frac{\mathrm{d}T_0}{\mathrm{d}z}w'\right)\\ &+\frac{2\mu_{\mathrm{k}0}}{c_\mathrm{v}}\frac{\mathrm{d}u_0}{\mathrm{d}z}\left(\frac{\partial u'}{\partial z} + \frac{\partial w'}{\partial x}\right) + \frac{\mu_0}{c_\mathrm{v}\rho_0}\left(\frac{\mathrm{d}u_0}{\mathrm{d}z}\right)^2\left(0.71\frac{T'}{T_0} - \frac{\rho'}{\rho_0}\right)\\ &+\frac{\mu_{\mathrm{k}0}\gamma}{\mathrm{Pr}}\left(\frac{\partial^2 T'}{\partial x^2} + \frac{\partial^2 T'}{\partial z^2}\right) + \frac{\gamma}{\rho_0\mathrm{Pr}}\frac{\mathrm{d}\mu_0}{\mathrm{d}z}\frac{\partial T'}{\partial z}\\ &+\frac{\gamma}{\rho_0\mathrm{Pr}}\frac{\mathrm{d}T_0}{\mathrm{d}z}\left[0.71\frac{\mathrm{d}\mu_0}{\mathrm{d}z}\left(\frac{T'}{T_0}\right) + 0.71\mu_0\frac{\partial}{\partial z}\left(\frac{T'}{T_0}\right)\right] - \frac{1}{c_\mathrm{v}}\left(\frac{1}{\rho}q_{\mathrm{ID}}\right)'.\end{aligned} \tag{A31}$$

respectively,

A3 Plane wave solution

We assume that all perturbations vary harmonically in time and in the x-direction, that is,

$$f'(x,z,t) = \overline{f}(z)\mathrm{e}^{\mathrm{j}(\omega t - k_\mathrm{x} x)}, \tag{A32}$$

where and ω is the angular frequency and k_x the horizontal wavenumber. It then follows that

$$\frac{\partial f'}{\partial t} = \mathrm{j}\omega f', \; \frac{\partial f'}{\partial x} = -\mathrm{j}k_\mathrm{x} f', \; \frac{\partial^2 f'}{\partial x^2} = -k_\mathrm{x}^2 f'. \tag{A33}$$

and finally, the ion-drag term in Eq. (??)is given by

The linearized continuity equation becomes

$$\frac{\overline{\rho}}{\rho_0} = \frac{k_\mathrm{x}}{\Omega}\overline{u} - \frac{\mathrm{j}}{\Omega H_\rho}\overline{w} + \frac{\mathrm{j}}{\Omega}\frac{\mathrm{d}\overline{w}}{\mathrm{d}z}, \tag{A34}$$

where

$$\Omega = \omega - k_\mathrm{x} u_0 \tag{A35}$$

Note that the ion drag terms $\widehat{f}_{\mathrm{ID}x}$, $\widehat{f}_{\mathrm{ID}z}$, and $\widehat{P}_\mathrm{ID}$ are computed as described in the main text. In short, in a first step, we assume the representations $n_i'(x,z,t) = \overline{n}_i(z)\exp[\mathrm{j}(\omega t - k_\mathrm{x} x)]$ and $\overline{n}_i(z) = n_{0i}(z)\widehat{n}_i(z)$, and use the continuity equation (??) to obtain is the intrinsic frequency. Further, using

$$\frac{\mathrm{d}}{\mathrm{d}z}\left(\frac{\overline{\rho}}{\rho_0}\right) = \frac{1}{\rho_0}\frac{\mathrm{d}\overline{\rho}}{\mathrm{d}z} + \frac{1}{H_\rho}\frac{\overline{\rho}}{\rho_0} \tag{A36}$$

together with

$$\frac{\mathrm{d}\Omega}{\mathrm{d}z} = -k_\mathrm{x}\frac{\mathrm{d}u_0}{\mathrm{d}z}, \; \frac{\mathrm{d}\rho_0}{\mathrm{d}z} = -\frac{\rho_0}{H_\rho}, \tag{A37}$$

we obtain

$$\begin{aligned}\frac{1}{\rho_0}\frac{\mathrm{d}\overline{\rho}}{\mathrm{d}z} + \frac{1}{H_\rho}\frac{\overline{\rho}}{\rho_0} &= \frac{k_\mathrm{x}^2}{\Omega^2}\frac{\mathrm{d}u_0}{\mathrm{d}z}\overline{u} - \frac{\mathrm{j}}{\Omega H_\rho}\left(\frac{k_\mathrm{x}}{\Omega}\frac{\mathrm{d}u_0}{\mathrm{d}z} - \frac{1}{H_\rho}\frac{\mathrm{d}H_\rho}{\mathrm{d}z}\right)\overline{w} \\ &+ \frac{k_\mathrm{x}}{\Omega}\frac{\mathrm{d}\overline{u}}{\mathrm{d}z} + \frac{\mathrm{j}}{\Omega}\left(\frac{k_\mathrm{x}}{\Omega}\frac{\mathrm{d}u_0}{\mathrm{d}z} - \frac{1}{H_\rho}\right)\frac{\mathrm{d}\overline{w}}{\mathrm{d}z} + \frac{\mathrm{j}}{\Omega}\frac{\mathrm{d}^2\overline{w}}{\mathrm{d}z^2}.\end{aligned} \tag{A38}$$

In a second first step, we use Eq. (??) together with Eqs. (??A34) and (??)to derive a representation for $\widehat{\nu}_{ni}$, which is then substituted A38), together with the linearized forms of the momentum and the heat equation given in Eqs. (??)and (??)to compute the desired quantitiesA29)–(A31), to express the governing equations in terms of $\overline{u}$, $\overline{w}$, $\overline{T}/T_0$, and their vertical derivatives.

The linear In a second step, we introduce the dimensionless state variables $\widehat{u}$, $\widehat{w}$, and $\widehat{T}$, defined by

$$\overline{u}(z) = \frac{\omega_0}{k_\mathrm{x}}\widehat{u}(z), \; \overline{w}(z) = \frac{\omega_0}{k_\mathrm{x}}\widehat{w}(z), \; \overline{T}(z) = T_0(z)\widehat{T}(z), \tag{A39}$$

where ω_0 is a reference frequency, together with their vertical derivatives

$$\widehat{\mathcal{U}} = \frac{\mathrm{d}\widehat{u}}{\mathrm{d}z},\ \widehat{\mathcal{W}} = \frac{\mathrm{d}\widehat{w}}{\mathrm{d}z},\ \widehat{\mathcal{T}} = \frac{\mathrm{d}\widehat{T}}{\mathrm{d}z}. \tag{A40}$$

The state vector is organized as

$$\mathbf{e} = [\widehat{u}, \widehat{w}, \widehat{T}, \widehat{\mathcal{U}}, \widehat{\mathcal{W}}, \widehat{\mathcal{T}}]^{\mathrm{T}}$$

and the corresponding system of ordinary differential equations (??)–(??)can be written in matrix form as is given by

$$\frac{1}{k_{\mathrm{x}}}\frac{\mathrm{d}\widehat{u}}{\mathrm{d}z} = \frac{1}{k_{\mathrm{x}}}\widehat{\mathcal{U}}, \tag{A41}$$

$$\frac{1}{k_{\mathrm{x}}}\frac{\mathrm{d}\widehat{w}}{\mathrm{d}z} = \frac{1}{k_{\mathrm{x}}}\widehat{\mathcal{W}}, \tag{A42}$$

$$\frac{1}{k_{\mathrm{x}}}\frac{\mathrm{d}\widehat{T}}{\mathrm{d}z} = \frac{1}{k_{\mathrm{x}}}\widehat{\mathcal{T}}, \tag{A43}$$

where

$$\begin{aligned}
k_{\mathrm{x}}\mu_{\mathrm{k0}}\left(\frac{1}{k_{\mathrm{x}}}\frac{\mathrm{d}\widehat{\mathcal{U}}}{\mathrm{d}z}\right) = {} & \left[\mathrm{j}\Omega + \frac{4}{3}k_{\mathrm{x}}^2\mu_{\mathrm{k0}} + \frac{k_{\mathrm{x}}}{\Omega}\left(\frac{1}{\rho_0}\frac{\mathrm{d}\mu_0}{\mathrm{d}z}\frac{\mathrm{d}u_0}{\mathrm{d}z} - \mathrm{j}k_{\mathrm{x}}\frac{c_{\mathrm{s}}^2}{\gamma}\right)\right]\widehat{u} \\
& + \left[\frac{\mathrm{d}u_0}{\mathrm{d}z} + \mathrm{j}k_{\mathrm{x}}\frac{1}{\rho_0}\frac{\mathrm{d}\mu_0}{\mathrm{d}z} - \frac{\mathrm{j}}{\Omega H_\rho}\left(\frac{1}{\rho_0}\frac{\mathrm{d}\mu_0}{\mathrm{d}z}\frac{\mathrm{d}u_0}{\mathrm{d}z} - \mathrm{j}k_{\mathrm{x}}\frac{c_{\mathrm{s}}^2}{\gamma}\right)\right]\widehat{w} \\
& - \frac{k_{\mathrm{x}}}{\omega_0}\left(\mathrm{j}k_{\mathrm{x}}\frac{c_{\mathrm{s}}^2}{\gamma} + 0.71\frac{1}{\rho_0}\frac{\mathrm{d}\mu_0}{\mathrm{d}z}\frac{\mathrm{d}u_0}{\mathrm{d}z}\right)\widehat{T} - \frac{1}{\rho_0}\frac{\mathrm{d}\mu_0}{\mathrm{d}z}\widehat{\mathcal{U}} \\
& + \left[\frac{1}{3}\mathrm{j}k_{\mathrm{x}}\mu_{\mathrm{k0}} + \frac{\mathrm{j}}{\Omega}\left(\frac{1}{\rho_0}\frac{\mathrm{d}\mu_0}{\mathrm{d}z}\frac{\mathrm{d}u_0}{\mathrm{d}z} - \mathrm{j}k_{\mathrm{x}}\frac{c_{\mathrm{s}}^2}{\gamma}\right)\right]\widehat{\mathcal{W}} \\
& - 0.71\frac{\mu_0}{\rho_0}\frac{\mathrm{d}u_0}{\mathrm{d}z}\frac{k_{\mathrm{x}}}{\omega_0}\widehat{\mathcal{T}} + \frac{k_{\mathrm{x}}}{\omega_0}\overline{\left(\frac{1}{\rho}f_{\mathrm{IDx}}\right)},
\end{aligned} \tag{A44}$$

For a numerical solution, the atmosphere is divided into thin layers, and the altitude dependent matrix A is approximated by its value in the middle of each layer.

Some comments can be made here. The background quantities ρ_0, T_0, $p_0 = \rho_0 R_{\mathrm{M}} T_0$, u_0 and n_{0i} are assumed to be input parameters of the model

$$\begin{aligned}
k_{\mathrm{x}}\left(\frac{4}{3}\mu_{\mathrm{k0}} - \frac{\mathrm{j}c_{\mathrm{s}}^2}{\gamma\Omega}\right)\left(\frac{1}{k_{\mathrm{x}}}\frac{\mathrm{d}\widehat{\mathcal{W}}}{\mathrm{d}z}\right) = {} & \left(-\frac{2}{3}\mathrm{j}k_{\mathrm{x}}\frac{1}{\rho_0}\frac{\mathrm{d}\mu_0}{\mathrm{d}z} + \frac{c_{\mathrm{s}}^2k_{\mathrm{x}}^2}{\gamma\Omega^2}\frac{\mathrm{d}u_0}{\mathrm{d}z}\right)\widehat{u} \\
& + \left[\mathrm{j}\Omega + k_{\mathrm{x}}^2\mu_{\mathrm{k0}} - \frac{\mathrm{j}c_{\mathrm{s}}^2}{\gamma\Omega H_\rho}\left(\frac{k_{\mathrm{x}}}{\Omega}\frac{\mathrm{d}u_0}{\mathrm{d}z} - \frac{1}{H_\rho}\frac{\mathrm{d}H_\rho}{\mathrm{d}z}\right)\right]\widehat{w} \\
& - \frac{c_{\mathrm{s}}^2}{\gamma}\frac{k_{\mathrm{x}}}{\omega_0}\left(\frac{1}{H_\rho} - \frac{1}{T_0}\frac{\mathrm{d}T_0}{\mathrm{d}z}\right)\widehat{T} + \left(\frac{1}{3}\mathrm{j}k_{\mathrm{x}}\mu_{\mathrm{k0}} + \frac{k_{\mathrm{x}}c_{\mathrm{s}}^2}{\gamma\Omega}\right)\widehat{\mathcal{U}} \\
& + \left[\frac{\mathrm{j}c_{\mathrm{s}}^2}{\gamma\Omega}\left(\frac{k_{\mathrm{x}}}{\Omega}\frac{\mathrm{d}u_0}{\mathrm{d}z} - \frac{1}{H_\rho}\right) - \frac{4}{3}\frac{1}{\rho_0}\frac{\mathrm{d}\mu_0}{\mathrm{d}z}\right]\widehat{\mathcal{W}} \\
& + \frac{c_{\mathrm{s}}^2}{\gamma}\frac{k_{\mathrm{x}}}{\omega_0}\widehat{\mathcal{T}} + \frac{k_{\mathrm{x}}}{\omega_0}\overline{\left(\frac{1}{\rho}f_{\mathrm{IDz}}\right)},
\end{aligned} \tag{A45}$$

$$
\begin{aligned}
k_{\mathrm{x}}\frac{\mu_{\mathrm{k0}}\gamma}{\mathrm{Pr}}\left(\frac{1}{k_{\mathrm{x}}}\frac{\mathrm{d}\widehat{\mathcal{T}}}{\mathrm{d}z}\right) &= \omega_0\left[-\mathrm{j}(\gamma-1)+\frac{1}{\Omega}\frac{\mu_0}{c_{\mathrm{v}}T_0\rho_0}\left(\frac{\mathrm{d}u_0}{\mathrm{d}z}\right)^2\right]\widehat{u} \\
&+\frac{\omega_0}{k_{\mathrm{x}}}\left[\frac{1}{T_0}\frac{\mathrm{d}T_0}{\mathrm{d}z}+\mathrm{j}\frac{2\mu_{\mathrm{k0}}k_{\mathrm{x}}}{c_{\mathrm{v}}T_0}\frac{\mathrm{d}u_0}{\mathrm{d}z}-\frac{\mathrm{j}}{\Omega H_\rho}\frac{\mu_0}{c_{\mathrm{v}}T_0\rho_0}\left(\frac{\mathrm{d}u_0}{\mathrm{d}z}\right)^2\right]\widehat{w} \\
&+\left[\mathrm{j}\Omega+\frac{\mu_{\mathrm{k0}}\gamma}{\mathrm{Pr}}k_{\mathrm{x}}^2-C_1\frac{\gamma}{\rho_0\mathrm{Pr}}\frac{\mathrm{d}\mu_0}{\mathrm{d}z}\frac{1}{T_0}\frac{\mathrm{d}T_0}{\mathrm{d}z}-0.71\frac{\mu_0}{c_{\mathrm{v}}T_0\rho_0}\left(\frac{\mathrm{d}u_0}{\mathrm{d}z}\right)^2\right]\widehat{T} \\
&-\frac{2\mu_{\mathrm{k0}}}{c_{\mathrm{v}}T_0}\frac{\omega_0}{k_{\mathrm{x}}}\frac{\mathrm{d}u_0}{\mathrm{d}z}\widehat{\mathcal{U}}+\frac{\omega_0}{k_{\mathrm{x}}}\left[(\gamma-1)+\frac{\mathrm{j}}{\Omega}\frac{\mu_0}{c_{\mathrm{v}}T_0\rho_0}\left(\frac{\mathrm{d}u_0}{\mathrm{d}z}\right)^2\right]\widehat{\mathcal{W}} \\
&-\frac{\gamma}{\mathrm{Pr}}\left(\frac{1}{\rho_0}\frac{\mathrm{d}\mu_0}{\mathrm{d}z}+C_2\mu_{\mathrm{k0}}\frac{1}{T_0}\frac{\mathrm{d}T_0}{\mathrm{d}z}\right)\widehat{\mathcal{T}}+\frac{1}{c_{\mathrm{v}}T_0}\overline{\left(\frac{1}{\rho}q_{\mathrm{ID}}\right)}. \qquad \text{(A46)}
\end{aligned}
$$

Equations (A44), (A45), in which case, the derivatives are computed by finite-differences, and the derivatives $\mathrm{d}p_0/\mathrm{d}z$ and (A46) with the constants $C_1 = 1.71$ and $C_2 = 2.71$ correspond to the general model, in which all altitude derivatives of the background parameters u_0, T_0, H_ρ, and μ_0 are retained. The terms shown in black and blue in these equations, with the constants $C_1 = 1.0$ and $\mathrm{d}\rho_0/\mathrm{d}z$ with the relations $C_2 = 2.0$, correspond to the model of Vadas and Nicolls (2012). Moreover, Eqs. (A44), (A45), and (A46), when only the black terms are retained and the constants are set to $C_1 = C_2 = 0$, are consistent in form with Eqs. (3.32), (3.31), and (3.33) in Knight et al. (2024), respectively. Note that in Knight et al. (2024), the wave propagates in three-dimensional space, the harmonic dependence of the perturbed quantities is taken as $\exp[-\mathrm{j}(\omega t - k_{\mathrm{x}}x - k_{\mathrm{y}}y)]$, rather than $\exp[\mathrm{j}(\omega t - k_{\mathrm{x}}x)]$, the characteristic solutions have an $\exp(\mathrm{j}mz)$ dependence, rather than $\exp(k_{\mathrm{x}}\lambda z)$, and the state vector is defined as $[\overline{u}, \overline{w}, \widehat{T}, \overline{\mathcal{U}}, \overline{\mathcal{W}}, \widehat{\mathcal{T}}]^T$ instead of $[\widehat{u}, \widehat{w}, \widehat{T}, \widehat{\mathcal{U}}, \widehat{\mathcal{W}}, \widehat{\mathcal{T}}]^T$, where $\overline{\mathcal{U}} = \mathrm{d}\overline{u}/\mathrm{d}z$ and $\overline{\mathcal{W}} = \mathrm{d}\overline{w}/\mathrm{d}z$. Essentially, the difference between the model of Vadas and Nicolls (2012) and that of Knight et al. (2024) is that, in the latter, the derivative of the dynamic viscosity $\mathrm{d}\mu_0/\mathrm{d}z$ is omitted. In the code, for testing purposes, we included a hard-coded logical flag that selects the linearized model to be used. Our numerical simulations show that there are no significant differences between the general model and that of Vadas and Nicolls (2012), and that the effect of the assumption $\mathrm{d}\mu_0/\mathrm{d}z = 0$ is relatively small. This latter assumption was discussed in detail in Knight et al. (2024). In the general model, the derivative $\mathrm{d}\mu_0/\mathrm{d}z$ is computed as

$$
\frac{\mathrm{d}\mu_0}{\mathrm{d}z} = 0.71\mu_0\frac{1}{T_0}\frac{\mathrm{d}T_0}{\mathrm{d}z},
$$

where is the atmospheric scale height. whereas the derivatives of u_0, T_0, and H_ρ are computed using central finite differences.

The model can be particularized as follows:

1. for an isothermal atmosphere with constant wind velocity (characterized by For an isothermal ($T_0 = \mathrm{constant}$and $u_0 = \mathrm{constant}$), we set), homogeneous ($\mu_{\mathrm{k0}} = \mu_0/\rho_0 = \mathrm{constant}$), and windless atmosphere ($u_0 = 0$), we set

$$
\frac{\mathrm{d}u_0}{\mathrm{d}z} = 0,\ \frac{\mathrm{d}T_0}{\mathrm{d}z} = 0,\ \Omega = \omega_0,\ \frac{\mathrm{d}H_\rho}{\mathrm{d}z} = 0,\ \text{and}\ \frac{1}{\rho_0}\frac{\mathrm{d}\mu_0}{\mathrm{d}z} = -\frac{\mu_{\mathrm{k0}}}{H_\rho}. \qquad \text{(A47)}
$$

2. for a homogeneous atmosphere (characterized by $\mu_\mathrm{k} = \mu_0/\rho_0 =$ constant and $\lambda_\mathrm{k} = \lambda_0/\rho_0 =$ constant), we use the computational formulas In this case, the density scale height H_ρ coincides with the atmospheric scale height H_a, which satisfies

$$\frac{1}{\rho_0}\frac{\mathrm{d}\rho_0}{\mathrm{d}z} = \frac{1}{p_0}\frac{\mathrm{d}p_0}{\mathrm{d}z} = -\frac{1}{H_\mathrm{a}} \tag{A48}$$

and is given by

$$H_\mathrm{a} = \frac{p_0}{\rho_0 g} = \frac{R_\mathrm{M} T_0}{g} = \text{constant}. \tag{A49}$$

3. for For an atmosphere without ion drag, we set

$$f_\mathrm{IDx} = 0,\ f_\mathrm{IDz} = 0, \text{ and } q_\mathrm{ID} = 0. \tag{A50}$$

A2. Simplified models

A4 Dispersion equation

Consider an isothermal, homogeneous, and windless atmosphere, that is, For $\widehat{f}(z) \propto \exp(k_\mathrm{x}\lambda z)$, we obtain

$$\widehat{\mathcal{F}} = \frac{\mathrm{d}\widehat{f}}{\mathrm{d}z} = k_\mathrm{x}\lambda\widehat{f},\ \frac{\mathrm{d}\widehat{\mathcal{F}}}{\mathrm{d}z} = k_\mathrm{x}^2\lambda^2\widehat{f}, \tag{A51}$$

Assuming $\mathbf{f}'_\mathrm{ID} \approx \rho_0\nu_{0ni}[\mathbf{u}' - (\mathbf{u}'\cdot\widehat{\mathbf{b}})\widehat{\mathbf{b}}]$ and $P'_\mathrm{ID} \approx 0$ (compare with where f denotes u, w, and T, and $\mathcal{F}$ denotes $\mathcal{U}$, $\mathcal{W}$, and $\mathcal{T}$. Inserting Eq. (A51) into Eqs. (??)and (??)), we are led to the following linear system of ordinary differential equations($\omega_0 = \omega$): where the dimensionless parameters η A44)–(A46) yields a homogeneous system of equations. Requiring the determinant of this system to vanish, and ν are given by Eq. (??), while the parameters α, β, and σ are given respectively, by neglecting the ion-drag terms, leads to the following dispersion equation:

$$\begin{aligned}
&-\frac{\Omega}{c_\mathrm{s}^2}\left[\Omega - \mathrm{j}\frac{\gamma\mu_\mathrm{k0}}{\mathrm{Pr}}k_\mathrm{x}^2\left(1-\lambda^2\right)\right]\left[\Omega - \mathrm{j}\mu_\mathrm{k0}k_\mathrm{x}^2\left(1-\lambda^2\right)\right]\left[\Omega - \mathrm{j}\frac{4\mu_\mathrm{k0}}{3}k_\mathrm{x}^2\left(1-\lambda^2\right)\right]\\
&+\left[\Omega - \mathrm{j}\mu_\mathrm{k0}k_\mathrm{x}^2\left(1-\lambda^2\right)\right]\left[\Omega - \mathrm{j}\frac{\mu_\mathrm{k0}}{\mathrm{Pr}}k_\mathrm{x}^2\left(1-\lambda^2\right)\right]\left[k_\mathrm{x}^2\left(1-\lambda^2\right) + \frac{k_\mathrm{x}\lambda}{H_\rho}\right] - \frac{k_\mathrm{x}^2 c_\mathrm{s}^2}{\gamma^2 H_\rho^2}(\gamma-1)\\
&= 0.
\end{aligned} \tag{A52}$$

For $\mathbf{e} = [\widehat{u}, \widehat{w}, \widehat{p}, \widehat{T}, \widehat{\mathcal{U}}, \widehat{\mathcal{T}}]^T$, the matrix differential equation associated to the system of differential equations (??) –(??) is given by Eq. (??) . By further assuming that the geomagnetic field is either in The dispersion equation (A52) is the counterpart of dispersion relation (3.35) in Knight et al. (2024), under the aforementioned equivalences. Remarkably, it does not include derivatives of the background parameters u_0, T_0, H_ρ, and μ_0. This result follows from the variable-change method discussed by Knight et al. (2024) in their Section 2.2.

For an isothermal, homogeneous, and windless atmosphere without ion drag, the horizontal or the vertical direction, that is, by neglecting the terms containing the product $\cos I \sin I$ in Eqs. (??) and (??), we are led to the model developed by Francis (1973). In this case, the characteristic equation, also known as the dispersion equation , is reduces to the cubic equation (Midgley and Liemohn, 1966)

$$C_3R^3 + C_2R^2 + C_1R + C_0 = 0, \tag{A53}$$

with the coefficients for $R = -\lambda^2 + \alpha\lambda + 1$,where $\alpha = 1/k_\mathrm{x}H_\mathrm{a}$, or equivalently, $R = \kappa^2 - \mathrm{j}\alpha\kappa + 1$, where

$$\kappa = \mathrm{j}\lambda = \frac{1}{k_\mathrm{x}}\left(k_\mathrm{z} + \mathrm{j}\frac{1}{2H_\mathrm{a}}\right). \tag{A54}$$

The coefficients of the cubic equations are given by

$$C_3 = -3\eta\nu(1+4\eta), \tag{A55}$$

$$C_2 = \frac{3\eta(1+4\eta)}{\gamma-1} + \nu\beta(1+7\eta) + 3\eta, \tag{A56}$$

$$C_1 = -[\beta^2 - 2\eta\alpha^2(1+3\eta)]\nu - \frac{\beta(1+7\eta)}{\gamma-1} - \beta, \tag{A57}$$

$$C_0 = \frac{\beta^2 - 2\eta\alpha^2(1+3\eta)}{\gamma-1} + \alpha^2(1+3\eta), \tag{A58}$$

where

$$\eta = \mathrm{j}\frac{\omega_0\mu_0}{3p_0},\ \nu = \mathrm{j}\frac{k_\mathrm{x}^2\Lambda_0T_0}{\omega_0p_0},\ \Lambda_0 = \frac{\gamma c_\mathrm{v}\mu_0}{\mathrm{Pr}},\ \beta = \frac{\omega_0^2}{k_\mathrm{x}^2gH_\mathrm{a}}. \tag{A59}$$

If R_m, $m = 1,\ldots,3$ are the solutions of the dispersion equation, the corresponding vertical wavenumbers $k_{\mathrm{z}m}^{\pm}$ are computed as given by

$$k_{\mathrm{z}m}^{\pm} = \mp k_\mathrm{x}\sqrt{R_m - 1 - \frac{\alpha^2}{4}}. \tag{A60}$$

The wavenumbers $k_{\mathrm{z}m}^{+}$ with $\mathrm{Im}(k_{\mathrm{z}m}^{+}) < 0$ are associated with ascending modes, and whereas the wavenumbers $k_{\mathrm{z}m}^{-}$ with $\mathrm{Im}(k_{\mathrm{z}m}^{-}) > 0$ with correspond to descending modes. If we organize the wavenumbers $k_{\mathrm{z}m}^{+}$ Ordering the ascending wavenumbers as

$$\mathrm{Im}(k_{\mathrm{z}3}^{+}) < \mathrm{Im}(k_{\mathrm{z}2}^{+}) < \mathrm{Im}(k_{\mathrm{z}1}^{+}) < 0,$$

then we identify (i) $k_{\mathrm{z}1}^{+}$ and $k_{\mathrm{z}1}^{-}$ will correspond to as ascending and descending gravity-wave modes, respectively, (ii) $k_{\mathrm{z}2}^{+}$ and $k_{\mathrm{z}2}^{-}$ to as ascending and descending viscosity-wave modes, respectively, and (iii) $k_{\mathrm{z}3}^{+}$ and $k_{\mathrm{z}3}^{-}$ to as ascending and descending thermal conduction-wave thermal-conduction wave modes, respectively. Note that when the ion drag is completely neglected, the model simplifies to that of Midgley and Liemohn (1966)A similar cubic equation was derived by Francis (1973) under the assumption that the geomagnetic field is either in the horizontal or the vertical direction.

Consider For an isothermal, homogeneous, and windless atmosphere, and neglect without viscosity and ion drag. In this case, the linear system of ordinary differential equations simplify to (Volland, 1969b)

and the additional equation Thus, the matrix differential equation (**??**) is solved for $\mathbf{e} = [\widehat{w}, \widehat{p}, \widehat{T}, \widehat{\mathcal{T}}]^T$, and the dispersion equation is the , the dispersion equation (A53) reduces to the quadratic equation

$$C_2R^2 + C_1R + C_0 = 0, \tag{A61}$$

with

$$C_2 = \nu\beta, \tag{A62}$$

$$C_1 = -\beta^2\nu - \beta\frac{\gamma}{\gamma-1}, \tag{A63}$$

$$C_0 = \frac{\beta^2}{\gamma-1} + \alpha^2. \tag{A64}$$

For $\mathrm{Im}(k_{z2}^+) < \mathrm{Im}(k_{z1}^+) < 0$, the permissible modes are (i) the ascending and descending gravity-wave modes associated to the pair (k_{z1}^+, k_{z1}^-), and (ii) the ascending and descending thermal conduction-wave modes associated to the pair (k_{z2}^+, k_{z2}^-).

We conclude this appendix by presenting Hines' criticism of standard multilayer methods (Hines, 1973). Although this criticism does not pertain to our adopted method (a nonstandard multilayer method), we find itvaluable to discuss. This is especially pertinent since the solution methods we proposed can be applied to any linear system of ordinary differential equationswith constant coefficients. Hines mentioned that in a standard multilayer method,

Appendix B: Derivation of the ion-drag terms

In this appendix we derive the expressions for the ion-drag terms that enter the hydrodynamic equations (A44)–(A46).

B1 Ion equations

For each ion species i, the ion continuity equation is

$$\frac{\partial n_i}{\partial t} + \nabla\cdot(n_i\mathbf{u}_i) = P_i - n_i\mathcal{L}_i, \tag{B1}$$

and the corresponding ion momentum equation, including pressure gradient, electric field, magnetic field, gravity, and collisions, is

$$\begin{aligned}\frac{\partial \mathbf{u}_i}{\partial t} + (\mathbf{u}_i\cdot\nabla)\mathbf{u}_i = &-\frac{1}{m_i n_i}\nabla p_i + \frac{q_i}{m_i}\mathbf{E} + \frac{q_i}{m_i}\mathbf{u}_i\times\mathbf{B} + \mathbf{g}\\ &- \nu_{in}(\mathbf{u}_i - \mathbf{u}) - \sum_j \nu_{ij}(\mathbf{u}_i - \mathbf{u}_j).\end{aligned} \tag{B2}$$

Here n_i, $\mathbf{u}_i$, T_i, m_i, and $p_i = n_i k_\mathrm{B} T_i$ are the number density, velocity, temperature, mass, and pressure of ion species i; $\mathbf{E}$ is the electric field, $\mathbf{B}$ the magnetic field, q_i the ion charge, $\mathbf{g}$ the gravitational acceleration, and k_B the Boltzmann constant. The quantities P_i and $\mathcal{L}_i$ denote the ionization production rate and the loss rate due to chemical processes of ion i, respectively. The neutral wind velocity is $\mathbf{u}$, and the collision frequencies ν_{in} and ν_{ij} describe ion–neutral and ion–ion collisions.

In addition to ion equations, we consider the electron momentum equation

$$0 = -\frac{1}{m_e n_e}\nabla p_e - \frac{e}{m_e}\mathbf{E} - \frac{e}{m_e}\mathbf{u}_e\times\mathbf{B}, \tag{B3}$$

where n_e, $\mathbf{u}_e$, T_e, m_e, and $p_e = n_e k_\mathrm{B} T_e$ are the number density, velocity, temperature, mass, and pressure of electrons. In Eq. (B3), electron inertia is neglected because of the small electron mass, while electron collisional terms are neglected because $\nu_e \ll \Omega_e$, where ν_e denotes the electron collision frequencies and Ω_e is the electron cyclotron frequency.

In the ion momentum equation we neglect the ion inertia and the ion–ion collisions, and introduce the drift velocity $\mathbf{u}_{\mathrm{D}}$ by writing $\mathbf{u}_i = \mathbf{u} + \mathbf{u}_{\mathrm{D}}$. This yields

$$m_i \nu_{in} \mathbf{u}_{\mathrm{D}} = q_i \left[\mathbf{E} + (\mathbf{u} + \mathbf{u}_{\mathrm{D}}) \times \mathbf{B}\right] - \frac{1}{n_i} \nabla p_i + m_i \mathbf{g}. \tag{B4}$$

The momentum equation is projected along the direction of the magnetic field $\widehat{\mathbf{b}}$ and perpendicular to it. The parallel and perpendicular force-balance equations are

$$m_i \nu_{in} u_{\mathrm{D}\parallel} = q_i E_\parallel - \frac{1}{n_i} (\nabla p_i)_\parallel + m_i g_\parallel, \tag{B5}$$

and

$$m_i \nu_{in} \mathbf{u}_{\mathrm{D}\perp} = q_i \left[\mathbf{E}_\perp + (\mathbf{u}_\perp + \mathbf{u}_{\mathrm{D}\perp}) \times \mathbf{B}\right] - \frac{1}{n_i} (\nabla p_i)_\perp + m_i \mathbf{g}_\perp, \tag{B6}$$

respectively, where in general $\mathbf{a}_\parallel = (\mathbf{a} \cdot \widehat{\mathbf{b}})\widehat{\mathbf{b}} = a_\parallel \widehat{\mathbf{b}}$ and $\mathbf{a}_\perp = \mathbf{a} - \mathbf{a}_\parallel$. The parallel transport equation for electrons reduces to

$$E_\parallel = -\frac{1}{e n_e} \frac{\partial p_e}{\partial b}. \tag{B7}$$

The parallel and perpendicular force-balance equations are solved as follows. We first consider the ambipolar diffusion velocity, and then the electromagnetic drift velocity.

1. **Ambipolar diffusion velocity.** For a single dominant ion species of charge $q_i = +e$, the parallel force balance equation for ions becomes

$$m_i \nu_{in} u_{\mathrm{D}\parallel} = e E_\parallel - \frac{1}{n_i} \frac{\partial p_i}{\partial b} + m_i g_\parallel, \tag{B8}$$

where $\partial p_i / \partial b = \nabla p_i \cdot \widehat{\mathbf{b}}$. Inserting Eq. (B7) into Eq. (B8), gives

$$m_i \nu_{in} u_{\mathrm{D}\parallel} = -\left(\frac{1}{n_e} \frac{\partial p_e}{\partial b} + \frac{1}{n_i} \frac{\partial p_i}{\partial b}\right) + m_i g_\parallel, \tag{B9}$$

where $g_\parallel = \mathbf{g} \cdot \widehat{\mathbf{b}}$. Using the ideal-gas relations $p_i = n_i k_{\mathrm{B}} T_i$ and $p_e = n_e k_{\mathrm{B}} T_e$, assuming quasi-neutrality $n_e = n_i$, and thermal equilibrium $T_i = T_e = T$, we obtain

$$u_{\mathrm{D}\parallel} = -D_{\mathrm{A}} \left(\frac{1}{n_i} \frac{\partial n_i}{\partial b} + \frac{1}{T} \frac{\partial T}{\partial b}\right) + \frac{g_\parallel}{\nu_{in}}, \tag{B10}$$

where

$$D_{\mathrm{A}} = \frac{2 k_{\mathrm{B}} T}{m_i \nu_{in}} \tag{B11}$$

is the choice of the unknowns (the components of the vector $\mathbf{e}$)should depend on the physical meaning of the continuity condition at the layer interfaces. The choice (**??**)ambipolar diffusion coefficient.

2. **Electromagnetic drift velocity.** Neglecting perpendicular pressure-gradient and gravity terms, which are often small compared to the electromagnetic drift terms, and assuming a collisionless or weakly collisional limit in which the ion–neutral drag term is negligible, the perpendicular momentum balance reduces to

$$\mathbf{E}_{\perp} + (\mathbf{u}_{\perp} + \mathbf{u}_{\mathrm{D}\perp}) \times \mathbf{B} = 0. \tag{B12}$$

With $\mathbf{u}_{i\perp} = \mathbf{u}_{\perp} + \mathbf{u}_{\mathrm{D}\perp}$, this gives $\mathbf{u}_{i\perp} \times \mathbf{B} = -\mathbf{E}_{\perp}$, whose solution is the electromagnetic drift velocity

$$\mathbf{u}_{\mathrm{E}} = \frac{\mathbf{E}_{\perp} \times \mathbf{B}}{B^2} = \frac{\mathbf{E} \times \mathbf{B}}{B^2}. \tag{B13}$$

Consequently,

$$\mathbf{u}_{\mathrm{D}\perp} = \mathbf{u}_{\mathrm{E}} - \mathbf{u}_{\perp}. \tag{B14}$$

Collecting all contributions, the ion velocity can be written as

$$\mathbf{u}_i = \mathbf{u}_{\|} + \mathbf{u}_{\mathrm{D}\|} + \mathbf{u}_{\mathrm{E}}, \tag{B15}$$

where $\mathbf{u}_{\|} = (\mathbf{u} \cdot \widehat{\mathbf{b}})\widehat{\mathbf{b}}$ is the same as the one used by Volland (1969b) and implies the continuity of the pressure $\widehat{p}$. Midgley and Liemohn (1966) used instead the continuity of $\widehat{p} + \mathrm{j}\widehat{w}/(k_{\mathrm{x}} H_{\mathrm{a}})$, which reflects the continuity of the pressure perturbation $p' + \mathrm{j}wp_0/(\omega H_{\mathrm{a}})$ evaluated at the interface between two layers ; this interface being displaced by a distance $\mathrm{j}w/\omega$ from its ambient position because of the perturbing effect of the wavefield-aligned neutral velocity, $\mathbf{u}_{\mathrm{D}\|} = u_{\mathrm{D}\|}\widehat{\mathbf{b}}$ is the ambipolar diffusion velocity given by Eq. (B10), and $\mathbf{u}_{\mathrm{E}}$ is the electromagnetic drift velocity given by Eq. (B13). This expression follows from the decomposition $\mathbf{u}_i = \mathbf{u} + \mathbf{u}_{\mathrm{D}}$, together with $\mathbf{u}_{\mathrm{D}\perp} = \mathbf{u}_{\mathrm{E}} - \mathbf{u}_{\perp}$, so that the perpendicular neutral velocity cancels.

In our model, the ion velocity is assumed to be aligned with the magnetic field lines. This assumption is introduced to decouple the hydrodynamic and ion equation systems. Accordingly, the ion velocity is approximated by

$$\mathbf{u}_i \approx (\mathbf{u} \cdot \widehat{\mathbf{b}})\widehat{\mathbf{b}} + u_{\mathrm{D}\|}\widehat{\mathbf{b}}. \tag{B16}$$

This approximation is justified when perpendicular ion transport is small compared to the dominant field-aligned diffusion. The resulting formulation captures the leading-order effects of ambipolar diffusion along the magnetic field lines, while deliberately neglecting perpendicular electrodynamic coupling, such as cross-field advection and $\mathbf{E} \times \mathbf{B}$ drifts. Consequently, the model is applicable to regimes in which field-aligned transport dominates and perpendicular electrodynamic effects play a secondary role. We note, however, that the neglect of the electromagnetic drift velocity is not appropriate for all geophysical regimes. At high latitudes, ion convection is largely controlled by magnetospheric forcing (Dungey, 1961), and realistic modeling generally requires externally imposed convection electric fields, for example from empirical models such as Weimer (2005). At mid-latitudes, perpendicular ion motion may be influenced by inter-hemispheric coupling and neutral-wind differences between conjugate hemispheres (Laundal et al., 2025; Buchert, 2020). A fully self-consistent electrodynamic formulation, in which the electric field is obtained from an electrostatic potential Φ via $\mathbf{E} = -\nabla\Phi$, with Φ determined from quasi-neutral current continuity and the conductivity-tensor relation (Weimer, 2005), is therefore beyond the scope of the present study but constitutes an important extension for future work.

In the following, for simplicity, the subscript $\|$ is omitted, and we write $\mathbf{u}_{\mathrm{D}}$ and u_{D} instead of $\mathbf{u}_{\mathrm{D}\|}$ and $u_{\mathrm{D}\|}$, respectively. Let

$$\mathbf{g} = (0,0,-g),\ \widehat{\mathbf{b}} = (-\cos I, 0, -\sin I),\ \mathbf{u} = (u,0,w), \tag{B17}$$

where I is the geomagnetic inclination. The field-aligned derivative is

$$\frac{\partial}{\partial b} = \nabla\cdot\widehat{\mathbf{b}} = -\left(\cos I\frac{\partial}{\partial x} + \sin I\frac{\partial}{\partial z}\right),$$

and the scalar field-aligned diffusion velocity becomes (cf. Eq. (B10))

$$u_{\mathrm{D}} = D_{\mathrm{A}}\left(\cos I\frac{1}{n_i}\frac{\partial n_i}{\partial x} + \sin I\frac{1}{n_i}\frac{\partial n_i}{\partial z} + \cos I\frac{1}{T}\frac{\partial T}{\partial x} + \sin I\frac{1}{T}\frac{\partial T}{\partial z}\right) + \frac{g}{\nu_{in}}\sin I. \tag{B18}$$

B2 Linearized equations

The linearized continuity equation, together with the linearized expressions for the diffusion velocity, ion-drag force, and ion-drag heating, are as follows.

1. **Ion continuity equation**. Neglecting the perturbed production and loss terms, the perturbed ion continuity equation is

$$\frac{\partial n_i'}{\partial t} + n_i'\nabla\cdot\mathbf{u}_{i0} + \mathbf{u}_{i0}\cdot\nabla n_i' + n_{i0}\nabla\cdot\mathbf{u}_i' + \mathbf{u}_i'\cdot\nabla n_{i0} = 0. \tag{B19}$$

   Using Eq. (B17) and the standard assumptions $n_{i0} = n_{i0}(z)$, $\mathbf{u}_0(z) = (u_0(z), 0, 0)$, and $u_{\mathrm{D}0} = u_{\mathrm{D}0}(z)$, we obtain

$$\begin{aligned}
\frac{\partial}{\partial t}\left(\frac{n_i'}{n_{i0}}\right) = &-u_{\mathrm{D}0}\left[\frac{\partial}{\partial b}\left(\frac{n_i'}{n_{i0}}\right) - \frac{1}{n_{i0}}\frac{\mathrm{d}n_{i0}}{\mathrm{d}z}\sin I\left(\frac{n_i'}{n_{i0}}\right)\right] + \frac{\mathrm{d}u_{\mathrm{D}0}}{\mathrm{d}z}\sin I\left(\frac{n_i'}{n_{i0}}\right)\\
&+\left(\frac{\partial u'}{\partial b} - \frac{1}{n_{i0}}\frac{\mathrm{d}n_{i0}}{\mathrm{d}z}\sin I u'\right)\cos I + \left(\frac{\partial w'}{\partial b} - \frac{1}{n_{i0}}\frac{\mathrm{d}n_{i0}}{\mathrm{d}z}\sin I w'\right)\sin I\\
&-\left(\frac{\partial u_{\mathrm{D}}'}{\partial b} - \frac{1}{n_{i0}}\frac{\mathrm{d}n_{i0}}{\mathrm{d}z}\sin I u_{\mathrm{D}}'\right) + u_0\cos I\frac{\partial}{\partial b}\left(\frac{n_i'}{n_{i0}}\right)\\
&-\cos I\sin I\left(\frac{\mathrm{d}u_0}{\mathrm{d}z} + u_0\frac{1}{n_{i0}}\frac{\mathrm{d}n_{i0}}{\mathrm{d}z}\right)\left(\frac{n_i'}{n_{i0}}\right).
\end{aligned} \tag{B20}$$

2. **Diffusion velocity**. For the perturbed diffusion velocity u_{D}' , we have the representation

$$\begin{aligned}
u_{\mathrm{D}}' = &-D_{\mathrm{A}0}\frac{\partial}{\partial b}\left(\frac{T'}{T_0}\right) - D_{\mathrm{A}0}\frac{\partial}{\partial b}\left(\frac{n_i'}{n_{i0}}\right)\\
&+\left(\frac{1}{n_{i0}}\frac{\mathrm{d}n_{i0}}{\mathrm{d}z} + \frac{1}{T_0}\frac{\mathrm{d}T_0}{\mathrm{d}z}\right)\sin I D_{\mathrm{A}}' - \frac{g\sin I}{\nu_{in0}}\left(\frac{\nu_{in}'}{\nu_{in0}}\right).
\end{aligned} \tag{B21}$$

3. **Ion-drag force and ion-drag heating.** For the ion-drag force per unit mass (cf. Eq. (A10) of Appendix A),

$$\frac{1}{\rho}\mathbf{f}_{\mathrm{ID}} = \nu_{ni}(\mathbf{u} - \mathbf{u}_i),$$

we obtain

$$\left(\frac{1}{\rho}f_{\mathrm{IDx}}\right)' = \nu_{ni0}\Big[\sin^2 I u' - \sin I \cos I w' + \cos I u'_{\mathrm{D}} + \left(u_{\mathrm{D0}}\cos I + u_0 \sin^2 I\right)\left(\frac{\nu'_{ni}}{\nu_{ni0}}\right)\Big], \tag{B22}$$

$$\left(\frac{1}{\rho}f_{\mathrm{IDz}}\right)' = \nu_{ni0}\Big[-\sin I \cos I u' + \cos^2 I w' + \sin I u'_{\mathrm{D}} + \left(u_{\mathrm{D0}}\sin I - u_0 \cos I \sin I\right)\left(\frac{\nu'_{ni}}{\nu_{ni0}}\right)\Big]. \tag{B23}$$

For the ion-drag heating per unit mass (cf. Eq. (A11) of Appendix A)

$$\frac{1}{\rho}q_{\mathrm{ID}} = \nu_{ni}|\mathbf{u} - \mathbf{u}_i|^2,$$

we find

$$\left(\frac{1}{\rho}q_{\mathrm{ID}}\right)' = \nu_{ni0}\Big[2\left(\sin^2 I u_0 u' - \cos I \sin I u_0 w' + u_{\mathrm{D0}} u'_{\mathrm{D}}\right) + \left(u_0^2 \sin^2 I + u_{\mathrm{D0}}^2\right)\left(\frac{\nu'_{ni}}{\nu_{ni0}}\right)\Big]. \tag{B24}$$

Under the assumption that, in the ionosphere, the atomic oxygen O and O^+-ions are the main neutral and ionic constituents, we compute the background neutral-ion and ion-neutral collision frequencies as (Shibata, 1983; Stubbe, 1968)

$$\nu_{ni0} = 7.22 \times 10^{-17} T_0^{0.37} n_{i0}, \ \nu_{in0} = \frac{\nu_{ni0}}{n_{i0}} n_n, \ n = \mathrm{O}, i = \mathrm{O}^+$$

and their perturbed values as

$$D'_{\mathrm{A}} = D_{\mathrm{A0}}\left(\frac{T'}{T_0} - \frac{\nu'_{in}}{\nu_{in0}}\right), \tag{B25}$$

$$\frac{\nu'_{in}}{\nu_{in0}} = 0.37\frac{T'}{T_0} + \frac{\rho'}{\rho_0}, \tag{B26}$$

$$\frac{\nu'_{ni}}{\nu_{ni0}} = 0.37\frac{T'}{T_0} + \frac{n'_i}{n_{i0}}. \tag{B27}$$

B3 Decoupled system of equations

From Eqs. (B20)–(B24) we deduce that the hydrodynamic equations should be solved together with the ion continuity and momentum equations by introducing two additional state variables, namely n'_i/n_{i0} and u'_{D}. The resulting system then consists of eight equations, obtained by augmenting the hydrodynamic system with the ion continuity and momentum equations. This fully coupled approach was used by Shibata (1983).

In our analysis we instead employ a simplified, approximate model that decouples the hydrodynamic and ion equations. We have several options.

1. **Klostermeyer Approximation**. Klostermeyer (1972) solved the ion-continuity equation by neglecting the diffuse velocity and neutral winds, i.e.,
$$\frac{\partial}{\partial t}\left(\frac{n_i'}{n_{i0}}\right) = -\left(\cos I\frac{\partial u'}{\partial x} + \sin I\frac{\partial u'}{\partial z} + \frac{1}{n_{i0}}\frac{\mathrm{d}n_{i0}}{\mathrm{d}z}\sin I u'\right)\cos I - \left(\cos I\frac{\partial w'}{\partial x} + \sin I\frac{\partial w'}{\partial z} + \frac{1}{n_{i0}}\frac{\mathrm{d}n_{i0}}{\mathrm{d}z}\sin I w'\right)\sin I, \tag{B28}$$
and then computed the ion-drag force and ion-drag heating by including the background neutral wind, i.e.,
$$\left(\frac{1}{\rho}f_{\mathrm{IDx}}\right)' = \nu_{ni0}\left[\sin^2 I u' - \sin I\cos I w' + u_0\sin^2 I\left(\frac{\nu_{ni}'}{\nu_{ni0}}\right)\right], \tag{B29}$$
$$\left(\frac{1}{\rho}f_{\mathrm{IDz}}\right)' = \nu_{ni0}\left[-\sin I\cos I u' + \cos^2 I w' - u_0\cos I\sin I\left(\frac{\nu_{ni}'}{\nu_{ni0}}\right)\right], \tag{B30}$$
and
$$\left(\frac{1}{\rho}q_{\mathrm{ID}}\right)' = \nu_{ni0}\left[2\left(\sin^2 I u_0 u' - \cos I\sin I u_0 w'\right) + u_0^2\sin^2 I\left(\frac{\nu_{ni}'}{\nu_{ni0}}\right)\right]. \tag{B31}$$
Klostermeyer's method is best viewed as a semi–diagnostic approximation: one solves a simplified ion continuity equation driven only by the wave-induced divergence, and then evaluates ion-drag force and heating, including u_0 and ν_{ni}', but assuming no diffusion velocity. In other words, field-aligned diffusion and background neutral wind are neglected in the ion continuity equation when computing n_i', and the ion drag is treated as a diagnostic based on the neutral wave field and background wind.

2. **Fast Field-Aligned Diffusion**. In the second method, we assume that field-aligned diffusion is sufficiently strong that the relative ion perturbation and the perturbed diffusion velocity are nearly constant along the magnetic field line (but can vary across it):
$$\frac{\partial}{\partial b}\left(\frac{n_i'}{n_{i0}}\right) = -\left(\cos I\frac{\partial}{\partial x} + \sin I\frac{\partial}{\partial z}\right)\left(\frac{n_i'}{n_{i0}}\right) \approx 0 \tag{B32}$$
and
$$\frac{\partial u_{\mathrm{D}}'}{\partial b} = \cos I\frac{\partial u_{\mathrm{D}}'}{\partial x} + \sin I\frac{\partial u_{\mathrm{D}}'}{\partial z} \approx 0. \tag{B33}$$
We then obtain
$$\begin{aligned}\frac{\partial}{\partial t}\left(\frac{n_i'}{n_{i0}}\right) = &\left(u_{\mathrm{D0}}\frac{1}{n_{i0}}\frac{\mathrm{d}n_{i0}}{\mathrm{d}z} - \cos I\frac{\mathrm{d}u_0}{\mathrm{d}z} - \cos I u_0\frac{1}{n_{i0}}\frac{\mathrm{d}n_{i0}}{\mathrm{d}z}\right.\\ &\left.+\frac{\mathrm{d}u_{\mathrm{D0}}}{\mathrm{d}z}\right)\sin I\left(\frac{n_i'}{n_{i0}}\right) + \frac{1}{n_{i0}}\frac{\mathrm{d}n_{i0}}{\mathrm{d}z}\sin I u_{\mathrm{D}}'\\ &-\left(\cos I\frac{\partial u'}{\partial x} + \sin I\frac{\partial u'}{\partial z} + \frac{1}{n_{i0}}\frac{\mathrm{d}n_{i0}}{\mathrm{d}z}\sin I\, u'\right)\cos I\\ &-\left(\cos I\frac{\partial w'}{\partial x} + \sin I\frac{\partial w'}{\partial z} + \frac{1}{n_{i0}}\frac{\mathrm{d}n_{i0}}{\mathrm{d}z}\sin I\, w'\right)\sin I\end{aligned} \tag{B34}$$

and

$$u'_{\rm D} = D_{\rm A0}\left[\cos I\,\frac{\partial}{\partial x}\left(\frac{T'}{T_0}\right) + \sin I\,\frac{\partial}{\partial z}\left(\frac{T'}{T_0}\right)\right] + \left(\frac{1}{n_{i0}}\frac{{\rm d}n_{i0}}{{\rm d}z} + \frac{1}{T_0}\frac{{\rm d}T_0}{{\rm d}z}\right)\sin I\,D'_{\rm A} - \frac{g\sin I}{\nu_{in0}}\left(\frac{\nu'_{in}}{\nu_{in0}}\right). \tag{B35}$$

The ion-drag force and ion-drag heating are still computed from Eqs. (B22)–(B24).

B4 Plane wave solutions

Let

$$n'_i(x,z,t) = \overline{n}_i(z)\,{\rm e}^{{\rm j}(\omega t - k_{\rm x}x)},\ \overline{n}_i(z) = n_{i0}(z)\,\widehat{n}_i(z), \tag{B36}$$

and (cf. Eq. (A32) of Appendix A)

$$f'(x,z,t) = \overline{f}(z)\,{\rm e}^{{\rm j}(\omega t - k_{\rm x}x)}.$$

As in Appendix A, we introduce the dimensionless state variables $\widehat{u}$, $\widehat{w}$, and $\widehat{T}$, defined by

$$\overline{u} = \frac{\omega_0}{k_{\rm x}}\widehat{u},\ \overline{w} = \frac{\omega_0}{k_{\rm x}}\widehat{w},\ \frac{\overline{T}}{T_0} = \widehat{T},$$

together with their derivatives

$$\frac{{\rm d}\overline{u}}{{\rm d}z} = \frac{\omega_0}{k_{\rm x}}\widehat{\mathcal{U}},\ \frac{{\rm d}\overline{w}}{{\rm d}z} = \frac{\omega_0}{k_{\rm x}}\widehat{\mathcal{W}},\ \frac{\rm d}{{\rm d}z}\left(\frac{\overline{T}}{T_0}\right) = \frac{{\rm d}\widehat{T}}{{\rm d}z} = \widehat{\mathcal{T}}$$

1. **Representation of $\overline{u}_{\rm D}$.** From Eq. (B35) we obtain

$$\overline{u}_{\rm D} = -{\rm j}k_{\rm x}D_{\rm A0}\cos I\,\widehat{T} + D_{\rm A0}\sin I\,\widehat{\mathcal{T}} + \left(\frac{1}{n_{i0}}\frac{{\rm d}n_{i0}}{{\rm d}z} + \frac{1}{T_0}\frac{{\rm d}T_0}{{\rm d}z}\right)\sin I\,\overline{D}_{\rm A} - \frac{g\sin I}{\nu_{in0}}\left(\frac{\overline{\nu}_{in}}{\nu_{in0}}\right). \tag{B37}$$

Using

$$\frac{\overline{D}_{\rm A}}{D_{\rm A0}} = \frac{\overline{T}}{T_0} - \frac{\overline{\nu}_{in}}{\nu_{in0}}, \tag{B38}$$

$$\frac{\overline{\nu}_{in}}{\nu_{in0}} = 0.37\frac{\overline{T}}{T_0} + \frac{\overline{\rho}}{\rho_0}, \tag{B39}$$

together with (cf. Eq. (A34) of Appendix A)

$$\frac{\overline{\rho}}{\rho_0} = \frac{k_{\rm x}}{\Omega}\overline{u} - \frac{\rm j}{\Omega H_\rho}\overline{w} + \frac{\rm j}{\Omega}\frac{{\rm d}\overline{w}}{{\rm d}z}$$

we express $\overline{u}_{\rm D}$ as

$$\overline{u}_{\rm D} = U_{\rm u}\widehat{u} + U_{\rm w}\widehat{w} + U_{\rm T}\widehat{T} + U_{\mathcal{W}}\widehat{\mathcal{W}} + U_{\mathcal{T}}\widehat{\mathcal{T}}, \tag{B40}$$

where the U coefficients are given by

$$U_\mathrm{u} = -\frac{\omega_0}{\Omega}\,(D_{\mathrm{A}0}E + G), \tag{B41}$$

$$U_\mathrm{w} = \mathrm{j}\,\frac{\omega_0}{\Omega}\,\frac{1}{k_\mathrm{x}H_\rho}\,(D_{\mathrm{A}0}E + G), \tag{B42}$$

$$U_\mathrm{T} = -\mathrm{j}k_\mathrm{x}D_{\mathrm{A}0}\cos I + 0.63\,D_{\mathrm{A}0}E - 0.37\,G, \tag{B43}$$

$$U_\mathcal{W} = -\mathrm{j}\,\frac{\omega_0}{\Omega}\,\frac{1}{k_\mathrm{x}}\,(D_{\mathrm{A}0}E + G), \tag{B44}$$

$$U_\mathcal{T} = D_{\mathrm{A}0}\sin I, \tag{B45}$$

with

$$E = \sin I\left(\frac{1}{n_{i0}}\frac{\mathrm{d}n_{i0}}{\mathrm{d}z} + \frac{1}{T_0}\frac{\mathrm{d}T_0}{\mathrm{d}z}\right),\ G = \frac{g\sin I}{\nu_{in0}}. \tag{B46}$$

2. **Representation of $\widehat{n}_i$.** From Eq. (B34) we obtain

$$\begin{aligned}
&\left(\mathrm{j}\omega - u_{\mathrm{D}0}\frac{1}{n_{i0}}\frac{\mathrm{d}n_{i0}}{\mathrm{d}z}\sin I + \frac{\mathrm{d}u_0}{\mathrm{d}z}\cos I\sin I\right.\\
&\left.+\,u_0\frac{1}{n_{i0}}\frac{\mathrm{d}n_{i0}}{\mathrm{d}z}\cos I\sin I - \frac{\mathrm{d}u_{\mathrm{D}0}}{\mathrm{d}z}\sin I\right)\widehat{n}_i\\
&= \frac{1}{n_{i0}}\frac{\mathrm{d}n_{i0}}{\mathrm{d}z}\sin I\,\overline{u}_\mathrm{D} + \left(\mathrm{j}k_\mathrm{x}\cos I - \frac{1}{n_{i0}}\frac{\mathrm{d}n_{i0}}{\mathrm{d}z}\sin I\right)\cos I\frac{\omega_0}{k_\mathrm{x}}\widehat{u}\\
&+\left(\mathrm{j}k_\mathrm{x}\cos I - \frac{1}{n_{i0}}\frac{\mathrm{d}n_{i0}}{\mathrm{d}z}\sin I\right)\sin I\,\frac{\omega_0}{k_\mathrm{x}}\widehat{w} - \cos I\sin I\,\frac{\omega_0}{k_\mathrm{x}}\widehat{\mathcal{U}} - \sin^2 I\,\frac{\omega_0}{k_\mathrm{x}}\widehat{\mathcal{W}}.
\end{aligned} \tag{B47}$$

After some manipulations, the expression for $\widehat{n}_i$ reads

$$\widehat{n}_i = N_\mathrm{u}\widehat{u} + N_\mathrm{w}\widehat{w} + N_\mathrm{T}\widehat{T} + N_\mathcal{U}\widehat{\mathcal{U}} + N_\mathcal{W}\widehat{\mathcal{W}} + N_\mathcal{T}\widehat{\mathcal{T}}, \tag{B48}$$

where the N coefficients are given by

$$N_\mathrm{u} = \frac{1}{N_0}\left[\left(\mathrm{j}k_\mathrm{x}\cos I - \frac{1}{n_{i0}}\frac{\mathrm{d}n_{i0}}{\mathrm{d}z}\sin I\right)\cos I\frac{\omega_0}{k_\mathrm{x}} + \frac{1}{n_{i0}}\frac{\mathrm{d}n_{i0}}{\mathrm{d}z}\sin I U_\mathrm{u}\right], \tag{B49}$$

$$N_\mathrm{w} = \frac{1}{N_0}\left[\left(\mathrm{j}k_\mathrm{x}\cos I - \frac{1}{n_{i0}}\frac{\mathrm{d}n_{i0}}{\mathrm{d}z}\sin I\right)\sin I\,\frac{\omega_0}{k_\mathrm{x}} + \frac{1}{n_{i0}}\frac{\mathrm{d}n_{i0}}{\mathrm{d}z}\sin I U_\mathrm{w}\right], \tag{B50}$$

$$N_\mathrm{T} = \frac{1}{N_0}\frac{1}{n_{i0}}\frac{\mathrm{d}n_{i0}}{\mathrm{d}z}\sin I U_\mathrm{T}, \tag{B51}$$

$$N_\mathcal{U} = -\frac{1}{N_0}\cos I\sin I\,\frac{\omega_0}{k_\mathrm{x}}, \tag{B52}$$

$$N_\mathcal{W} = -\frac{1}{N_0}\left(\sin^2 I\,\frac{\omega_0}{k_\mathrm{x}} - \frac{1}{n_{i0}}\frac{\mathrm{d}n_{i0}}{\mathrm{d}z}\sin I U_\mathcal{W}\right), \tag{B53}$$

$$N_\mathcal{T} = \frac{1}{N_0}\frac{1}{n_{i0}}\frac{\mathrm{d}n_{i0}}{\mathrm{d}z}\sin I U_\mathcal{T}, \tag{B54}$$

and

$$N_0 = \mathrm{j}\omega - u_{\mathrm{D0}} \frac{1}{n_{i0}} \frac{\mathrm{d}n_{i0}}{\mathrm{d}z} \sin I + \frac{\mathrm{d}u_0}{\mathrm{d}z} \cos I \sin I + u_0 \frac{1}{n_{i0}} \frac{\mathrm{d}n_{i0}}{\mathrm{d}z} \cos I \sin I - \frac{\mathrm{d}u_{\mathrm{D0}}}{\mathrm{d}z} \sin I. \tag{B55}$$

3. **Ion-drag force and ion-drag heating.** Using Eqs. (B40) and (B48), together with

$$\frac{\overline{\nu}_{ni}}{\nu_{ni0}} = 0.37 \frac{\overline{T}}{T_0} + \frac{\overline{n}_i}{n_{i0}} = 0.37 \widehat{T} + \widehat{n}_i, \tag{B56}$$

we obtain

$$\frac{1}{\nu_{ni0}} \overline{\left(\frac{1}{\rho} f_{\mathrm{IDx}} \right)} = F_{\mathrm{xu}} \widehat{u} + F_{\mathrm{xw}} \widehat{w} + F_{\mathrm{xT}} \widehat{T} + F_{\mathrm{x}\mathcal{U}} \widehat{\mathcal{U}} + F_{\mathrm{x}\mathcal{W}} \widehat{\mathcal{W}} + F_{\mathrm{x}\mathcal{T}} \widehat{\mathcal{T}}, \tag{B57}$$

$$\frac{1}{\nu_{ni0}} \overline{\left(\frac{1}{\rho} f_{\mathrm{IDz}} \right)} = F_{\mathrm{zu}} \widehat{u} + F_{\mathrm{zw}} \widehat{w} + F_{\mathrm{zT}} \widehat{T} + F_{\mathrm{z}\mathcal{U}} \widehat{\mathcal{U}} + F_{\mathrm{z}\mathcal{W}} \widehat{\mathcal{W}} + F_{\mathrm{z}\mathcal{T}} \widehat{\mathcal{T}}, \tag{B58}$$

$$\frac{1}{\nu_{ni0}} \overline{\left(\frac{1}{\rho} q_{\mathrm{ID}} \right)} = P_{\mathrm{u}} \widehat{u} + P_{\mathrm{w}} \widehat{w} + P_{\mathrm{T}} \widehat{T} + P_{\mathcal{U}} \widehat{\mathcal{U}} + P_{\mathcal{W}} \widehat{\mathcal{W}} + P_{\mathcal{T}} \widehat{\mathcal{T}}. \tag{B59}$$

With

$$A_{\mathrm{x}} = u_{\mathrm{D0}} \cos I + u_0 \sin^2 I,\ A_{\mathrm{z}} = u_{\mathrm{D0}} \sin I - u_0 \cos I \sin I,\ B = u_{\mathrm{D0}}^2 + u_0^2 \sin^2 I, \tag{B60}$$

the coefficients corresponding to f_{IDx} are

$$F_{\mathrm{xu}} = \sin^2 I \frac{\omega_0}{k_{\mathrm{x}}} + A_{\mathrm{x}} N_{\mathrm{u}} + \cos I\, U_{\mathrm{u}}, \tag{B61}$$

$$F_{\mathrm{xw}} = -\sin I \cos I \frac{\omega_0}{k_{\mathrm{x}}} + A_{\mathrm{x}} N_{\mathrm{w}} + \cos I\, U_{\mathrm{w}}, \tag{B62}$$

$$F_{\mathrm{xT}} = 0.37\, A_{\mathrm{x}} + A_{\mathrm{x}} N_{\mathrm{T}} + \cos I\, U_{\mathrm{T}}, \tag{B63}$$

$$F_{\mathrm{x}\mathcal{U}} = A_{\mathrm{x}} N_{\mathcal{U}}, \tag{B64}$$

$$F_{\mathrm{x}\mathcal{W}} = A_{\mathrm{x}} N_{\mathcal{W}} + \cos I\, U_{\mathcal{W}}, \tag{B65}$$

$$F_{\mathrm{x}\mathcal{T}} = A_{\mathrm{x}} N_{\mathcal{T}} + \cos I\, U_{\mathcal{T}}, \tag{B66}$$

the coefficients corresponding to f_{IDz} are

$$F_{\mathrm{zu}} = -\sin I \cos I \frac{\omega_0}{k_{\mathrm{x}}} + A_{\mathrm{z}} N_{\mathrm{u}} + \sin I \, U_{\mathrm{u}}, \tag{B67}$$

$$F_{\mathrm{zw}} = \cos^2 I \frac{\omega_0}{k_{\mathrm{x}}} + A_{\mathrm{z}} N_{\mathrm{w}} + \sin I \, U_{\mathrm{w}}, \tag{B68}$$

$$F_{\mathrm{zT}} = 0.37 \, A_{\mathrm{z}} + A_{\mathrm{z}} N_{\mathrm{T}} + \sin I \, U_{\mathrm{T}}, \tag{B69}$$

$$F_{\mathrm{z}\mathcal{U}} = A_{\mathrm{z}} N_{\mathcal{U}}, \tag{B70}$$

$$F_{\mathrm{z}\mathcal{W}} = A_{\mathrm{z}} N_{\mathcal{W}} + \sin I \, U_{\mathcal{W}}, \tag{B71}$$

$$F_{\mathrm{z}\mathcal{T}} = A_{\mathrm{z}} N_{\mathcal{T}} + \sin I \, U_{\mathcal{T}}, \tag{B72}$$

and the coefficients corresponding to q_{ID} are

$$P_{\mathrm{u}} = 2 \sin^2 I \frac{\omega_0}{k_{\mathrm{x}}} u_0 + B N_{\mathrm{u}} + 2 u_{\mathrm{D0}} U_{\mathrm{u}}, \tag{B73}$$

$$P_{\mathrm{w}} = -2 \cos I \sin I \frac{\omega_0}{k_{\mathrm{x}}} u_0 + B N_{\mathrm{w}} + 2 u_{\mathrm{D0}} U_{\mathrm{w}}, \tag{B74}$$

$$P_{\mathrm{T}} = 0.37 \, B + B N_{\mathrm{T}} + 2 u_{\mathrm{D0}} U_{\mathrm{T}}, \tag{B75}$$

$$P_{\mathcal{U}} = B N_{\mathcal{U}}, \tag{B76}$$

$$P_{\mathcal{W}} = B N_{\mathcal{W}} + 2 u_{\mathrm{D0}} U_{\mathcal{W}}, \tag{B77}$$

$$P_{\mathcal{T}} = B N_{\mathcal{T}} + 2 u_{\mathrm{D0}} U_{\mathcal{T}}. \tag{B78}$$

Note that, in the algorithm implementation, the derivatives $\mathrm{d}n_{i0}/\mathrm{d}z$ and $\mathrm{d}u_{\mathrm{D0}}/\mathrm{d}z$ are computed using central finite differences.

Appendix C: Solution methods for the grid-point values of the state vector

In this appendix, the global matrix method with matrix exponential and the scattering matrix method will be formulated for the grid-point values of the state vector. To guarantee this interfacial condition, the components of the vector $\mathbf{e}$ are chosen as

C1 Global matrix method with matrix exponential

In the layer l, with boundaries z_l and z_{l+1}, the discrete values $\mathbf{e}_{l+1} = \mathbf{e}(z_{l+1})$ and $\mathbf{e}_l = \mathbf{e}(z_l)$ are related through the relation (cf. Eq. (14))

$$\mathbf{e}_{l+1} = \mathrm{V}_l \mathrm{diag}[\mathrm{e}^{k_{\mathrm{x}} \lambda_{nl} \Delta_l}] \mathrm{V}_l^{-1} \mathbf{e}_l, \tag{C1}$$

Inserting or equivalently,

$$\mathrm{V}_l^{-1}\mathbf{e}_{l+1} = \mathrm{diag}[\mathrm{e}^{k_x\lambda_{nl}\Delta_l}]\mathrm{V}_l^{-1}\mathbf{e}_l. \tag{C2}$$

Taking into account that by Eqs. (13) and (14), we have $\mathbf{e}_l = \mathrm{V}_l\mathbf{a}_l$ and $\mathbf{e}_{l+1} = \mathrm{V}_{l+1}\mathbf{a}_{l+1}$,we see that Eq. (35) and (C2) are completely equivalent. Multiplying Eq. (C2) with the scaling matrix $\mathrm{K}_{l,}^1$, we obtain the layer equation

$$\mathbb{A}_l^1\mathbf{e}_{l+1} - \mathbb{A}_l^0\mathbf{e}_l = \mathbf{0}_{2M},\ l = 1,...,L-1, \tag{C3}$$

where

$$\mathbb{A}_l^1 = \mathrm{K}_{l,}^1\mathrm{V}_l^{-1}, \tag{C4}$$

$$\mathbb{A}_l^0 = \mathrm{K}_{l,}^0\mathrm{V}_l^{-1}, \tag{C5}$$

and K_l^1 and K_l^0, are given by Eqs. (36) and (37), respectively. Essentially, we have $L-1$ equations imposed on layers $1,\ldots,L-1$ for the L unknowns $\mathbf{e}_1,\ldots,\mathbf{e}_L$. On the layer $l=1$, the boundary condition (cf. Eq. (42)) $\mathbf{a}_1^+ = \mathbf{i}_1$, translates into (cf. Eq. (24))

$$[\mathrm{I}_M, 0_M]\mathrm{V}_1^{-1}\mathbf{e}_1 = \mathbf{i}_1, \tag{C6}$$

while on the layer $l = L$, the boundary condition (cf. Eq. (46)) $\mathbf{a}_L^- = \mathbf{0}_M$ translates into (cf. Eq. (25))

$$[0_M, \mathrm{I}_M]\mathrm{V}_L^{-1}\mathbf{e}_L = \mathbf{0}_M. \tag{C7}$$

As in Section 3, the layer equations (C3) together with the boundary conditions (C6) and (C7) for a unit scale factor, are assembled into a system of equations for the stratified atmosphere, i.e.,

$$\mathbb{A}\mathbf{e} = \mathbf{b}, \tag{C8}$$

where

$$\mathbb{A} = \begin{bmatrix} [0_M, \mathrm{I}_M]\mathrm{V}_L^{-1} & 0 & \ldots & 0 & 0 \\ \mathbb{A}_{L-1}^1 & -\mathbb{A}_{L-1}^0 & \ldots & 0 & 0 \\ \vdots & \vdots & \ddots & \vdots & \vdots \\ 0 & 0 & \ldots & \mathbb{A}_1^1 & -\mathbb{A}_1^0 \\ 0 & 0 & \ldots & 0 & [\mathrm{I}_M, 0_M]\mathrm{V}_1^{-1} \end{bmatrix}, \tag{C9}$$

$$\mathbf{e} = \begin{bmatrix} \mathbf{e}_L \\ \mathbf{e}_{L-1} \\ \vdots \\ \mathbf{e}_2 \\ \mathbf{e}_1 \end{bmatrix} \text{ and } \mathbf{b} = \begin{bmatrix} \mathbf{0}_M \\ \mathbf{0}_{2M} \\ \vdots \\ \mathbf{0}_{2M} \\ \mathbf{i}_1 \end{bmatrix}. \tag{C10}$$

When applying the lower boundary condition (56), $\mathbf{i}_1$ in Eq. (C10) should be replaced by $\mathrm{B}^{-1}\mathbf{b}_1$, where, for a unit scale factor, $\mathbf{b}_1 = [1, 0, 0]^\mathrm{T}$. After solving Eq. (C8), we compute the wave amplitudes by using Eq. (61).

Comments.

1. The ascending and descending solution modes can be derived by using the upward and downward recurrence relations (cf. Eqs. (28)–(31), (41) and (45))

$$\mathbf{e}_{l+1}^{+} = \mathrm{T}_l^{+}\mathbf{e}_l, \text{ for } l = 1, \ldots, L-1, \text{ with } \mathbf{e}_1^{+} = \mathbf{v}_1^{+}, \text{ and} \tag{C11}$$

$$\mathbf{e}_l^{-} = \mathrm{T}_l^{-}\mathbf{e}_{l+1}, \text{ for } l = L-1, \ldots, 1, \text{ with } \mathbf{e}_L^{-} = \mathbf{0}_{2M}, \tag{C12}$$

respectively, where

$$\mathrm{T}_l^{+} = \mathrm{V}_l \begin{bmatrix} \mathrm{diag}[\mathrm{e}^{k_\mathrm{x}\lambda_{ml}^{+}\Delta_l}] & 0_M \\ 0_M & 0_M \end{bmatrix} \mathrm{V}_l^{-1}, \tag{C13}$$

$$\mathrm{T}_l^{-} = \mathrm{V}_l \begin{bmatrix} 0_M & 0_M \\ 0_M & \mathrm{diag}[\mathrm{e}^{-k_\mathrm{x}\lambda_{ml}^{-}\Delta_l}] \end{bmatrix} \mathrm{V}_l^{-1}. \tag{C14}$$

Obviously, the relation $\mathbf{e}_l = \mathbf{e}_l^{+} + \mathbf{e}_l^{-}$, $l = 1, \ldots, L$, can be used to verify the numerical algorithm.

2. If we assume that the ascending modes are the dominant modes, i.e., $\mathbf{e}_l \approx \mathbf{e}_l^{+}$ for $l = 1, \ldots, L$, we may compute the state vector by means of the upward recurrence relation (cf. Eq. (C11))

$$\mathbf{e}_{l+1} = \mathrm{T}_l^{+}\mathbf{e}_l, \text{ for } l = 1, \ldots, L-1, \text{ with } \mathbf{e}_1 = \mathbf{v}_1^{+}. \tag{C15}$$

3. The layer equation (C3) was derived from the solution representation (C1). In fact, this equation is simply the matrix-exponential representation of the solution, i.e., $\mathbf{e}_{l+1} = \exp(\mathrm{A}_l k_\mathrm{x} \Delta_l)\mathbf{e}_l$, where the matrix exponential is calculated using an eigendecomposition of the propagation matrix A_l, i.e., $\mathrm{A}_l = \mathrm{V}_l \mathrm{diag}[\lambda_{nl}]\mathrm{V}_l^{-1}$. However, instead of an eigen-decomposition method, we can use the Padé approximation to compute the matrix exponential (Doicu and Trautmann, 2009a, b). The nth diagonal Padé approximation to the matrix exponential is $\exp(\mathrm{A}x) = [\mathrm{D}(\mathrm{A}x)]^{-1}\mathrm{N}(\mathrm{A}x)$, where $\mathrm{D}(\mathrm{A}x)$ and $\mathrm{N}(\mathrm{A}x)$ are polynomials in $\mathrm{A}x$ of degree n given respectively, by $\mathrm{D}(\mathrm{A}x) = \sum_{k=0}^{n}(-1)^k c_k x^k \mathrm{A}^k$ and $\mathrm{N}(\mathrm{A}x) = \mathrm{D}(-\mathrm{A}x) = \sum_{k=0}^{n} c_k x^k \mathrm{A}^k$. The coefficients c_k can be computed recursively by means of the relation

$$c_k = \frac{n-k+1}{k(2n-k+1)} c_{k-1}, \; k \geq 1 \tag{C16}$$

with the initial value $c_0 = 1$. The layer equation then becomes

$$\mathbb{A}_l^1 \mathbf{e}_{l+1} - \mathbb{A}_l^0 \mathbf{e}_l = \mathbf{0}_{2M}, \; l = 1, ..., L-1, \tag{C17}$$

where $\mathbb{A}_l^1 = \mathrm{D}(\mathrm{A}_l k_\mathrm{x} \Delta_l)$ and $\mathbb{A}_l^0 = \mathrm{N}(\mathrm{A}_l k_\mathrm{x} \Delta_l)$. The resulting system of layer equations, together with the boundary conditions, is assembled into a banded linear system. Eigendecomposition is required only in the lower and upper layers to apply the boundary conditions, whereas the Padé approximation is used in all interior layers. This approach is presumably more efficient than a full eigendecomposition. However, since the first-order Padé approximation corresponds to a centered finite-difference scheme, whereas the first-order Taylor expansion yields a forward finite-difference scheme, the method is less accurate. For this reason, the Padé approximation of the matrix exponential is not implemented in our computer code and is included here solely for theoretical completeness.

C2 Scattering matrix method

In principle, the scattering matrix method can also be formulated in terms of the discrete values of the state vector. Starting from the interaction principle equation (68), using Eq. (27), i.e., $\mathbf{e}_l^{\pm} = \mathrm{V}_l^{\pm}\mathbf{a}_l^{\pm}$, and Eqs. (24)–(25), i.e.,

$$\mathbf{a}_l^{+} = [\mathrm{I}_M, 0_M]\mathbf{a}_l = [\mathrm{I}_M, 0_M]\mathrm{V}_l^{-1}\mathbf{e}_l, \tag{C18}$$

$$\mathbf{a}_l^{-} = [0_M, \mathrm{I}_M]\mathbf{a}_l = [0_M, \mathrm{I}_M]\mathrm{V}_l^{-1}\mathbf{e}_l, \tag{C19}$$

we find that for the stack $\mathcal{S}_{l_0 l}$, the interaction principle equation involving the discrete values of the state vector is

$$\begin{bmatrix} \mathbf{e}_{l_0}^{-} \\ \mathbf{e}_{l+1}^{+} \end{bmatrix} = \begin{bmatrix} \mathscr{R}_{l_0 l}^{+} & \mathscr{T}_{l_0 l}^{-} \\ \mathscr{T}_{l_0 l}^{+} & \mathscr{R}_{l_0 l}^{-} \end{bmatrix} \begin{bmatrix} \mathbf{e}_{l_0}^{+} \\ \mathbf{e}_{l+1}^{-} \end{bmatrix}, \tag{C20}$$

where $\dim(\mathscr{R}_{l_0 l}^{\pm}) = \dim(\mathscr{T}_{l_0 l}^{\pm}) = 2M \times 2M$, and

$$\begin{bmatrix} \mathscr{R}_{l_0 l}^{+} & \mathscr{T}_{l_0 l}^{-} \\ \mathscr{T}_{l_0 l}^{+} & \mathscr{R}_{l_0 l}^{-} \end{bmatrix} = (\mathrm{I}_{4M} - \mathrm{A})^{-1}\mathrm{A}, \tag{C21}$$

with

$$\mathrm{A} = \begin{bmatrix} \mathrm{V}_{l_0}^{-}\mathcal{R}_{l_0 l}^{+}[\mathrm{V}_{l_0}^{-1}]_1 & \mathrm{V}_{l_0}^{-}\mathcal{T}_{l_0 l}^{-}[\mathrm{V}_{l}^{-1}]_2 \\ \mathrm{V}_{l}^{+}\mathcal{T}_{l_0 l}^{+}[\mathrm{V}_{l_0}^{-1}]_1 & \mathrm{V}_{l}^{+}\mathcal{R}_{l_0 l}^{-}[\mathrm{V}_{l}^{-1}]_2 \end{bmatrix}, \tag{C22}$$

$$\mathrm{V}_l = [\mathrm{V}_l^{+}, \mathrm{V}_l^{-}], \text{ and } \mathrm{V}_l^{-1} = \begin{bmatrix} [\mathrm{V}_l^{-1}]_1 \\ [\mathrm{V}_l^{-1}]_2 \end{bmatrix}. \tag{C23}$$

Since the matrices $\mathscr{R}_{l_0 l}^{\pm}$ and $\mathscr{T}_{l_0 l}^{\pm}$ are twice the size of the matrices $\mathcal{R}_{l_0 l}^{\pm}$ and $\mathcal{T}_{l_0 l}^{\pm}$, the associated computational cost is significantly higher. Owing to its low numerical efficiency, this method is therefore of purely theoretical interest and is not implemented in our computer code.

Appendix D: Implementation issues

In this appendix, we discuss several implementation issues related to the computation of lower and upper bounds for the wave period, the choice of frequency and time discretization for the Fourier transform, and the determination of the imaginary frequency shift.

D1 Wave period

To define practical bounds for the wave period λ_{t}, we solve the inviscid dispersion equation (cf. Eq. (A61) with $\nu = 0$ and with the intrinsic frequency $\Omega = \omega - k_{\mathrm{x}} u_0$ replacing ω)

$$\Omega^4 - \left[\omega_{\mathrm{a}}^2 + c_{\mathrm{s}}^2 \left(k_{\mathrm{x}}^2 + k_{\mathrm{z}}^2\right)\right] \Omega^2 + c_{\mathrm{s}}^2 k_{\mathrm{x}}^2 \omega_{\mathrm{g}}^2 = 0, \tag{D1}$$

for an assumed value of the vertical wavenumber k_{z}, where $\omega_{\mathrm{g}} = \sqrt{\gamma - 1} g / c_{\mathrm{s}}$ is the buoyancy (gravity-wave) frequency and $\omega_{\mathrm{a}} = \gamma g / (2 c_{\mathrm{s}})$ is the acoustic cutoff frequency. Thus, for a stratified atmosphere, the solution Ω_{inv} depends on the altitude z and the wavenumber k_{z}, and satisfies $\Omega_{\mathrm{inv}}(z, k_{\mathrm{z}}) < \omega_{\mathrm{g}}(z)$. In this context we define $\omega_{\mathrm{inv}}(k_{\mathrm{z}}) = \min_z [\Omega_{\mathrm{inv}}(z, k_{\mathrm{z}}) + k_{\mathrm{x}} u_0(z)]$. The equation is solved for two assumed minimum and maximum values of the vertical wavelength λ_{z}, namely $\lambda_{\mathrm{zmin}} = 125$ km and $\lambda_{\mathrm{zmax}} = 250$ km, implying $k_{\mathrm{zmin}} = 2\pi / \lambda_{\mathrm{zmax}}$ and $k_{\mathrm{zmax}} = 2\pi / \lambda_{\mathrm{zmin}}$. The corresponding solutions are denoted by $\omega_{\min} = \omega_{\mathrm{inv}}(k_{\mathrm{zmax}})$ and $\omega_{\max} = \omega_{\mathrm{inv}}(k_{\mathrm{zmin}})$, and the resulting time periods are $\lambda_{\mathrm{t,min}} = 2\pi / \omega_{\max}$ and $\lambda_{\mathrm{t,max}} = 2\pi / \omega_{\min}$. These values are likely underestimates, since dissipative effects ($\nu \neq 0$) tend to reduce the oscillation frequencies and thus increase the wave periods. For this reason, we round the bounds upward to the nearest multiple of 10 min, and set $\lambda_{\mathrm{t,min}} = 10 \lceil \lambda_{\mathrm{t,min}} / 10 \rceil$ and $\lambda_{\mathrm{t,max}} = 10 \lceil \lambda_{\mathrm{t,max}} / 10 \rceil$, where $\lceil x \rceil$ denotes the upward rounding of x to the next integer.

To provide a physical interpretation of this approach, we note that Eq. (**??**) into Eqs. (**??**)–(**??**), we are led to the system of equations where $\eta_1 = 1/(1 + 4\eta)$. On the other hand, Hines (1973) and Francis (1973) showed that the continuity of D1) yields

$$k_{\mathrm{z}}^2 = \frac{\Omega^2 - \omega_{\mathrm{a}}^2}{c_s^2} + k_{\mathrm{x}}^2 \left(\frac{\omega_{\mathrm{g}}^2}{\Omega^2} - 1 \right), \tag{D2}$$

or equivalently, of the pressure perturbation is more realistic. In this case, the components of the vector **e** are chosen so that, under the assumption $\Omega \ll \omega_{\mathrm{a}}$, we obtain

$$\frac{k_{\mathrm{z}}}{k_x} = \pm \sqrt{\frac{\omega_{\mathrm{g}}^2}{\Omega^2} - 1 - \frac{1}{4 k_{\mathrm{x}}^2 H_{\mathrm{a}}^2}}. \tag{D3}$$

If

$$\frac{\omega_{\mathrm{g}}^2}{\Omega^2} - 1 - \frac{1}{4 k_{\mathrm{x}}^2 H_{\mathrm{a}}^2} > 0 \text{ for all } z, \tag{D4}$$

then k_{z} is real and $\exp(-\mathrm{j} k_{\mathrm{z}} z) \in \mathbb{C}$; thus, the wave is propagating. When this condition is not satisfied, k_{z} is purely imaginary and $\exp(-\mathrm{j} k_{\mathrm{z}} z) \in \mathbb{R}$; thus, for $\mathrm{Im}(k_{\mathrm{z}}) < 0$, the wave is evanescent. This condition yields

$$\omega < \Omega_{\mathrm{inv}}(z, k_{\mathrm{z}} = 0) + k_{\mathrm{x}} u_0(z) \text{ for all } z, \tag{D5}$$

where

$$\Omega_{\mathrm{inv}}(z, k_{\mathrm{z}} = 0) = \frac{\omega_{\mathrm{g}}}{\sqrt{1 + \frac{1}{4 k_{\mathrm{x}}^2 H_{\mathrm{a}}^2}}} \tag{D6}$$

is the solution of the inviscid dispersion equation in the case $k_{\mathrm{z}}=0$ ($\lambda_{\mathrm{z}}\to\infty$). We conclude that the condition $\omega_{\mathrm{inv}}(k_{\mathrm{z}})=\min_z[\Omega_{\mathrm{inv}}(z,k_{\mathrm{z}})+k_{\mathrm{x}}u_0(z)]$ implies that the time period is chosen such that only propagating waves are considered. Condition (D5), written $\Omega(z)<\Omega_{\mathrm{inv}}(z,k_{\mathrm{z}}=0)$ was used by Knight et al. (2024) to determine the intrinsic evanescent frequencies that lead to the so-called "anomalous results". In practice, evanescent frequencies occur at altitudes up to at least 100 km; consequently, these anomalous results are of limited relevance for upper-thermospheric gravity-wave studies, since evanescence below about 100 km and critical layers in the lower thermosphere strongly attenuate such waves before they can reach higher altitudes (Knight et al., 2024).

D2 Frequency and time discretization for the Fourier transform

In the code, we do not use a Fast Fourier Transform (FFT). Instead, we perform a direct (discrete) Fourier Transform (FT) by explicitly discretizing the Fourier integral. The discretization parameters are chosen to resolve a source that is localized both in frequency and in time.

1. **Frequency band centered on ω_0**. The Fourier transform is performed over a frequency band centered on the reference frequency ω_0. We introduce a frequency standard deviation σ_ω defined as a fraction of ω_0, i.e., $\sigma_\omega=\omega_0/\kappa_\omega$, where $\kappa_\omega\geq 6$ is an input parameter. The effective frequency band of interest is chosen to cover approximately plus/minus three standard deviations of the source spectrum: $\omega_{\min}=\omega_0-3\sigma_\omega$ and $\omega_{\max}=\omega_0+3\sigma_\omega$. The total frequency interval and the frequency step are, respectively, $L_\omega=\omega_{\max}-\omega_{\min}=6\omega_0/\kappa_\omega$ and $\Delta\omega=L_\omega/(N_{\mathrm{FT}}-1)$, where N_{FT} is the number of discrete points. The discrete frequency grid ω_k is then constructed as $\omega_k=\omega_{\min}+(k-1)\Delta\omega$, $k=1,2,\ldots,N_{\mathrm{FT}}$.

2. **Time interval and time step**. The time grid is chosen to be consistent with the assumed temporal localization of the source and with the chosen frequency bandwidth. First, we define the time standard deviation σ_{t} as $\sigma_{\mathrm{t}}=1/\sigma_\omega$. The time interval L_{t} is chosen to contain N_{p} periods of the reference frequency. The time period is given by $\lambda_{\mathrm{t}}=2\pi/\omega_0$, and therefore, $L_{\mathrm{t}}=N_{\mathrm{p}}\lambda_{\mathrm{t}}$. The time step Δt is then computed as $\Delta t=L_{\mathrm{t}}/(N_{\mathrm{FT}}-1)$. The time grid t_k is defined on the interval $[t_{\min},t_{\max}]$, where $t_{\min}$ is an input parameter and $t_{\max}=t_{\min}+L_{\mathrm{t}}$, by $t_k=t_{\mathrm{min}}+(k-1)\Delta t$, $k=1,2,\ldots,N_{\mathrm{FT}}$. We also define a time shift by $t_0=(t_{\max}-t_{\min})/2$ which places the reference time close to the center of the time window.

In the code, N_{FT}, κ_ω, N_{p} and $t_{\min}$ are input parameters. Specifically, κ_ω determines the length of the frequency interval L_ω, whereas N_{p} determines the length of the time interval L_{t}. The discretization is considered adequate if the following conditions are satisfied:

1. The time window is long enough for the chosen frequency bandwidth. This requires that the number of time standard deviations contained in the interval satisfies $L_{\mathrm{t}}/\sigma_{\mathrm{t}}>6$, which ensures that the main part of the source is well contained within the time window and that truncation effects are negligible.

2. The Nyquist condition $\Delta t < \pi/\omega_{\max}$, and the dual Nyquist condition $\Delta\omega < 2\pi/L_{\mathrm{t}}$ are satisfied. These conditions ensure that the temporal signal is properly sampled in time and frequency, prevent aliasing effects, and guarantee a consistent discrete Fourier transform between the time and frequency domains

Since the Fourier transform is computed by direct discretization of the Fourier integral, no FFT-specific constraint is imposed between the frequency step $\Delta\omega$ and the time step Δt. In particular, the grid relation $\Delta t\,\Delta\omega = 2\pi/N_{\mathrm{FT}}$, which is characteristic of discrete Fourier transforms based on periodic sampling and exact discrete orthogonality, is not required here. Instead, the frequency and time grids are chosen independently, based on the desired frequency band and time window needed to resolve a source that is localized in both domains. This provides greater flexibility in selecting the bandwidth, resolution, and window length.

D3 Imaginary frequency shift

The imaginary frequency shift is determined using a heuristic approach that combines two criteria: application of the Layerwise Causality (LC) condition at selected altitude levels, and a Source-Function Reconstruction (SFR) test.

1. **LC condition at selected altitude levels**. Choose a subset $L_0 \subset \{1,2,\ldots,L\}$ of altitude indices, and let N_{L_0} be the number of elements of the set L_0, i.e., $N_{L_0} = |L_0|$. At each altitude level $l_0 \in L_0$, start with $\delta_{l_0} = \delta_{\text{start}}$ and increases δ_{l_0} in steps of $\Delta\delta$, i.e., $\delta_{l_0} \leftarrow \min(\delta_{l_0} + \Delta\delta, \delta_{\text{stop}})$, until the LC condition (c.f. Eq. (109))

$$d_{l_0}(\omega_k) = \mathrm{Re}[\lambda^{-}_{1l_0}(\omega_k - \mathrm{j}\delta_{l_0})] - \mathrm{Re}[\lambda^{+}_{1l_0}(\omega_k - \mathrm{j}\delta_{l_0})] > \epsilon_{\mathrm{LC}} \tag{D7}$$

is satisfied for all $\omega_k = \omega_{\min} + (k-1)\Delta\omega$, $k = 1,2,\ldots,N_{\mathrm{FT}}$, and some prescribed tolerance $\epsilon_{\mathrm{LC}} = 10^{-10}$. If there exists an altitude level for which it is not possible to satisfy the LC condition for all frequencies ω_k by increasing the imaginary frequency shift within the interval from the start value δ_{start} to the stop value δ_{stop}, then the subset-based LC criterion is said to fail. Otherwise, the LC frequency shift is computed as

$$\delta_{\mathrm{LC}} = \max_{l_0 \in L_0} \delta_{l_0}. \tag{D8}$$

2. **SFR**. A frequency shift δ is considered valid if the relative RMS error between the source function $s(t)$ and the inverse Fourier transform applied to $S(\omega - \mathrm{j}\delta)$ is below a prescribed tolerance $\epsilon_{\mathrm{SFR}} = 5\times 10^{-3}$. In practice, we compare the normalized functions

$$\widehat{s}(t) = \frac{s(t)}{\max_t \mathrm{Re}\{s(t)\}},\ \widehat{s}_\delta(t) = \frac{s_\delta(t)}{\max_t \mathrm{Re}\{s_\delta(t)\}},$$

where (compare with Eq. (116))

$$s_\delta(t) = A\mathrm{e}^{\delta(t-t_0)}\frac{1}{2\pi}\int_{-\infty}^{\infty}\mathscr{S}(\omega - \mathrm{j}\delta)\mathrm{e}^{\mathrm{j}\omega(t-t_0)}\mathrm{d}\omega, \tag{D9}$$

and the underlying system of equations is $s(t)$ and $\mathscr{S}(\omega)$ are given by Eqs. (84) and (92), respectively. The relative RMS error is computed as

$$\varepsilon_{s\delta} = \sqrt{\frac{\sum_{k=1}^{N_{\mathrm{FT}}} [\widehat{s}(t_k) - \widehat{s}_\delta(t_k)]^2}{\sum_{k=1}^{N_{\mathrm{FT}}} \widehat{s}(t_k)^2}} \tag{D10}$$

Both system of equations (??) –(??)with $t_k = t_{\min} + (k-1)\Delta t$, $k = 1, 2, \ldots, N_{\mathrm{FT}}$. In the algorithm,

(a) if $\varepsilon_{s\delta} > \epsilon_{\mathrm{SFR}}$, the frequency shift is relaxed according to $\delta \leftarrow \max(\delta - \Delta\delta, \delta_{\mathrm{stop}})$, and

(b) if $\varepsilon_{s\delta} > \epsilon_{\mathrm{SFR}}$ also holds for $\delta = \delta_{\mathrm{stop}}$, the SFR test fails.

The algorithm proceeds as follows.

Step 1: Initialization and SFR test at $\boldsymbol{\delta_{\min}}$

We choose $\delta_{\min} = \Delta\delta$ and (??)–(??)can be solved using the methods proposed in Section 4. $\delta_{\max} = k_\delta\,\Delta\delta$, where $\Delta\delta$ (e.g., $\Delta\delta = 10^{-6}\ \mathrm{s}^{-1}$) is the initial discrete step of the imaginary frequency shift and k_δ is an integer. We first apply the SFR test to the input $\delta_{\min}$, using $\delta_{\mathrm{stop}} = \Delta\delta$ and the step $\Delta\delta$ as a decreasing update of δ. With this choice, the algorithm effectively checks whether $\delta_{\min}$ passes the SFR test, that is, without invoking a frequency-shift relaxation. If the SFR test fails, we stop the algorithm. Otherwise, the value $\delta_{\min}$ is accepted as SFR-admissible. Based on the monotonic behavior of the SFR error in δ, we assume that any $\delta \le \delta_{\min}$ would also satisfy the SFR test.

Step 2: SFR test at $\boldsymbol{\delta_{\max}}$ and refinement of $\boldsymbol{\delta_{\max}}$

We apply the SFR test to the input $\delta_{\max}$, using $\delta_{\mathrm{stop}} = \delta_{\min}$ and the step $\Delta\delta$ again as a decreasing update of δ. Since the SFR test has already been successful at $\delta_{\min}$, this second SFR call is guaranteed to succeed: if necessary, the procedure can always relax δ down to $\delta_{\min}$. Let $\delta_{\mathrm{SFR}} = k_{\mathrm{SFR}}\,\Delta\delta$ denote the value returned by the SFR routine. We then reset $\delta_{\max} \leftarrow \delta_{\mathrm{SFR}}$. By construction, every $\delta \in [\delta_{\min}, \delta_{\max}]$ satisfies the SFR test.

Step 3: Construction and adjustment of an internal $\boldsymbol{\delta}$-grid

The next steps require an internal grid of discrete values of δ between $\delta_{\min}$ and $\delta_{\max}$, with a sufficiently large number of points (e.g., at least five) to reliably apply the LC procedure. This internal grid uses the spacing $\Delta\delta$, but is independent of the number N_δ used later in the final selection step. To avoid a degenerate interval and to obtain a reasonably fine internal spacing, we adjust $\delta_{\min}$ and $\Delta\delta$ according to the following rules: if $\delta_{\max} - \delta_{\min} < \Delta\delta/2$ (i.e., $\delta_{\max} \approx \delta_{\min}$), then set $\delta_{\min} \leftarrow \delta_{\max} - \Delta\delta/2$ and $\Delta\delta \leftarrow \Delta\delta/8$; else if $\Delta\delta/2 < \delta_{\max} - \delta_{\min} < 3\Delta\delta/2$ (i.e., $\delta_{\max} - \delta_{\min} \approx \Delta\delta$), then set $\Delta\delta \leftarrow \Delta\delta/4$; else if $3\Delta\delta/2 < \delta_{\max} - \delta_{\min} < 5\Delta\delta/2$ (i.e., $\delta_{\max} - \delta_{\min} \approx 2\Delta\delta$), then set $\Delta\delta \leftarrow 2\Delta\delta/3$. After this adjustment, the interval $[\delta_{\min}, \delta_{\max}]$ contains a suitable number of internal grid points spaced by $\Delta\delta$. These internal points are used only in the LC procedure described in the next step.

Step 4: LC procedure and update of $\boldsymbol{\delta_{\min}}$

We apply the subset-based LC procedure to δ, starting from the current value $\delta_{\min}$ and moving towards larger values, with an upper bound $\delta_{\text{stop}} = \delta_{\max} - \Delta\delta$ and an increasing step $\Delta\delta$. If there exists an altitude level for which the LC test fails, we stop the algorithm. Otherwise, let $\delta_{\text{LC}} = k_{\text{LC}}\,\Delta\delta$ denote the LC-based estimate returned by the procedure. We then update $\delta_{\min} \leftarrow \delta_{\text{LC}}$. By construction, for every $\delta \in [\delta_{\min}, \delta_{\max}]$, both the SFR test and the LC condition at the selected altitude levels are satisfied.

Step 5: Final selection of the frequency shift

The final selection step is based on a separate set of N_δ equidistant values of δ in the interval $\delta_{\min} \le \delta \le \delta_{\max}$. Here, N_δ is chosen independently of the internal grid used in Steps 3 and 4, and we define $\delta_j = \delta_{\min} + (j-1)\,\Delta\delta_{\text{final}}$, $j = 1, 2, \ldots, N_\delta$, with $\Delta\delta_{\text{final}} = (\delta_{\max} - \delta_{\min})/(N_\delta - 1)$. For each δ_j, we perform the following tasks:

1. Compute the wave parameters corresponding to δ_j.
2. Evaluate the maximum perturbed horizontal velocity, the maximum perturbed vertical velocity, and the maximum perturbed temperature.
3. Check whether the layerwise causality condition is satisfied over the entire altitude range.

Finally, among all frequency shifts for which the causality condition is satisfied over the full altitude range, the algorithm determines the center of mass in the space spanned by the maximum values of the perturbed horizontal velocity, vertical velocity, and temperature, and selects the solution whose maximum-amplitude vector is closest to this center of mass.

Comments:

1. The algorithm determines not a single value but an interval of admissible imaginary frequency shifts. This is necessary for two reasons.

   (a) First, the LC procedure evaluates the layerwise causality condition only at a selected subset of altitude levels. As a consequence, the value returned by the LC test guarantees causality only at these selected levels, but not necessarily across the entire altitude range. By retaining an interval rather than a single value, we ensure that the subsequent analysis can identify those values of the frequency shift that satisfy the LC condition everywhere, not just at the sampled altitudes.

   (b) Second, even when the LC condition is applied across the full altitude range, it is often the case that more than one frequency shift satisfies the LC condition over all altitudes. Since these admissible shifts may lead to solutions with different numerical behaviors, a mechanism is needed to select an optimal value. For this purpose, the algorithm evaluates the wave parameters for a discrete set of shifts within the admissible interval and selects the optimal value based on the distance to the center of mass.

2. In principle, a Global Causality (CG) test can be applied at selected frequencies. Such a test proceeds as follows. Choose a set of N_{K_0} equidistant frequencies $\omega_{k_0} \in \{\omega_k\}_{k=1}^{N_{\rm FT}}$ with $k_0 \in K_0 = \{1, 2, \ldots, N_{K_0}\}$. For each test frequency ω_{k_0}, start with $\delta_{k_0} = \delta_{\rm start}$ and increases δ_{k_0} in steps of $\Delta\delta$, i.e., $\delta_{k_0} \leftarrow \min(\delta_{k_0} + \Delta\delta, \delta_{\rm stop})$, until the GC condition (c.f. Eq. (105))

$$\max_{l=1,\ldots,L} \mathrm{Re}[\lambda_{1l}^{+}(\omega_{k_0} - \mathrm{j}\delta_{k_0})] < \min_{l=1,\ldots,L} \mathrm{Re}[\lambda_{1l}^{-}(\omega_{k_0} - \mathrm{j}\delta_{k_0})]$$

is satisfied. If there exists a test frequency for which the GC condition is not satisfied, we say that the subset-based GC criterion fails for $\delta_{\rm stop}$. Otherwise, the GC frequency shift is computed as

$$\delta_{\rm GC} = \max_{k_0 \in K_0} \delta_{k_0}.$$

This test can be applied after the first step to determine $\delta_{\max} = \delta_{\rm GC}$. However, our numerical experiments indicate that this test is computationally very expensive and typically yields an excessively large value of $\delta_{\rm GC}$. In the subsequent step, this large value would be reduced by the SFR test. Importantly, if one instead prescribes a moderate but still sufficiently large input value for $\delta_{\max}$, the source-function reconstruction test reduces $\delta_{\max}$ to the same final value as when starting from $\delta_{\rm GC}$. Since the LC test alone is sufficient to ensure causality, we therefore do not employ the GC test in practice and use a prescribed moderate value of $\delta_{\max}$.

Author contributions. AlD: writing (original draft preparation), and conceptualization. DSE: writing (original draft preparation), and validation. TT: writing (original draft preparation), and formal analysis.

Code and data availability. The designed model is freely available as open-source code at https://github.com/AlexandruDoicu/Gravity-Waves. The International Reference Ionosphere (IRI) code data files are available at https://ccmc.gsfc.nasa.gov/models/IRI~2016/. The SAMI2 model of the Naval Research Laboratory is avaliable at https://github.com/NRL-Plasma-Physics-Division/SAMI2.

Competing interests. The authors declare that they have no conflict of interest.

Acknowledgements. We are grateful to Harold Knight for his helpful and insightful comments and for his detailed explanations of the theoretical results of his work. We also thank Stephan Buchert for his pertinent comments, especially those concerning ion drag.

References

Buchert, S. C.: Entangled dynamos and Joule heating in the Earth's ionosphere, Annales Geophysicae, 38, 1019–1030, https://doi.org/10.5194/angeo-38-1019-2020, 2020.

Budak, V. P., Klyuykov, D. A., and Korkin, S. V.: Complete matrix solution of radiative transfer equation for PILE of horizontally homogeneous slabs, Journal of Quantitative Spectroscopy and Radiative Transfer, 112, 1141–1148, https://doi.org/10.1016/j.jqsrt.2010.08.028, 2011.

Budak, V. P., Efremenko, D. S., and Shagalov, O. V.: Efficiency of algorithm for solution of vector radiative transfer equation in turbid medium slab, Journal of Physics: Conference Series, 369, 012 021, https://doi.org/10.1088/1742-6596/369/1/012021, 2012.

Chandrasekhar, S.: Radiative Transfer, Dover Publications, Inc., New York, 1950.

Dalgarno, A. and Smith, F.: The thermal conductivity and viscosity of atomic oxygen, Planetary and Space Science, 9, 1–2, https://doi.org/10.1016/0032-0633(62)90064-8, 1962.

Doicu, A. and Trautmann, T.: Discrete-ordinate method with matrix exponential for a pseudo-spherical atmosphere: Scalar case, Journal of Quantitative Spectroscopy and Radiative Transfer, 110, 146–158, https://doi.org/10.1016/j.jqsrt.2008.09.04, 2009a.

Doicu, A. and Trautmann, T.: Discrete-ordinate method with matrix exponential for a pseudo-spherical atmosphere: Vector case, Journal of Quantitative Spectroscopy and Radiative Transfer, 110, 159–172, https://doi.org/10.1016/j.jqsrt.2008.09.013, 2009b.

Drob, D. P., Emmert, J. T., Meriwether, J. W., Makela, J. J., Doornbos, E., Conde, M., Hernandez, G., Noto, J., Zawdie, K. A., McDonald, S. E., Huba, J. D., and Klenzing, J. H.: An update to the Horizontal Wind Model (HWM): The quiet time thermosphere, Earth and Space Science, 2, 301–319, https://doi.org/10.1002/2014ea000089, 2015.

Dungey, J. W.: Interplanetary Magnetic Field and the Auroral Zones, Physical Review Letters, 6, 47–48, https://doi.org/10.1103/physrevlett.6.47, 1961.

Efremenko, D. and Kokhanovsky, A.: Foundations of Atmospheric Remote Sensing, Springer International Publishing, ISBN 9783030667450, https://doi.org/10.1007/978-3-030-66745-0, 2021.

Efremenko, D. S., Molina García, V., Gimeno García, S., and Doicu, A.: A review of the matrix-exponential formalism in radiative transfer, Journal of Quantitative Spectroscopy and Radiative Transfer, 196, 17–45, https://doi.org/10.1016/j.jqsrt.2017.02.015, 2017.

Emmert, J. T., Drob, D. P., Picone, J. M., Siskind, D. E., Jones, M., Mlynczak, M. G., Bernath, P. F., Chu, X., Doornbos, E., Funke, B., Goncharenko, L. P., Hervig, M. E., Schwartz, M. J., Sheese, P. E., Vargas, F., Williams, B. P., and Yuan, T.: NRLMSIS 2.0: A Whole-Atmosphere Empirical Model of Temperature and Neutral Species Densities, Earth and Space Science, 8, https://doi.org/10.1029/2020ea001321, 2021.

Francis, S. H.: Acoustic-gravity modes and large-scale traveling ionospheric disturbances of a realistic, dissipative atmosphere, Journal of Geophysical Research, 78, 2278–2301, https://doi.org/10.1029/ja078i013p02278, 1973.

Fritts, D. C., Laughman, B., Lund, T. S., and Snively, J. B.: Self-acceleration and instability of gravity wave packets: 1. Effects of temporal localization, Journal of Geophysical Research: Atmospheres, 120, 8783–8803, https://doi.org/10.1002/2015jd023363, 2015.

Heale, C. J., Snively, J. B., Hickey, M. P., and Ali, C. J.: Thermospheric dissipation of upward propagating gravity wave packets, Journal of Geophysical Research: Space Physics, 119, 3857–3872, https://doi.org/10.1002/2013ja019387, 2014.

Hedin, A. E.: MSIS-86 Thermospheric Model, Journal of Geophysical Research: Space Physics, 92, 4649–4662, https://doi.org/10.1029/ja092ia05p04649, 1987.

Hedin, A. E., Biondi, M. A., Burnside, R. G., Hernandez, G., Johnson, R. M., Killeen, T. L., Mazaudier, C., Meriwether, J. W., Salah, J. E., Sica, R. J., Smith, R. W., Spencer, N. W., Wickwar, V. B., and Virdi, T. S.: Revised global model of thermosphere winds using satellite and ground-based observations, Journal of Geophysical Research: Space Physics, 96, 7657–7688, https://doi.org/10.1029/91ja00251, 1991.

Hickey, M. and Cole, K.: A numerical model for gravity wave dissipation in the thermosphere, Journal of Atmospheric and Terrestrial Physics, 50, 689–697, https://doi.org/10.1016/0021-9169(88)90032-3, 1988.

Hickey, M. P., Taylor, M. J., Gardner, C. S., and Gibbons, C. R.: Full-wave modeling of small-scale gravity waves using Airborne Lidar and Observations of the Hawaiian Airglow (ALOHA-93) O(1S) images and coincident Na wind/temperature lidar measurements, Journal of Geophysical Research: Atmospheres, 103, 6439–6453, https://doi.org/10.1029/97jd03373, 1998.

Hickey, M. P., Schubert, G., and Walterscheid, R. L.: Propagation of tsunami-driven gravity waves into the thermosphere and ionosphere, Journal of Geophysical Research: Space Physics, 114, https://doi.org/10.1029/2009ja014105, 2009.

Hines, C. O.: Internal atmospheric gravity waves at ionosphric heights, Canadian Journal of Physics, 38, 1441–1481, https://doi.org/10.1139/p60-150, 1960.

Hines, C. O.: A critique of multilayer analyses in application to the propagation of acoustic-gravity waves, Journal of Geophysical Research, 78, 265–273, https://doi.org/10.1029/ja078i001p00265, 1973.

Huba, J. D.: On the Development of the SAMI2 Ionosphere Model, Perspectives of Earth and Space Scientists, 4, https://doi.org/10.1029/2022cn000195, 2023.

Huba, J. D., Joyce, G., and Fedder, J. A.: Sami2 is Another Model of the Ionosphere (SAMI2): A new low-latitude ionosphere model, Journal of Geophysical Research: Space Physics, 105, 23 035–23 053, https://doi.org/10.1029/2000ja000035, 2000.

Huba, J. D., Joyce, G., and Krall, J.: Three-dimensional equatorial spread F modeling, Geophysical Research Letters, 35, https://doi.org/10.1029/2008gl033509, 2008.

Inoue, Y. and Horowitz, S.: Numerical Solution of Full-Wave Equation With Mode Coupling, Radio Science, 1, 957–970, https://doi.org/10.1002/rds196618957, 1966.

Kattawar, G. W., Plass, G. N., and Catchings, F. E.: Matrix Operator Theory of Radiative Transfer 2: Scattering from Maritime Haze, Applied Optics, 12, 1071, https://doi.org/10.1364/ao.12.001071, 1973.

Klostermeyer, J.: Numerical calculation of gravity wave propagation in a realistic thermosphere, Journal of Atmospheric and Terrestrial Physics, 34, 765–774, https://doi.org/10.1016/0021-9169(72)90109-2, 1972.

Klostermeyer, J.: Computation of acoustic-gravity waves, Kelvin-Helmholtz instabilities,and wave-induced eddy transport in realistic atmospheric models, Journal of Geophysical Research: Oceans, 85, 2829–2839, https://doi.org/10.1029/jc085ic05p02829, 1980.

Knight, H., Broutman, D., Eckermann, S., and Doyle, J.: A single-mode approximation for gravity waves in the thermosphere, Journal of Atmospheric and Solar-Terrestrial Physics, 224, 105 749, https://doi.org/10.1016/j.jastp.2021.105749, 2021.

Knight, H., Broutman, D., and Eckermann, S.: Full-wave anelastic and compressible Fourier methods for gravity waves in the thermosphere, Wave Motion, 110, 102 894, https://doi.org/10.1016/j.wavemoti.2022.102894, 2022.

Knight, H., Broutman, D., and Eckermann, S.: Compressible and anelastic governing-equation solution methods for thermospheric gravity waves with realistic background parameters, Theoretical and Computational Fluid Dynamics, 38, 479–509, https://doi.org/10.1007/s00162-024-00709-x, 2024.

Knight, H. K., Broutman, D., and Eckermann, S. D.: A causality-preserving Fourier method for gravity waves in a viscous, thermally diffusive, and vertically varying atmosphere, Wave Motion, 88, 226–256, https://doi.org/10.1016/j.wavemoti.2019.06.001, 2019.

Knight, H. K., Richards, P. G., Martinis, C. R., and Goncharenko, L. P.: Modeling MSTIDs Produced by Gravity Waves With Parameters Obtained From All-Sky Imager Observations and Comparisons to Incoherent Scatter Radar Observations, Journal of Geophysical Research: Space Physics, 130, https://doi.org/10.1029/2025ja033906, 2025.

Laundal, K. M., Skeidsvoll, A. S., Popescu Braileanu, B., Hatch, S. M., Olsen, N., and Vanhamäki, H.: Global inductive magnetosphere-ionosphere- thermosphere coupling, Annales Geophysicae, 43, 803–833, https://doi.org/10.5194/angeo-43-803-2025, 2025.

Lindzen, R. S. and Kuo, H.-L.: A Reliable Method for the Numerical Integration of a Large Class of Ordinary and Partial Differential Equations, Monthly Weather Review, 97, 732–734, https://doi.org/10.1175/1520-0493(1969)097<0732:armftn>2.3.co;2, 1969.

Liu, X., Xu, J., Yue, J., and Vadas, S. L.: Numerical modeling study of the momentum deposition of small amplitude gravity waves in the thermosphere, Annales Geophysicae, 31, 1–14, https://doi.org/10.5194/angeo-31-1-2013, 2013.

Maeda, S.: Numerical solutions of the coupled equations for acoustic-gravity waves in the upper thermosphere, Journal of Atmospheric and Terrestrial Physics, 47, 965–972, https://doi.org/10.1016/0021-9169(85)90074-1, 1985.

Midgley, J. E. and Liemohn, H. B.: Gravity waves in a realistic atmosphere, Journal of Geophysical Research, 71, 3729–3748, https://doi.org/10.1029/jz071i015p03729, 1966.

Nakajima, T. and Tanaka, M.: Matrix formulations for the transfer of solar radiation in a plane-parallel scattering atmosphere, Journal of Quantitative Spectroscopy and Radiative Transfer, 35, 13–21, https://doi.org/10.1016/0022-4073(86)90088-9, 1986.

Pfeffer, R. L. and Zarichny, J.: Acoustic-Gravity Wave Propagation from Nuclear Explosions in the Earth's Atmosphere, Journal of the Atmospheric Sciences, 19, 256–263, https://doi.org/10.1175/1520-0469(1962)019<0256:agwpfn>2.0.co;2, 1962.

Plass, G. N., Kattawar, G. W., and Catchings, F. E.: Matrix Operator Theory of Radiative Transfer 1: Rayleigh Scattering, Applied Optics, 12, 314, https://doi.org/10.1364/ao.12.000314, 1973.

Pütz, C., Schlutow, M., and Klein, R.: Initiation of ray tracing models: evolution of small-amplitude gravity wave packets in non-uniform background, Theoretical and Computational Fluid Dynamics, 33, 509–535, https://doi.org/10.1007/s00162-019-00504-z, 2019.

Pérez-Álvarez, R. and García-Moliner, F.: Transfer Matrix, Green Function, And Related Techniques: Tools For The Study Of Multilayer Heterostructures, Universitat Jaume I, Castelló de la Plana, Spain, 2004.

Pütz, C., Schlutow, M., and Klein, R.: Initiation of ray tracing models: evolution of small-amplitude gravity wave packets in non-uniform background, Theoretical and Computational Fluid Dynamics, 33, 509–535, https://doi.org/10.1007/s00162-019-00504-z, 2019.

Richards, P. G. and Peterson, W. K.: Measured and modeled backscatter of ionospheric photoelectron fluxes, Journal of Geophysical Research: Space Physics, 113, https://doi.org/10.1029/2008ja013092, 2008.

Shibata, T.: A numerical calculation of the ionospheric response to atmospheric gravity waves in the F-region, Journal of Atmospheric and Terrestrial Physics, 45, 797–809, https://doi.org/10.1016/s0021-9169(22)00009-5, 1983.

Stamnes, K.: The theory of multiple scattering of radiation in plane parallel atmospheres, Reviews of Geophysics, 24, 299–310, https://doi.org/10.1029/rg024i002p00299, 1986.

Stamnes, K. and Swanson, R.: A New Look at the Discrete Ordinate Method for Radiative Transfer Calculations in Anisotropically Scattering Atmospheres, J. Atmos. Sci., 38, 387–389, https://doi.org/10.1175/1520-0469(1981)038<0387:ANLATD>2.0.CO, 1981.

Stubbe, P.: Frictional forces and collision frequencies between moving ion and neutral gases, Journal of Atmospheric and Terrestrial Physics, 30, 1965–1985, https://doi.org/10.1016/0021-9169(68)90004-4, 1968.

Vadas, S. L. and Nicolls, M. J.: The phases and amplitudes of gravity waves propagating and dissipating in the thermosphere: Theory, Journal of Geophysical Research: Space Physics, 117, https://doi.org/10.1029/2011ja017426, 2012.

van de Hulst, H.: A new look at multiple scattering, Tech. rep., NASA Inst. Space Studies, 1963.

Volland, H.: Full wave calculations of gravity wave propagation through the thermosphere, Journal of Geophysical Research, 74, 1786–1795, https://doi.org/10.1029/ja074i007p01786, 1969a.

Volland, H.: The upper atmosphere as a multiply refractive medium for neutral air motions, Journal of Atmospheric and Terrestrial Physics, 31, 491–514, https://doi.org/10.1016/0021-9169(69)90002-6, 1969b.

Weimer, D. R.: Improved ionospheric electrodynamic models and application to calculating Joule heating rates, Journal of Geophysical Research: Space Physics, 110, https://doi.org/10.1029/2004ja010884, 2005.

Wick, G. C.: Über ebene Diffusionsprobleme, Zeitschrift für Physik, 121, 702–718, https://doi.org/10.1007/bf01339167, 1943.

Yeh, K. C. and Liu, C. H.: Acoustic-gravity waves in the upper atmosphere, Reviews of Geophysics, 12, 193–216, https://doi.org/10.1029/rg012i002p00193, 1974.